SYNTHESIS, CHARACTERIZATION AND CATALYTIC PROPERTIES OF MODIFIED BETA ZEOLITES

A THESIS

SUBMITTED TO THE

UNIVERSITY OF POONA

FOR THE DEGREE OF

DOCTOR OF PHILOSOPHY

(IN CHEMISTRY)

BY

K. SATYA NARAYANA REDDY

CATALYSIS DIVISION

NATIONAL CHEMICAL LABORATORY

PUNE - 411 008, INDIA

NOVEMBER 1992

Dedicated to

my beloved

Parents

and

Grandmother

CERTIFICATE

Certified that the work incorporated in the thesis entitled "**Synthesis, Characterization and Catalytic Properties of Modified Beta Zeolites**" submitted by Mr. **K. Satya Narayana Reddy** for the degree of Doctor of Philosophy was carried out by the candidate under my supervision in the National Chemical Laboratory, Pune, India. Such material as has been obtained from other sources has been duly acknowledged.

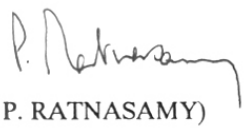

(Dr. P. RATNASAMY)

Supervisor

ACKNOWLEDGEMENTS

I would like to express my deep sense of gratitude to my supervisor, Dr. P. Ratnasamy, Deputy Director, National Chemical Laboratory, for his valuable guidance and inspiration.

I am deeply indebted to Dr. V.P. Shiralkar for his stimulating discussions and constant professional and personal help rendered during the course of the present investigation. Without his help, it would not have been possible for me to complete my research work successfully.

I wish to offer my sincere thanks to Dr. A.N. Kotasthane for his valuable discussions and suggestions during the present study.

I take this opportunity to thank Dr. S. Sivasanker, Dr. A.V. Ramaswamy, Dr. B.S. Rao, I. Balakrishnan and all other colleagues and friends in Catalysis Division for their help and co-operation rendered during the present study.

I am thankful to my senior colleagues Dr. G.N. Rao and Dr. K.M. Reddy, for their immense co-operation and motivation during this study.

I am thankful to the Director, National Chemical Laboratory, for allowing me to submit this work in the form of a thesis for the award of Ph. D degree. Financial assistance from University Grants Commission, New Delhi, is gratefully acknowledged.

My special word of thanks is due to Pranitha for her inspiration, constant encouragement and moral support.

Date: 6-11-1992

(K. SATYA NARAYANA REDDY)

Contents...

CHAPTER 1

GENERAL INTRODUCTION

1.1. INTRODUCTION

Zeolites are hydrated, crystalline aluminosilicates containing a rigid three dimensional framework structure enclosing cavities and channels. Zeolites are interesting materials because their pores are uniform in size and are in the size range of small molecules (see Fig.1.1). By virtue of these properties, zeolites can discriminate molecules on the basis of their size and this ability qualified them as 'molecular sieves'.

In many applications, particularly in petroleum and petrochemicals, they totally dominate many established and most new processing. The molecular control of ingress and egress to reactive sites, as well as control of the size and stereochemistry of the site itself, facilitates unprecedented molecular control of chemical reactions, and the ultimate in "molecular engineering" of molecules less than 10 Å in size.

Zeolites have found widespread use as adsorbents, ion exchangers, detergent-builders and catalysts, and are now being investigated for uses where the materials must have precise functions, for example, nonlinear optical materials, or electron and ion conductors.

1.2. ZEOLITES

In 1756 the Swedish minerologist Cronstedt observed[1] that mineral stilbite gave off steam, when heated. This result led him to coin the term zeolite, which is derived from the two Greek words "Zeo", to boil, and "lithos", stone.

From a chemist's standpoint, zeolites are inorganic polymers based on an infinitely extending three-dimensional, four connected framework of AlO_4 and SiO_4 tetrahedra linked to each other by the corner sharing of oxygen ions. Each AlO_4 tetrahedron in the framework bears a net negative charge which is balanced by a cation. The crystal structure of a zeolite is defined by the specific order in which a network of tetrahedral units are linked together. A representative emperical formula for a zeolite is written as[2]:

$$M_{2/n}O \cdot Al_2O_3 \cdot x\ SiO_2 \cdot y\ H_2O$$

where 'M' is an exchangeable cation, generally from the groups I or II of the periodic table. Organic cations may also be used to balance the framework charge; 'n' represents the cation valence. The value of 'x' is equal to or greater than 2; because two Al^{3+} ions do not occupy adjacent tetrahedral sites in accordance with the Lowenstein's rule[3].

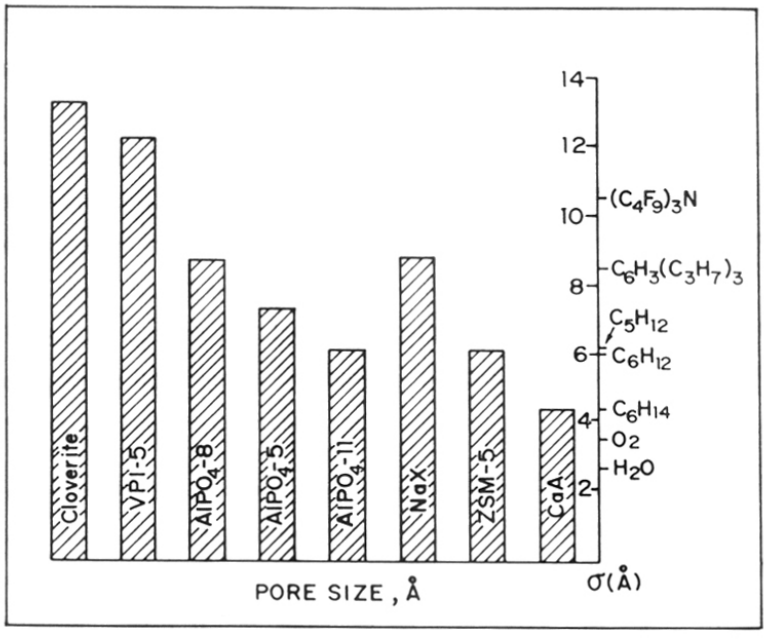

Fig.1.1: Correlation between pore size of molecular sieves and the diameter (σ) of various molecules.

The framework structure contains channels or interconnected voids that are occupied by the cations and water molecules. The cations are mobile and ordinarily undergo ion exchange. The water may be removed reversibly, generally by the application of heat, which leaves intact a crystalline host structure permeated by the micropores and voids which may amount upto 50 % of the crystals by volume.

1.3. ZEOLITE STRUCTURE

The primary building block of the zeolite structure is a tetrahedron of four oxygen atoms surrounding a central silicon atom - $(SiO_4)^{4-}$, Fig.1.2a. These are connected through their corners of shared oxygen atoms to form a wide range of small secondary building units, Fig.1.2b. These are interconnected to form a wide range of polyhedra, Fig.1.2c, which in turn connect to form the infinitely extended frameworks of the various specific zeolite crystal structures, Fig.1.2d. (In these structural diagrams the corners of the polyhedra represent Si or Al atoms, and the connecting lines, the shared oxygen atoms). Individual structures may comprise only one basic unit or many of them; the record is held by the mineral paulingite which contains five such polyhedra. To estimate the large number of possible structures, therefore, is a mathematical problem of combining polyhedra in different ways.

There are two types of structures: one provides internal pore system comprised of inter-connected cage like voids; the second provides a system of uniform channels which, in some instances, are one dimensional channel systems. Zeolites may conveniently be divided into one-, two-, and three-dimensional pore structures. The preferred type has two- or three-dimensional channels to provide rapid intracrystalline diffusion in adsorption and catalytic applications. Since 1950, approximately 150 synthetic zeolites[4] have been made, though only about 37 natural zeolites are known. It is estimated by the crystallographers[5] that the zeolite structures known till today represent less than 10 % of all possible zeolite structure types that could be theoretically formed.

1.4. CLASSIFICATION OF ZEOLITES

Classification of zeolites has been made on the basis of their morphology, crystal structure, chemical composition, effective pore diameter and natural occurrence. The classification of

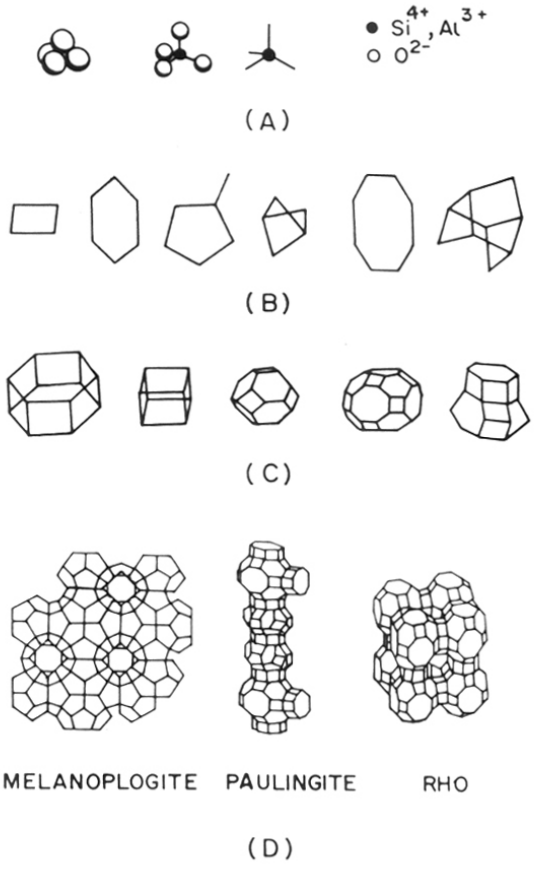

Fig.1.2: a) Primary Units b) Secondary Units c) Tertiary Units and d) Zeolite structures.

zeolites based on morphology was made by Bragg[6]. This classification was further modified on the basis of secondary building units present in the crystal structure by Meier[7] and Barrer[8] (Table 1.1).

Classification of zeolites according to their chemical composition has been made on the basis of increasing framework Si/Al ratio[8-10]. The four somewhat arbitrary categories are: 1) "low" 2) "intermediate" 3) "high" silica zeolites, and 4) "silica" molecular sieves.

The thermal stability increases from about 700°C in the low silica zeolites to 1300°C in the high silica molecular sieves. The surface selectivity which is highly hydrophilic in the low silica zeolites is hydrophobic in the high silica zeolites and the silica molecular sieves. The acidity tends to increase in strength with increasing Si/Al ratio. As the Si/Al ratio increases, the cation concentration and ion exchange capacity (proportional to aluminium content) decreases. The structures of the low silica zeolites are predominantly formed with 4, 6, and 8 rings of tetrahedra. In the intermediate silica zeolites, the onset of 5-rings in mordenite and omega zeolite is observed. In the high silica zeolite structures and the silica molecular sieves, a predominance of 5-rings of tetrahedra is found.

It is also convenient to classify zeolites according to their effective pore diameter, since this indicates the largest size molecule that can be adsorbed into their pore system. Barrer[11] has made such a classification of zeolites into five groups. Later, Sand[12] modified this classification into three major groups viz., small (e.g. erionite, ZK-5, chabazite, Rho), medium (ZSM-5, ZSM-11, ferrierite, EU-1) and large pore (mordenite, Y, beta, ZSM-12) zeolites, according to the largest membered ring present in the structure of each zeolites. Recently, Davis *et al.* discovered[13] a very large pore aluminophosphate molecular sieve called VPI-5 containing 18-membered ring pore openings. An isomorph of VPI-5 called MCM-9 containing Si atoms is also discovered[14]. Very recently, an extra large pore gallo-phosphate molecular sieve containing 20-membered ring pore openings, called Cloverite has been discovered[15].

1.5. NOMENCLATURE

There is no systematic nomenclature developed for molecular sieve materials. The discoverer of the synthetic species based on a characteristic X-ray powder diffraction pattern and chemical composition assigns trivial symbols. The early synthetic materials discovered by Milton, Breck and co-workers at Union Carbide used the arabic alphabet, e.g., zeolites A, B, X,

TABLE 1.1: Classification of zeolites according to structure type[7,8].

Sl.No.	Structure type	Main species	Iso structural species
1.	**Analcime group:** (interconnected 4- and 6-membered rings	analcime	leucite, pollucite, viseite, wairakite 6-Ca-D, Na-B.
2.	**Natrolite group:** (4-1 membered rings)	natrolite	laubanite, mesolite, meta-natrolite
3.	**Chabazite group:** (parallel 6- or double 6-membered rings)	chabazite	Linde D, herschelite, Linde R
4.	**Phillipsite group:** (approximated parallel 4-membered rings)	phillipsite	harmotome, ZK-19, Na-P_1, Linde W
5.	**Heulandite group** (characteristic configuration with 4- or 5-membered rings)	heulandite	clinoptilolite
6.	**Mordenite group:** (each tetrahedra of the framework belongs to at least one 5-membered ring)	mordenite	Na-D, Zeolon, ZSM-21, ZSM-35, ZSM-38, ptilolite
7.	**Faujasite group:** (frameworks based on poly-hedral cages of cubic or near cubic symmetry)	faujasite	Linde X, Linde Y, ZSM-20, ZK-4, ZK-21, ZK-22, N-A, Alpha
8.	**Laumontite group:**	Laumontite	leonhardite
9.	**Pentasil group:**	ZSM-5, ZSM-11	
10.	**Clathrate group:**	melanophlogite, ZSM-39	

Y, L. The use of Greek alphabet was initiated by Mobil and Union Carbide with the zeolites alpha, beta, and omega. Many of the synthetic zeolites which have the structural topology of mineral species were assigned the name of the mineral, for example synthetic mordenite, chabazite, erionite and offretite.

The International Zeolite Association Structure Commission and **IUPAC** have assigned structural codes to the known synthetic and natural zeolites[16,17] for known framework topology irrespective of composition, distribution of T-atoms and unit cell symmetry. Illustrative codes are LTA for Linde zeolite A, FAU for molecular sieves with faujasite topology Eg., zeolites X and Y, MOR for the mordenite topology, MFI for ZSM-5, MEL for ZSM-11, MTW for ZSM-12, and AFI for the aluminophosphate $AlPO_4$-5 topology.

1.6. ZEOLITE SYNTHESIS

Zeolites occur in nature in vugs and vesicles of basaltic lava, in specific kinds of rocks subjected to moderate geological temperature and pressure and in altered and reacted volcanic ash deposits. Many of these natural zeolites have been commercialized for purification of natural gas (chabazite), radioactive waste disposal (clinoptilolite), ammonia recovery from sewage effluents (clinoptilolite), and various petroleum and petrochemical catalyst applications (erionite, mordenite). The formation of such zeolites with volcanic glass and saline water as reactants must have occurred in temperature range 300-350 K and at pH > 13, requiring several years of crystallization[9,18,19].

Zeolites are synthesized hydrothermally by the combination of alkali metal ions, source of silica and alumina. The type of the zeolite formed depends mainly on the nature and concentration of bases (organic and inorganic), composition of reactants, reaction temperature, sequence of mixing the constituents and reaction time.

In the early 1950s, zeolite with low silica to alumina ratios ($SiO_2/Al_2O_3 \leq 10$) were discovered, by crystrallizing reactive aluminosilicate gels with alkali and alkaline earth metal hydroxides. The synthesis gels exhibited very high pH (≥ 13) and were crystallized at 100°C or less. Well known examples of such zeolites are A[20], X[21], Y[22], L[23] and mordenite[24]. In 1960s, the organic quaternary cations (templates) were introduced in the zeolite synthesis[25]. The use of organic cations[26] is an important step in the hydrothermal synthesis of high-silica zeolites, whose characteristic features are high acidity, high resistance to water and acids, and high thermal

stability. The manner in which such templates affect the zeolite crystallization is not straightforward. The progress in zeolite synthesis has been the discovery of the high silica zeolite beta[27], and the ZSM (Zeolite Socony Mobil) series[28-37] (ZSM-5, ZSM-11, ZSM-12, ZSM-20, ZSM-23, ZSM-25, ZSM-45, ZSM-48, ZSM-50, ZSM-51) using organic quaternary ammonium cations and amines (Table 1.2)[26].

The first members of another family of molecular sieves silicalite-1[38], silicalite-2[39] and TEA-silicate[40] have also been discovered. The organic additives may function as a structure-directing agent, gel modifier, buffer, and void filler[41]. Zeolites can also be synthesized in the presence of metal chelate complexes[42]. Alkali metal cations also play an important role in the formation of crystallite size and morphology of the zeolites during the synthesis[43].

Synthesis of zeolites is carried out from a gel or a solution containing silica, alumina and organic cations in highly alkaline medium. The first step involves the dissolution or depolymerization of aluminium and silicon to form silicate and aluminate anions. These are then brought together (by templates and/or metal ions) to form a gel by condensation or polymerization.

Sand[44] has summarized the following important events occuring during crystallization of zeolites:

* precipitation of a gel phase.
* dissolution of the gel.
* nucleation of zeolite(s).
* continued crystallization and crystal growth of the zeolite(s).
* dissolution of the initial metastable phase(s).
* nucleation of the more "**stable**" metastable phase or phases.
* continued crystallization and crystal growth of the new crystalline phase(s) while the initial crystals are dissolving.
* dissolution of metastable phase(s).
* nucleation of the equilibrium phase(s).
* crystallization and crystal growth of the final crystalline phases.

Based on the experimental evidence, two mechanisms have been suggested for the transformation of gels into zeolites. Kerr[45,46] reported on the crystallization of zeolites A and X in specific systems in which he postulated the growth of crystals from solution. McNicol *et.al*[47] concluded that the nucleation and the crystal growth of the zeolite within the gel phase. It has been evidenced for example by crystallizing zeolites from clear solutions under hot stage

Table 1.2: Organic template - zeolite structure relationship[26]

Organic template	structure
Tetraethylammonium (TEA)	Beta
	ZSM-48
	ZSM-12
	ZSM-20
	ZSM-25
	mordenite
Tetrapropylammonium (TPA)	ZSM-5
n-propylamine	ZSM-5
Tetrabutylammonium (TBA)	ZSM-11
Choline	ZSM-38
	ZSM-43
	ZSM-34
	CZH-5
Tetramethylammonium (TMA)	ZSM-39
Pyrrolidine	ZSM-5
	ZSM-21
	ZSM-29
	ZSM-35
	ZSM-48
	ZSM-50
1,2-diaminoethane	ZSM-5
	ZSM-21
	ZSM-35
1,8-diaminooctane	ZSM-11
	ZSM-48
Hexamethonium Bromide (HMBr)	EU-1
	EU-2
Neopentylamine	mordenite

microscope[48]. The nucleation and subsequent crystallization can occur readily in the solution. However, in solution phase transformation crystallization starts at the liquid-solid interface (gel or reactor wall).

1.7. MODIFICATION OF ZEOLITES

The as-synthesized zeolites usually contain substantial amounts of alkali metal ions or organic templates. The activity and selectivity of zeolites as catalysts are determined by the Brönstead acid sites associated with the aluminium in the framework. To use the zeolites in acid catalyzed reactions, they have to be converted into the protonic form.

It is also necessary to modify the as-synthesized zeolite so as to improve the thermal stability and acidic strength. The zeolite molecular sieves can be suitably modified by one or more of the following ways.

1.7.1 Isomorphous substitution

In recent years isomorphous substitution of Si by foreign elements[49] as B[50-52], Fe[51], Ga[51], Ti[53], V[54], etc. has been largely studied and has been shown to result in different catalytic properties. Materials of $AlPO_4$-n family have opened new fields of interests and prospectives with the possibility of isomorphous substitution by many elements[55,56], as Si, Co, Mn and many others. Carbon and sulfide-type molecular sieves have also been synthesized. The purpose of obtaining isomorphous substitution and new molecular sieve materials was obviously to modify the chemical and physical properties of zeolitic-type materials and therefore their catalytic properties. Barrer classfied four types of isomorphous replacement in zeolites[57]:

1. One guest molecule by another (i.e.: substitution of sodium chloride by sodium sulphate transforms sodalite into Nosean).
2. One cation by another (i.e.: the more common method is the treatment of a zeolite with an aqueous solution of the salt containing the different cation; it is the base of water sweetening).
3. One element by one of its isotopes (i.e.: mainly hydrogen, oxygen and silicon).
4. One element in tetrahedral position by another (i.e.: substitution of silicon or aluminium with sterically compatible elements).

The type one substitution has low relevance from the point of view of zeolite applications.

The type two substitution is important because it is possible to obtain active catalysts and to eliminate certain cations contaminating water or solutions.

The type three substitution could be useful to investigate the zeolite synthesis and for characterization purposes.

Studies on the type four substitution were initiated many years ago. Goldsmith[58] referred in 1952 his success in the synthesis of thomsonite samples in which Si was replaced by Ge in the zeolite framework. Again in the fifties appeared the remarkable work of Barrer *et.al*[59]: Thomsonite, zeolite A, Faujasite and Harmotome were obtained having gallium and/or germanium in the lattice.

1.7.2. Cation exchange

Most of the zeolites are synthesized in a cationic form in which the positively charged cations balance the negatively charged framework system. These extra-framework cations can be replaced by other cations[9].

The rate of and degree of cation exchange depends on the following factors:

1). The type of cation being exchanged, the size and charge.
2). The nature, size and strength of any cation co-ordination complex.
3). The temperature of the ion exchange treatment.
4). The thermal treatment of the zeolite, before or after exchange.
5). The structural properties of the zeolite and its silica/alumina ratio.
6). The locations of the cations in the zeolite structure.
7). The concentration of the cation exchange solution.
8). The previous treatment of the zeolite.

1.7.3. Metal loading

For many industrial reactions, e.g., those involving hydrogenation or oxidation, it is necessary to have additional components in the catalyst to perform the total or partial catalytic function. Such components are frequently metals, their oxides, or sulfides similar to those used in nonzeolite or amorphous catalyst systems.

Zeolite-containing catalysts can be loaded with metals in several ways. These include ion exchange of the zeolite from solution, impregnation from solution, adsorption from the gas phase

and co-mulling during the catalyst formation of the solid metal component or its solution. Metals which are desirable for the introduction into the zeolite and/or catalysts include the common hydrogenation and oxidation components such as Ni, Co, Pt, Ag, Pd, Mo, W, Cr, and the like.

1.8. ACIDITY AND BASICITY IN ZEOLITES

The acidity and basicity are important characteristics of zeolites. The acidity in zeolites arises from the substitution of a trivalent metal atom such as Al, Ga, Fe, B, etc., for Si in the framework positions. When the charge compensating cation is hydrogen atom (proton) the zeolite framework exhibits a Brönsted acidity[60]. The treatment of protonic zeolites at high temperature causes the transformation of Brönsted acid sites into Lewis acid sites. Lewis acidity arises from a trigonal Al or cationic species, alkali, alkaline earth or other cations. Brönsted acidity depends on the content of trivalent metal ion in the framework position.

Similarly, basicity in zeolites may also exist in two forms. The Brönsted bases are the negative -OH groups and the Lewis basic sites are the framework oxygen atoms. The extent of charge on the oxygen determines their basic strength. The application of basic zeolites in catalysis and adsorption has been reported[61,62]. Recently, Barthomeuf *et. al*[63] had shown that the basic strength of the zeolite depends not only on the chemical composition but also on the structural environment of the framework oxygen.

1.9. SHAPE SELECTIVITY IN ZEOLITES

Shape selective catalysis by zeolites is based on the presence of active catalyst sites inside the zeolite pore system. For shape selectivity to occur, essentially all the catalytic active sites must be in the interior of the pores. The actual pore size within a given ring structure can be varied within limits by the cation present in the system. Weisz and Frilette[64] were apparently the first to describe shape selectivity, and they, together with Chen and Degnan[65] and Miale and co-workers[66] have published extensively on variety of applications. The pore size and shape may affect the selectivity of a reaction in four ways.

1.9.1. Reactant Shape Selectivity

This occurs when the aperture size of the zeolite is such that it admits only certain smaller molecules and excludes larger molecules (Fig.1.3.a); hence, in a mixture, effectively only the smaller molecules react.

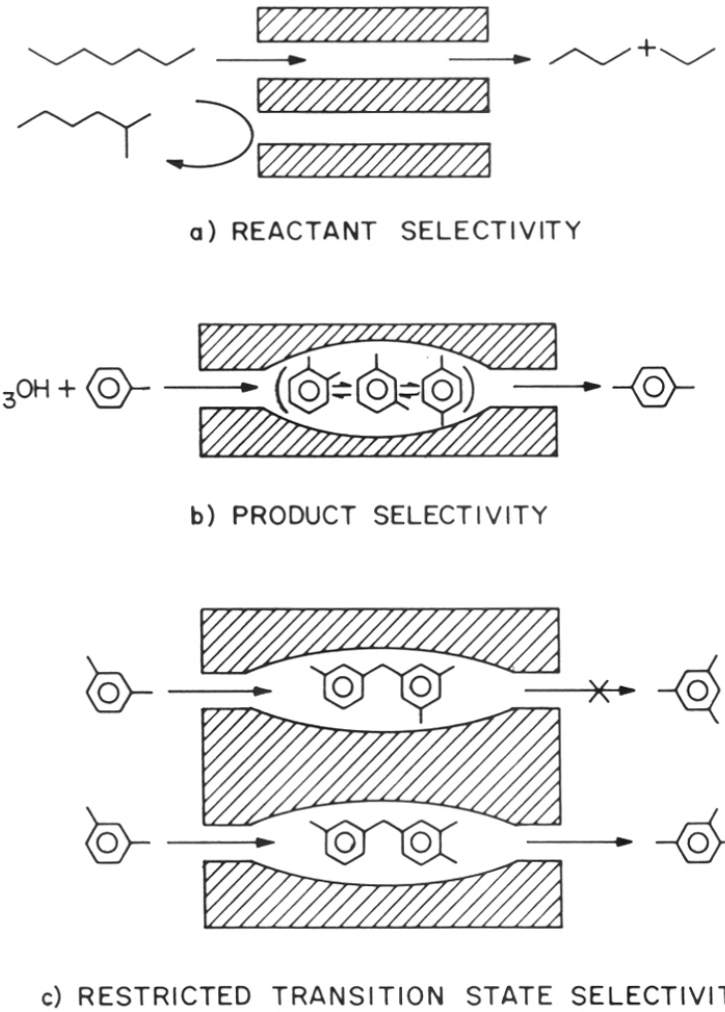

Fig.1.3: Shape Selectivity in Zeolites.

1.9.2. Product Shape Selectivity

In catalysis over zeolites, product selectivity (Fig.1.3.b) is observed when some of the products formed within the pores are too bulky to diffuse out as products or if they are not too bulky, their size, compared with other molecules produced, results in a large difference in diffusion rates. The bulky molecules are either converted to smaller molecules, or build up in the catalyst pores and deactivate it. For example, *p*-xylene is produced preferentially in modified zeolites over the more bulky *o*- and *m*-isomers due to the pore diameter restrictions. Thus, the formation of high diffusivity products by diffusion reaction-interactions[67] is thereby favoured.

1.9.3. Restricted Transition State Shape Selectivity

Restricted transition state selectivity (Fig.1.3.c) occurs when shape selective restrictions act on the intrinsic kinetics rather than via diffusion limitations. The phenomenon can limit or prevent the formation of the intermediate structures and thereby inhibit certain reaction pathways. The reactions requiring smaller transition states proceed unhindered. This type of shape selectivity was first proposed by Csicsery[68] in order to explain the absence of symmetrical trialkylbenzenes in the product from the disproportionation of dialkylbenzenes over mordenite.

1.9.4. Molecular Traffic Control

A new type of shape selectivity in zeolites, containing intersecting channels of different diameters has been proposed by Derouane and Gabelica[69]. According to this concept, in the case of zeolites with more than one type of intersecting channels, the reactants enter preferentially through one set of channels and the products leave the system by a different set, thus minimizing counter diffusion. However, the existence of the molecular traffic control is not yet supported by experimental findings.

Several model reactions have been used to determine the shape selectivity of zeolites quantitatively.

* Constraint Index[70]
* Refined Constraint Index[71]
* Spaciousness Index[72]
* *o-p*-index in *m*-xylene isomerization[73]
* DEB distribution in EB disproportionation[74].

1.10. PHYSICO-CHEMICAL CHARACTERIZATION OF ZEOLITES

1.10.1. X-ray Diffraction

X-ray powder diffraction is one of the most important techniques used in the study of zeolites. It is used to (i) identify the zeolite structure (finger print of individual structures)[75] (ii) check its phase purity (iii) find out the crystallinity and (iv) estimate unit cell parameters[76]. Bibby *et.al*[77] reported the use of X-ray diffraction technique for the estimation of the average alumina content, from the change in unit cell volume in the ZSM-5 crystals. The use of unit cell volume studies in confirming the structural incorporation of elements other than aluminium has been reported[78].

The advent of modern methods of X-ray diffraction technique is in solving the structures, in particular, by powder diffraction techniques including *ab-initio* structure determinations and *Rietveld refinements*[79,80] have helped in the elucidation of structures of new zeolites.

1.10.2. Infrared Spectroscopy

Infrared spectroscopy is one of the earliest techniques used to study zeolite hydroxyls, it provides qualitative information on zeolite acidity with probe molecules such as pyridine. In addition, it provides a method of studying extra-framework cations. Flanigen[81] and Ward[82] discussed the i.r. studies in the framework and hydroxyl regions. Maroni *et.al*[83] and Janin *et.al*[84] have discussed the use of different probe molecules to study the acidity of zeolites by diffuse reflectance and transmission techniques; and Baker *et.al*[85] discussed the study of extra-framework cations with far-i.r. spectroscopy.

In the i.r. spectrum of zeolites in the range of 200-1300 cm^{-1} the lattice vibration can be observed. These vibrations can be divided into structure-sensitive (external linkages) and structure-insensitive (internal tetrahedra) bands. Flanigen[86] reported the following position of these bands:

Structure sensitive vibrations

- asymmetric stretch	1050 - 1150 cm^{-1}
- symmetric stretch	750 - 820 cm^{-1}
- double ring vibrations	500 - 650 cm^{-1}
- pore opening vibration	300 - 420 cm^{-1}

Structure insensitive vibrations

- asymmetric stretch	950 - 1250 cm^{-1}
- symmetric stretch	650 - 720 cm^{-1}
- T-O bending	420 - 500 cm^{-1}

The incorporation of P, B, Ga, Fe and Ti into the silicate frameworks has been found to shift the framework i.r. vibrations. The substitution of B into the zeolite framework results in the shift of asymmetric vibrations towards higher wave-numbers due to lighter mass of B[87]. Again, as expected for substitution by heavier Ga atom into the faujasite and sodalite frameworks exhibit symmetric stretching vibrations at lower wave numbers than the corresponding aluminosilicates[88]. Similar shifts are also observed in ferrisilicate molecular sieves[89].

The bands characteristic of the hydroxyl functions in the i.r. spectrum around 3500-3700 cm^{-1} have been associated with the acidity[90]. In the case of large pore zeolites, Ward *et.al*[82] observed hydroxyl stretching vibrations in the region of 3600-3650 cm^{-1}. Medium and small pore zeolites are found to exhibit similar hydroxyl vibration at slightly lower wave-numbers[91].

1.10.3. Nuclear Magnetic Resonance Spectroscopy

Since the introduction of the Magic Angle Spinning technique to NMR spectroscopy, it is possible to obtain high resolution spectra from solid samples. Lippmaa *et.al*[92] were the first who applied in 1981 this method to record the ^{29}Si spectra of zeolites. Nagy and Derouane discussed the application of various NMR nuclei to study the zeolites[93]. Much attention has been focussed on ^{29}Si and ^{27}Al MAS NMR spectra in order to investigate:

* Si and Al ordering[94]
* crystallographically equivalent and non-equivalent Si[95] and Al[96] ions in various sites.
* framework Si/Al ratio[97]
* the co-ordination number of Si[98] and Al[99]
* spectral correlation with Si-O-T bond angles[100] and Si-O bond lengths[101].

^{27}Al MAS NMR has been applied primarily to observe the tetrahedral (framework) or octahedral (nonframework) form of Al in zeolites[102].

Freude *et.al*[103] and Scholle *et.al*[104] have used ^{1}H MAS NMR to study the zeolite acidity. Three types of proton signals were observed. These are due to (i) water protons, (ii) surface silanols and (iii) Brönsted acid protons. Barrer *et.al*[105] studied the adsorbent-adsorbate interaction by using the ^{13}C MAS NMR technique.

1.10.4. Sorption and diffusion in zeolites

Zeolites are microporous crystalline materials with ability to sorb selected molecules inside the channels and cavities. In zeolites usually intracrystalline surface area constitutes about 97% of total surface area. Study of the sorption characteristics of zeolites can provide information about their void volume, the size of the pore opening, the level of crystallinity, the acidity, and diffusion properties and pore blockages, if any.

Sorption of various gases and vapours on natural as well as synthetic zeolites has been extensively studied by Barrer[106,107]. Anderson *et.al*[108] have carried out the sorption of hydrocarbons to characterize their pore openings. Flanigen *et.al*[109], while studying the sorption properties of silicalite, have found that benzene with a diameter 0.585 nm is adsorbed, while neopentane with a diameter of 0.62 nm is not adsorbed. Olson *et.al*[110] observed that the hydrophobicity of the zeolite is inversely proportional to the aluminium content in the framework positions.

In heterogeneous catalysis, adsorption and diffusion properties play an important role in the rate of chemical reaction at the catalytic active site. A detailed review on diffusion in zeolites is given by Barrer[111]. The diffusion in zeolites may be devided into three types viz., **Configurational diffusion, Knudsen diffusion and Bulk diffusion**.

1.11. ZEOLITES IN CATALYSIS

The industrial use of zeolites as catalysts started at the beginning of the 1960s with the replacement of cracking catalysts based on amorphous aluminosilicates[112]. As far as catalysis is concerned, zeolites share the following six properties that make them attractive as heterogeneous catalysts[113].

* Well-defined crystalline structure
* High internal surface areas (>600 m^2/g)
* Uniform pores with one or more discrete sizes.
* Good thermal stability'
* Ability to sorb and concentrate hydrocarbons
* Highly acidic sites when ion exchanged with protons.

Zeolites are inorganic cation exchangers. Their catalytic activity is associated with the presence of acid centres (Brönsted and Lewis) in the intracrystalline surface. The acid strength and number of the acid centres can be adjusted in a controlled manner during synthesis, isomorphous substitution of Al and/or subsequent ion exchange.

The most importanat application of zeolites is in reactions catalyzed by proton acids and Lewis acids, where the change from a homogeneous to a heterogeneous procedure brings advantages in respect of easy separation, and disposal of the catalyst, avoidance of corrosion etc.

1.11.1. Zeolite Catalysts in Petrochemical Processes

The use of silicon-rich zeolites as highly acidic, extremely shape selective and heat-stable catalysts led to new industrial petrochemical processes:[114,115] Selectoforming[116], olefin oligomerization[117], dewaxing[118] and MTG (methanol to gasoline) processes[119] thereby have established themselves as industrial processes alongside cracking and hydrocracking. They are also used for the dehydrocyclization of ethane, propane or LPG (liquid petroleum gas) to arenes[120] and in the somewhat more distant future by the MTO (methanol to olefin) process[121]. However, the petrochemical industry also uses selective reactions such as the Mobil-Badger process for the alkylation of arenes[122], the *para*-directed isomerization of xylenes[123] and the disproportionation[122,123] or alkylation of monosubstituted arenes[124].

A number of shape selective zeolite based processes are commercially available to improve the octane quality of the reformate and gasoline streams. These are (i) Selectoforming (ii) M-forming (iii) M-2 forming (iv) Cyclar process and (v) AromaxsM.

1.11.2. Zeolite Catalysts in Organic Synthesis

The combination of acidity and shape selectivity in the zeolite catalysts is an important factor for organic syntheses. The tendency to utilize this potential for specific, highly selective synthesis in the field of intermediates and fine chemicals has continued steadily in recent years. The numerous modifications of zeolites in respect of the number and strength of acid centres, isomorphous substitution[125] and doping with metals, provide an opportunity of employing catalysts that are tailored to suit the reactions desired, especially in organic synthesis. Recently, excellent reviews are published on the application of zeolites in organic synthesis[126,127].

A. Aromatic Substitution Reactions

Zeolite catalyzed alkylation of benzene, toluene and naphthalene have been studied. Alkylation ideally takes place in the gas phase. In many alkylation reactions with longer-chain alkenes, it is necessary to revert to the liquid phase. As the chain length increases, cracking reactions must be expected in the gas phase. It is then preferable to use the large-pore ZSM-12, X, Y zeolites[128]. For example, using ZSM-12 zeolite, isopropyltoluene is formed at a selectivity approximately 95% at conversion exceeding 95%. The most important gas phase alkylation of oligocyclic arenes is the methylation of naphthalene[129].

Like alkylation, the acylation of arenes can also be carried out using zeolites. The acylation of toluene with C_1-C_{20} -carboxylic acids using Ce-Y zeolite in the liquid phase has been done[130]. A surprising fact in the chlorination of benzene is that the substitution product chlorobenzene is obtained on Y zeolite, whereas on ZSM-5 the addition product hexachlorocyclohexane is formed[131].

B. Isomerization Reactions

Isomerization of 2,4-dichlorophenol to 2,5-dichlorophenol[132], 2-chlorothiopene to 3-chlorothiopene and 3,4-dichloro toluene to 2,5-dichlorotoluene over ZSM-5 zeolites is studied. Polynuclear aromatic compounds can also be isomerized using zeolites. 1-methylnaphthalene is converted into 2-methylnaphthalene over H-Na-Y zeolite[133].

C. Oxidation Reactions

The direct hydroxylation of phenol with H_2O_2 to di-hydroxybenzenes over TS-1 has been studied[134]. TS-1 is also active in the reaction of benzyl alcohol to benzaldehyde and cyclohexanol to cyclohexanone[135]. The oxidation of lower olefins to carbonyl compounds can be carried out in the gas phase on Pd/Cu-Y zeolites[136].

D. Condensation Reactions

Condensation reactions are catalyzed by acids or bases. Over acid aluminium zeolites, acetone is converted into mesityl oxide, isobutene, phorones, mesitylene and alkyl phenols[137]. The reaction of olefins with formaldehyde, for example, the synthesis of isoprene from isobutene,

is well known reaction[138]. Another class of condensation reactions with NH_3 is the synthesis of N-heterocyclic compounds. Picolines are obtained by the condensation of acetaldehyde with NH_3 over ZSM-5 and Cd-ZSM-5 zeolites[139].

1.12. STRUCTURE OF ZEOLITE BETA

Zeolite beta is a high silica, large pore crystalline material first synthesized by Wadlinger *et al.*[27]. Zeolite beta is a highly intergrown hybrid of two[140-143] distinct, but closely related structures that both have fully three-dimensional pore system with 12-membered rings. Zeolite beta belongs to a family of zeolites, the two end members of which have tetragonal (Polymorph A) and monoclinic (Polymorph B) symmetry (Fig.1.4). In both the crystallographic systems, 12-membered ring straight channels are present in two crystallographic directions, while the 12-membered ring channels in the third crystallographic direction is sinusoidal. The main difference between the two polymorphs is in the pore dimensions of the straight channel which is narrower for the tetragonal structure. Moreover, the sinusoidal channels are more tortuous in the tetragonal compared to those in the monoclinic structure (Fig.1.5).

All members of this family of zeolites have two sets of perpendicular channels, which intersect to form a three-dimensional array of cages that have three 12-ring apertures. In polymorph A which is tetragonal with a = 1.25 nm and c = 2.66 nm, the cages are arranged in a helical fashion around a fourfold screw axis, which may be either right-(space group $P4_122$) or left-($P4_322$) handed. In polymorph B, that is monoclinic C_2/c, with a = 1.76 nm, b = 1.78, c = 1.44 nm and $\beta = 114.5°$, the stacking of layers alternates in handedness and the structure is thus achiral. The unit cell volumes calculated for polymorph A and B are 4.142 and 4.118 nm^3 and the no. of T-atoms per unit cell are 64.

Zeolite beta have several unique and interesting features. It is only the high silica zeolite to have a fully three-dimensional 12-membered ring pore system and is also the only large pore zeolite to posses chiral pore intersections. Finally, unlike other zeolites, it is the only zeolite to have a near-random degree of stacking faults and adsorbs equal amounts of n-hexane and cyclohexane giving its sorption capacity of about 0.23 $ml.g^{-1}$.

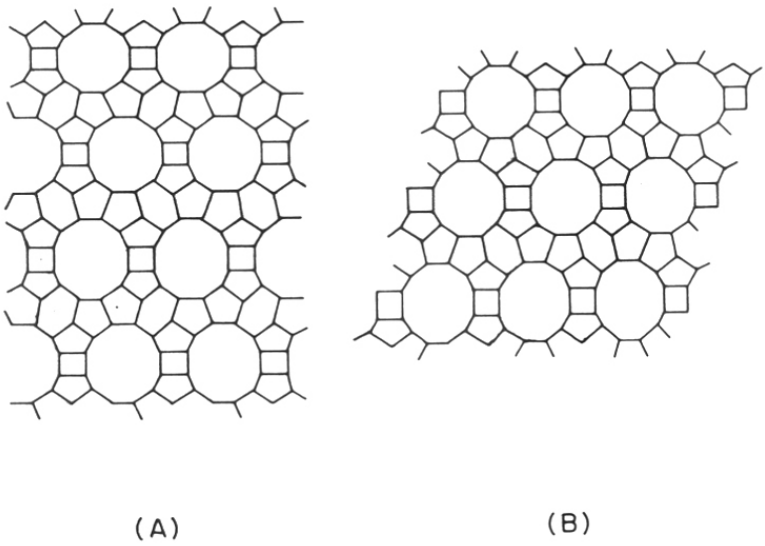

Fig.1.4: Structure of zeolite beta. (A) Polymorph A, (B) Polymorph B and (C) low-resolution model of zeolite beta pore structure showing an interpenetrating arrangement of channels.

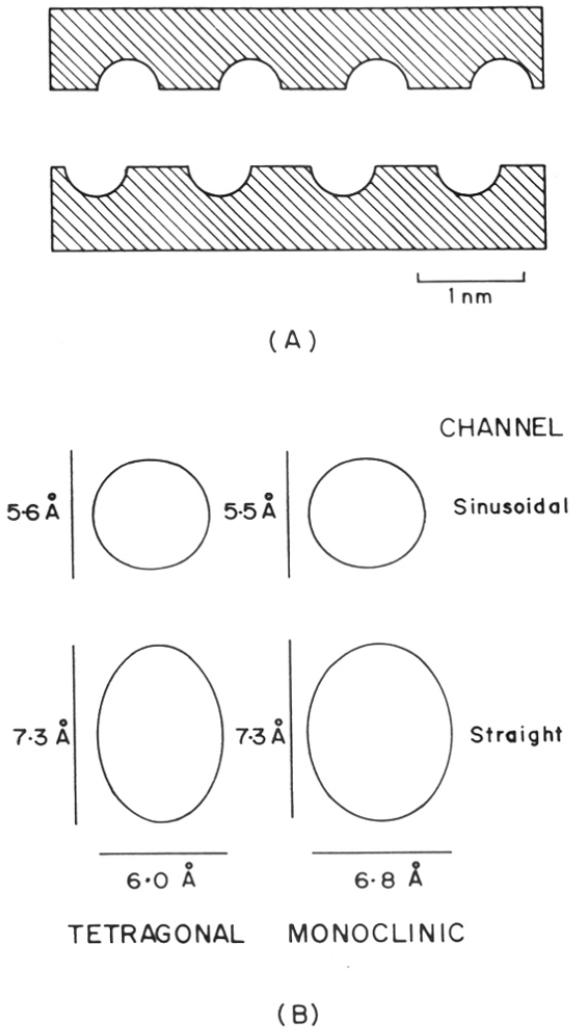

Fig.1.5: A) Cross section of the linear channel of zeolite beta B) Pore openings of zeolite beta.

1.13. SCOPE OF THE THESIS

The main objective of this work is to study the synthesis, characterization and catalytic properties of beta and modified beta zeolites in more detail. The results obtained in the synthesis and the modification of zeolite beta are discussed in chapter-2. This chapter demonstrates the feasibility of synthesis of beta using commercially economical raw materials such as silica sol and tetraethylammonium bromide instead of conventionally used tetraethylorthosilicate and tetraethylammonium hydroxide. A higher (> 98 % based on silica and alumina) yield of zeolite crystals was achieved. The modifications of zeolite beta by various methods are also described in this chapter. The physico-chemical characteristics of modified beta zeolites are presented in chapter-3. Isopropylation of benzene and toluene to cumene and cymenes over zeolite beta and other large pore zeolites like mordenite and ZSM-12 are described in chapter-4. The hydroisomerization of *n*-hexane to methylpentanes and dimethylbutanes on Pt-loaded beta zeolites are described in chapter-5. Chapter-6 summarizes the salient findings of thesis work.

1.14. REFERENCES:

1. Cronstedt, A.F., *Adak. Handl. Stockholm,* **17**, 120 (1756).
2. Breck, D.W., *J. Chem. Edn.*, **41**, 678 (1964).
3. Loewenstein, W., *Am. Minerals*, **39**, 92 (1954).
4. Whyte, Jr.T.E. and Dalla Betta, R.A., *Catal. Rev. Sci. Engg.*, **24(4)**, 567 (1982).
5. Sand, L.B., *Res. proposal to the office of Fossil Energy, Dept. of Energy*, (Re No. FE-NPI-80-001), (1982).
6. Bragg, W.L., *'The Atomic Structure of Minerals'*, Cornell University press, Ithaca, New York, (1937).
7. Meier, W.M., *Molecular sieves, Soc. of Chem. Ind.*, London., p.10 (1968).
8. Barrer, R.M., *'Hydrothermal Chemistry of Zeolites'*, London, Academic press (1982).
9. Breck, D.W., *'Zeolite Molecular Sieves: Structure, chemistry and use'*, London, Wiley (1974).
10. Flanigen, E.M., *'in Proceedings of the 5th International Conference of Zeolites'*, (Rees, L.V.C., Eds.), Naples, Italy, June 2-6, p.760 (1980).
11. Barrer, R.M., *'Zeolites and Clay Minerals as Sorbents and Molecular Sieves'*, Academic press, London and New York, Ch.2 (1978)
12. Sand, L.B., *Econ. Geol.*, p.191 (1967).
13. Davis, M.E., Saldarriaga, C., Montes, C., Graces, J. and Crowder, C., *Nature*, **331**, 968 (1988).
14. Derouane, E.G., Valyocsik, E.W. and von Ballmoos, R., Eur. Pat. Appl. 1,46,384 (1984).
15. Estermann, M. McCusker, L.B., Baerlocher, C., Merrouche, A. and Kessler, H., *Nature*, **352**, 320 (1991).
16. Barrer, R.M., *Pure and Appl. Chem.*, **51**, 1091 (1979).
17. Meier, W.M. and Olson, D.H., *'Atlas of zeolite structure types'*, London, Butterworths, (1987).
18. Mumpton, F.A., *Min. Soc. Am.*, Washington, (1977).
19. Sand, L.B. and Mumpton, F.A., (Eds.),' *Natural Zeolites, Occurance, Properties, Use'*, Pergamon press, Oxford (1978).
20. Breck, D.W., Eeversole, W.G., Milton, R.M., Reed, T.B. and Titomas, T.L., *J. Am. Chem. Soc.*, **78**, 5964 (1956).
21. Milton, R.M., US Pat. 2,282,244 (1959).
22. Breck, D.W., US Pat. 3,130,007 (1964).

23. Breck, D.W., US Pat. 3,216,789 (1965).
24. US Pat. 3,442,795.
25. Barrer, R.M. and Denny, P.J., *J. Chem. Soc.* 971 (1961).
26. Lok, B.M., Cannan, T.R. and Messina, C.A., *Zeolites*, **3**, 282 (1983).
27. Wadlinger, R.L., Kerr, G.T. and Rosinski, E.J., US Pat. 3,308,069 (1967).
28. Argauer, R.J. and Landolt, G.R., US Pat. 3,702,886 (1972).
29. Chu, P., US Pat. 3,709,979 (1973).
30. Rosinski, E.J. and Rubin, M.K., US Pat. 3,832,449 (1974).
31. Ciric, J., US Pat. 3,972,983 (1976).
32. Plank, C.J., Rosinski, E.J. and Rubin, M.K., US Pat. 4,076,842 (1978).
33. Dohety, H.G., Rosinski, E.J. and Plank, C.J., Eur. Pat. Appl. 15,702 (1980).
34. Kuel, G.H., US Pat. 4,495,303.
35. Rollman, L.D. and Valyocsik, E.W., Eur. Pat. Appl. 15,132 (1980).
36. Chu, P., Vartuti, J.C. and Herbst, A.J., Eur. Pat. Appl. 1,27,399 (1984).
37. Casci, J.L., Lowe, B.M. and Whittam, T.V., Eur. Pat. Appl. 42,226 (1981).
38. Grose, R.W. and Flanigen, E.M. US Pat. 4,061,724 (1977).
39. Bibby, D.M., Milestone, N.B. and Aldridge, L.P., *Nature*, **280**, 664 (1979).
40. Grose, R.W. and Flanigen, E.M., US Pat. 4,104,294 (1978).
41. Szostak, R., *'Molecular Sieves: Principles of Synthesis and Identifications'*, Van Nostrand Reinhold, New York (1989).
42. Rankel, L.A. and Valyocsik, E.W., US Pat. 4,500,503 (1985).
43. Gabelica, Z., Blom, N. and Derouane, E.G., *Appl. Catal.*, **5**, 227 (1983).
44. Sand, L.B., *Pure and Appl. Chem.*, **52**, 2105 (1980).
45. Kerr, G.T., *J. Phys. Chem.*, **70**, 1047 (1966).
46. Kerr, G.T., *J. Phys. Chem.*, **72**, 1385 (1968).
47. McNicol, B.D., Pott, G.T. and Loos, R.K., *J. Phys. Chem.*, **76**, 3388 (1972).
48. Guth, J.L. and Caullet, P., *J. Chim. Phys.*, **83**, 155 (1986).
49. Heinemann, H., in *'Catalysis: Science and Technology'*, (Anderson, J.R. and Boudart, M., Eds.), Springer, **1**, 1 (1981).
50. Becker, K., John, H., Steinberg, K., Weber, M. and Nestler, K., in *'Catalysis on Zeolites'*, (Kallo, D. and Minachev, Kh.M., Eds.), Akademia Kiado, Budapest p.515 (1988).

51. Naccache, C. and Ben Tarrit, Y., in *'Zeolite Science and Technology'*, (Ribeiro, F.R., Rodrigues, A.E., Rollmann, L.D. and Naccache, C., Eds.), Martinus Nijhoff, The Hague, p.373 (1984).

52. Minachev, Kh.M., Kharlamov, V.V. and Garanin, V.I., in *'Catalysis on Zeolites'*, (Kallo, D. and Minachev, Kh.M., Eds.), Akadamia Kiado, Budapest p.489 (1988).

53. Perego, G., Bellussi, G., Corono, C., Taramasso, M. and Buonomo, F., *Stud. Suf. Sci. and Catal.*, **28**, 129 (1986).

54. Kornatowski, J., Sychev, M., Goncharuk, V. and Baur, W.H., *Stud. Sur. Sci. and Catal.*, **65**, 581 (1991).

55. Nefedov, B.K., Sergeeva, N.S. and Krasnova, L.L., *Izv. Akad. Nauk* (SSSR), Ser. Khim. 614 (1977).

56. Niwa, M., Izuka, T. and Lunsford, J.H., *J. Chem. Soc. Chem. Com.*, 684 (1979).

57. Barrer, R.M., in *'Proc. of 6th International Zeolite Conference'*, (Olson, D.H. and Bisio, A., Eds.), Reno, July 10-15, 1983, Butterworth Ltd., UK, 870 (1984).

58. Goldsmith, J.R., *Min. Mag.*, **29**, 952 (1952).

59. Barrer, R.M., Baynham, J.W., Bultitude, F.W. and Meier, W.M., *J. Chem. Soc.*, 195 (1959).

60. Ward, J.W., *'Zeolites Chemistry and Catalysis'*, (Rabo, J.A., Eds.), ACS, monograph, Ch.2, **171**, 118 (1976).

61. Yashima, T., Sato, K., Hayasaka, T. and Hara, N., *J. Catal.*, **26**, 303 (1972).

62. Ono, Y., *Stud. Sur. Sci. and Catal.*, **5**, 19 (1980).

63. Barthomeuf, D., *Stud. Sur. Sci. and Catal.*, **65**, 157 (1991).

64. Weisz, P.B. and Frilette, V.S., *J. Phys. Chem.*, **64**, 382 (1960).

65. Chen,N.Y. and Degnan, T.F., *Chem. Engg. Prog.*, p.32 (Feb. 1988).

66. Miale, J.N., Chen, N.Y. and Weisz, P.B., *J. Catal.*, **6**, 278 (1966).

67. Weisz, P.B., *Stud. Sur. Sci. and Catal.* **7A**, 3 (1981).

68. Csicsery, S.M., *J. Catal.*, **23**, 124 (1971).

69. Derouane, E.G. and Gabelica, Z., *J. Catal.*, **65**, 486 (1980).

70. Frilette, V.J., Haag, W.O. and Lego, R.M., *J. Catal.*, **67**, 218 (1981).

71. Martens, J.A. Tielen, M., Jacobs, P.A. and Weitkamp, J., *Zeolites*, **4**, 98 (1984).

72. Weitkamp, J., Ernst, S., and Karge, H.G., *Erdol Kohle-Erdgas-Petrochem.*, **37**, 457 (1984).

73. Dewing, J.J., *J. Mol. Catal.*, **61**, 173 (1990).

74. Weitkamp, J., Ernst, S., Jacobs, P.A. and Karge, H.G., *Erdol Khole-Erdgas-Petrochem.*, **39**, 33 (1984).

75. von Ballmoos, R., *'Collection of simulated XRD powder patterns for zeolites'*, Butterworths, London (1984).

76. Ref. No.41, p.83 (1989).

77. Bibby, D.M., Aldridge, L.P. and Milestone, N.B., *J. Catal.*, **72**, 373 (1971).

78. Meyers, B.L., Ely, S.R., Kutz, N.A., Kaduk, J.A. and Bossche, E.V., *J. Catal.*, **91**, 352 (1985).

79. Rudolf, P.R., Saldarriaga, M.C. and Clearfield, A., *J. Phys. Chem.*, **90**, 6122 (1986).

80. Baerlochev, Ch., *Zeolites*, **6**, 325 (1983).

81. Flanigen, E.M., *'Zeolite Chemistry and Catalysis'*, ACS monograph (Rabo, J.A., Eds.), **171**, 80 (1976).

82. Ward, J.W., *'Zeolite Chemistry and Catalysis'*, ACS monograph (Rabo, J.A., Eds.), **171**, 118 (1976).

83. Maroni, V.A., Martin, K.A. and Johnson, S.A., *ACS Symp. Ser.*, **368**, 85 (1988).

84. Janin, A., Lavalley, J.C., Macedo, A. and Raatz, F., *ACS Symp. Ser.*, **368**, 117 (1988).

85. Baker, M.D., Godber, J. and Ozin, G.A., *ACS Symp. Ser.*, **368**, 136 (1988).

86. Flanigen, E.M., Khatami, H. and Szymanski, H.A., *Adv. Chem. Ser.*, **101**, 201 (1971).

87. Kutz, N., *Heterogeneous Catalysis-II*, (Sharpiro, B.L., Eds.), p.121 (1984).

88. Szostak, R. and Thomas, T.L., *J. Catal.*, **101**, 549 (1986).

89. Szostak, R. and Thomas, T.L., *J. Chem. Soc. Chem. Com.*, 113 (1986).

90. Jacobs, P.A., *'Carbaniogenic Activity of Zeolites'*, Elsvier, Amsterdam, p.39 (1977).

91. Jacobs, P.A. and von Ballmoos, *J. Phys. Chem.*, **86**, 3050 (1982).

92. Lippmaa, E., Magi, M., Samoson, A., Engelhardt, G. and grimmer, A.-R., *J. Am. Chem. Soc.*, **102**, 4889 (1980).

93. Nagy, J.B. and Derouane, E.G., *ACS Symp. Ser.*, **368**, 2 (1988).

94. Lippmaa, E., Magi, M., Samoson, A., Tarmak, M. and Engelhardt, G., *J. Am. Chem. Soc.*, **103**, 4992 (1981).

95. Fyfe, C.A., Gobbi, G.C., Klinowski, J., Thomas, J.M. and Ramdas, S., *Nature*, **296**, 530 (1982).

96. Fyfe, C.A., Gobbi, G.C., Klinowski, J. and Thomas, J.M., *J. Phys. Chem.*, **86**, 1247 (1982).

97. Engelhardt, G., Lohose, U., Lippmaa, E., Tarmak, M. and Magi, M., *Z. Anorg. Allg. Chem.*, **482**, 49 (1981).

98. Mastikhin, V.M. and Zamaraev, K.I., *Z. Phys. Chemie*, **152**, 332 (1987).

99. Muller, D., Gessnev, W., Behrens, H.J. and Schelev, G., *Chem. Phys. Lett.*, **79**, 59 (1981).

100. Thomas, J.M., Fyfe, C.A., Ramdas, S., Klinowski, J. and Gobbi, G.C., *J. Phys. Chem.*, **86**, 3061 (1982).

101. Ramdas, S. and Klinowski, J., *Nature*, **308**, 521 (1984).

102. Brunner, E., Ernst, H., Freude, D., Hunger, M., Krause, C.B., Preger, D., Reschetilowski, W., Schwieger, W. and Berg, K.H., *Zeolites*, **9**, 282 (1989).

103. Freide. D., Hunger, M. and Pfeifer, H., *Z. Phys. Chemie*, **152**, 429 (1987).

104. Scholle, K.F.M.G.J., veeman, W.S., Post, J.G., and von Hoof, *Zeolites*, **3**, 214 (1983).

105. Barrer, R.M. and Ibbitson, D.A., *Trans. Faraday Soc.*, **40**, 206 (1944).

106. Barrer, R.M. and Breck, D.W., *Trans. Faraday Soc.*, **59**, 2569 (1963).

107. Barrer, R.M., *Proc. Roy. Soc.*, **A 167**, 392 (1938).

108. Anderson, J.R., Foger, K., Mole, T., Rajyadhyaksha, R.A. and Senders, J.V., *J. Catal.*, **58**, 114 (1979).

109. Flanigen, E.M., Bennett, J.M., Grose, R.W., Cohen, J.P., Patton, R.L., Kirchner, R.M. and Smith, J.V., *Nature*, **271**, 512 (1978).

110. Olson, D.H., Haag, W.O. and Lago, R.M., *J. Catal.*, **61**, 390 (1980).

111. Barrer, R.M., *Adv. Chem. Ser.*, **102**, 41 (1971).

112. Weisz, P.B., Frilette, V.J., Maatman, R.W. and Mower, E.B., *J. Catal.*, **1**, 307 (1962).

113. Chen, N.Y. and Degnan, J.F., *Chem. Engg. Prog.*, **84(2)**, 32 (1988).

114. Weisz, P.B., *Pure. Appl. Chem.*, **52**, 2091 (1980).

115. Chen,N.Y. and Garwood, W.E., *Catal. Rev. Sci. Engg.*, **28**, 185 (1986).

116. Chen, N.Y., Mazink, J., Schwartz, A.B. and Weisz, P.B., *Oil Gas J.*, **66**, 154 (1968).

117. Garwood, W.E., *ACS Symp. Ser.*, **218**, 383 (1983).

118. Smith, K.W., Star, W.C. and Chen, N.Y., *Oil Gas J.*, **78**, 75 (1980).

119. Meisel, S.C., McCullough, J.P., Lechthaler, C.J. and Weisz, P.B., *Chemtech*, **6**, 86 (1976).

120. Chester, A.W. and Tung, F., US Pat. 4,350,835 (1982).

121. Haag, W.O., in *'Proc. of the 6th Intl. Zeolite Conference'* (Olson, D.H. and Bisio, A., Eds.), NV 1983, Butterworth, Guildford p.466 (1984).

122. Dwyer, F.G., Lewis, P.J. and Schneider, F.M., *Chem. Eng.*, **83**, 90 (1976).

123. Kaeding, W.W., Chu, C., Young, L.B. and Butter, S.A., *J. Catal.* **69**, 392 (1981).

124. Parker, D.G., *Appl. Catal.*, **9**, 53 (1984).

125. Thielen, M., Geelen, M. and Jacobs, P.A., in *'Proc. ZEOCAT Symp.'*, Siofok (Hungary) p.1 (1985).

126. Hölderich, W., Hesse, M. and Näumann, F., *Angew. Chemie*, **27(2)**, 226 (1988).

127. van Bekkum, H. and Kouwenhoven, H.W., *Recl. Trav. Chim*, Pays-Bas **108**, 283 (1989).

128. Burress, G.T., Eur. Pat. Appl. 12,514 (1980).

129. Eichler, K., Lenpoid, E., DBP 3,334,084 (1985).

130. Chiche, B., Finiels, A., Gauthier, C., Geneste, P., Graille, J., Pioch, D., *J. Org. Che.*, **51**, 2128 (1986).

131. Huizinga, T., Scholten, J.J.F., Wortel, T.M. and van Bekkum, H., *Tet. Lett.*, **21**, 3809 (1980).

132. Battes, H., Leupoid, E., DBP 3,345,808 (1985).

133. Solinas, V., Monaci, R., Marongiu, B. and Forni, L., *Appl. Catal.*, **9**, 109 (1984).

134. Eposito, A., Taramasso, M., Neri, C., Buonomo, F., Br. Pat. 2,116,974 (1985).

135. Eposito, A., Neri, C. and Buonomo, F., US Pat. 4.480,135 (1984).

136. Minachev, Kh.M., Nefedov, O.M., Kharlamov, V.V., Panov, S.Y. and Politanskii, S.F., *Izv. Akad. Nauk SSSR Ser. Khim.*, 1490 (1981).

137. Ref. 125, p.609.

138. Weissermel, K. and Arpe, H.-J., *Industrialle Organische Chemie. Verlag Chemie*, Weinheim p.108 (1978).

139. Chang, C.D. and Lang, W.H., US Pat. 4,220 783 91979).

140. Treacy, M.M.J. and Newsam, J.M., *Nature*, **332**, 249 (1988).

141. Newsam, J.M., Treacy, M.M.J., Koetsier, W.T. and de Gruyter, C.B., *Proc. R. Soc. London*, **A 420**, 375 (1988).

142. Higgins, J.B., La Pierre, R.B., Schlenker, J.L., Rohrman, A.C., Wood, J.D., Kerr, G.T. and Rohrbaugh, W.J., *Zeolites*, **8**, 446 (1988).

CHAPTER 2

SYNTHESIS AND MODIFICATION OF BETA ZEOLITES

2.1. PART-I: SYNTHESIS OF ZEOLITE BETA

2.1.1. INTRODUCTION

Zeolite beta, a high-silica zeolite, was first synthesized by Wadlinger *et.al* in 1967[1]. The SiO_2/Al_2O_3 ratio of the as-synthesized zeolite beta is in the range of 10 - 200. It is an aluminosilicate, crystallized from a gel containing alkali and TEA cations[2,3]. It crystallizes usually as an intergrowth of two[4,5] or three[6,7] polymorphs. The zeolite adsorbs equal amounts of n-hexane and cyclohexane, its pore volume being about 0.23 ml/g[1,6].

There are a number of reports[2,3,8] on the synthesis of zeolite beta under static or stirred conditions using tetraethylorthosilicate (TEOS) as a source of silica and tetraethylammonium hydroxide (TEA-OH) as an organic template in the presence of alkali (Na^+ and/or K^+) ions. TEOS could be replaced by amorphous silica[9], colloidal silica[10] and silica gel[11]. Recently, the crystallization period for the synthesis of zeolite beta was drastically brought down below 24 h., when potassium ions were used[8] in addition to sodium ions and TEA-OH.

In this chapter, factors influencing the synthesis of zeolite beta using silica sol as a source of silica and tetraethylammonium bromide (TEA-Br) as an organic template in combination with ammonium hydroxide (NH_4OH) have been investigated. The kinetic features of the crystallization process, such as temperature, alkali ion and hydroxyl ion concentration, gel dilution, etc., are also studied.

2.1.2. EXPERIMENTAL

A. Synthesis

Synthesis runs were carried out using different compositions in stainless steel autoclaves of 200 ml capacity (Fig.2.1) at autogenous pressure and at various temperatures. The crystallization was carried out hydrothermally using silica sol (28.9% SiO_2 Sycol 1230, Bombay, India), tetraethylammonium bromide (TEA-Br, 98% SRL, Bombay), sodium aluminate (43.8% Al_2O_3, 39% Na_2O), sodium hydroxide (NaOH 99% AR) and ammonium hydroxide (51% wt/wt) solutions. In a typical preparation, 15 ml. of NH_4OH was mixed slowly under stirring to a

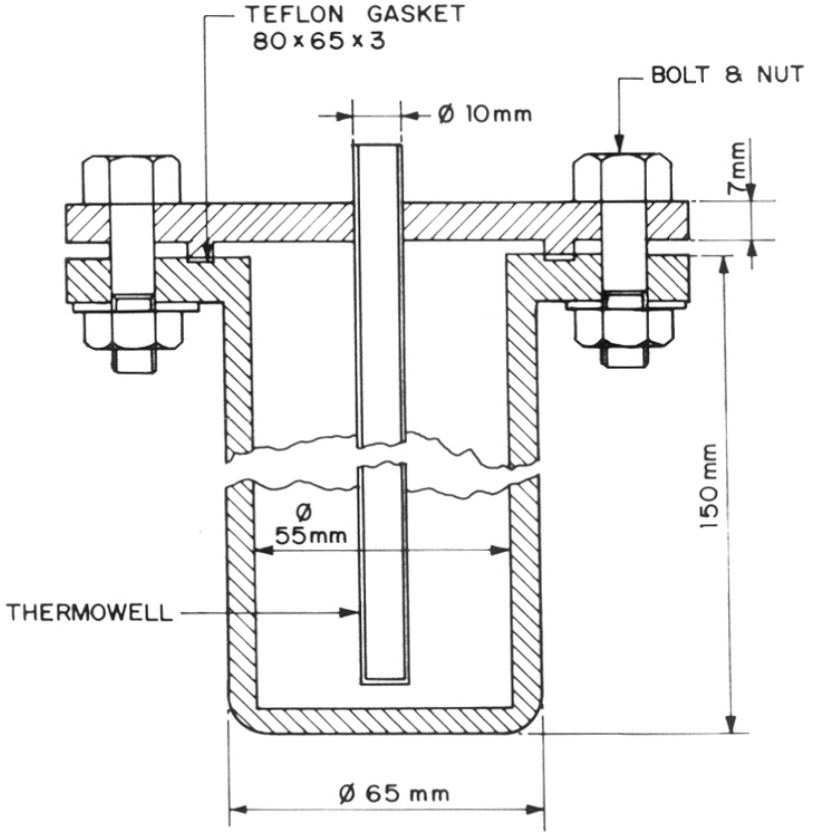

Fig.2.1: Stainless-steel autoclave with teflon gasket used for hydrothermal synthesis.

solution of 16.0 g. of TEA-Br in 20 g. of deionized water. To the above gel mixture, 1.67 g. sodium aluminate in 20 g. of deionized water with 0.9 g. of NaOH in 10 g. of deionized water was added slowly under stirring. 53.7 g. of silica sol was then added to this mixture under vigorous stirring. The resultant slurry was stirred for 1 h. to get a homogeneous gel mixture. This final gel was then transferred to a stainless steel autoclave. The molar composition of the gel was 3.1 Na_2O : 15 $(NH_4)_2O$: 5.0 $(TEA)_2O$: 35 SiO_2 : Al_2O_3 : 656 H_2O. The crystallization kinetics was studied under static conditions by comparing the extent of crystallization of the gel mixture at different intervals of time. The solid materials thus obtained were filtered, washed with deionized water and dried at 373 K for 4 h.

B.Characterization

i. X-ray diffraction

The as-synthesized zeolite samples were analyzed by X-ray powder diffraction for qualitative and quantitative phase identification. Rigaku (model D/MAX - VC, Japan) X-ray diffractometer with Ni filtered CuKα-radiations (λ = 1.5404 Å) was used for the analysis of the samples. For the quantitative phase identification and relative crystallinity, the most crystalline material obtained in the present study was used as a reference sample. The degree of crystallinity of the solid product was estimated from the formula[12].

$$\% \text{ X-ray crystallinity} = \frac{\text{peak area at } 2\theta = 22.40^{\circ} \text{ of the sample}}{\text{peak area at } 2\theta = 22.40^{\circ} \text{ of the reference sample}} \times 100$$

ii. Infrared spectroscopy

The infrared spectra of the samples were recorded in the frequency range between 400-1300 cm^{-1} on a PYE UNICAM SP 300 spectrometer using the nujol mull technique. The percent crystallinity of the samples was calculated from the area under the structure-sensitive band at 590 cm^{-1}. The extent of crystallization was estimated using the formula[12].

$$\% \text{ IR crystallinity} = \frac{\text{peak area of the band at 590 } cm^{-1} \text{ of the sample}}{\text{peak area of the band at 590 } cm^{-1} \text{ of the reference sample}} \times 100$$

iii. Thermal analysis

Simultaneous TG-DTA-DTG analysis of different crystalline samples were performed on an automatic derivatograph (SETARAM TG-DTA 92). The thermograms of the samples were recorded under the following conditions.

Weight of the sample	= 40 mg.
Heating rate	= 10 $K.min^{-1}$
Pressure	= Flowing air at atmospheric pressure

Finely powdered α - alumina was used as a reference material.

iv. Scanning electron microscopy

The morphology of zeolite beta samples was investigated using scanning electron microscopy (JEOL, JSM - 5200). The samples were mounted on a carrier made from alumina and were coated with a film of gold to prevent surface charging and to protect the zeolite material from thermal damage by the electron beam. In all the samples a uniform film thickness of about 0.1 mm was maintained.

v. Sorption measurements

The zeolite samples in the sodium form (obtained by calcining the as-synthesized form at 773 K) were also further characterized by the adsorption of different probe molecules gravimetrically, using a microbalance (model, Cahn-2000 G) connected to a vacuum/gas handling system. Prior to adsorption, the samples were outgassed in vacuum at 673 K for several hours.

2.1.3. RESULTS AND DISCUSSION

A. Kinetics of crystallization

i. Effect of temperature

The synthesis runs were carried out using equimolar mixtures of TEA-Br and NH_4OH as a templating agent. Zeolite beta was crystallized using silica sol as a source of silicon having the gel composition in terms of moles of oxides as 3.1 Na_2O : 15 $(NH_4)_2O$: 5.0 $(TEA)_2O$: 35 SiO_2 : Al_2O_3 : 656 H_2O.

The kinetics of crystallization of zeolite beta was investigated in the temperature range of 373 - 413 K by comparing the extent of crystallization of the gel-mixture at different intervals of crystallization time. The extent of crystallization is conventionally evaluated[13] either by sorption of water vapour/nitrogen[14] at fixed relative pressure on a completely dehydrated zeolite or by the ratio of sum of the areas[15] of intense XRD peaks of the sample under consideration to that of the most crystalline sample obtained during the study. The curves (Fig.2.2) for the crystallization kinetics were obtained by the following the XRD procedure, to study the effect of temperature on the formation of zeolite beta crystals. The curves in Fig.2.2, typically exhibit a sigmoidal or S-shaped nature, characteristic of a process involving two distinct stages, viz:

(a) an induction period when nuclei are formed; and

(b) a crystal growth period when nuclei grow into crystals.

The intercept made by the curve on the time axis (abscissa) is defined as the induction period (the time needed to form crystallization centres or nuclei). It is found from Fig.2.2, that the induction period is inversely proportional to the temperature. The rate of nucleation may be assumed to be proportional to the reciprocal of the induction period and hence varies directly with the crystallization temperature. The rate of crystallization increases slowly with time upto 10-15% crystallinity. Thereafter, crystallization rate increases rapidly and passes through a maximum and remains constant till 80% crystallinity is achieved. The crystallization rate then decreases till the 100% crystalline product is obtained.

Application of the Avrami-Erofeev equation

Since the curve in Fig.2.2 is almost linear between 20-80% crystallinity, the crystallization of zeolite beta was treated as a first order reaction. Therefore, the kinetics of crystallization can be described, at least in principle, by a linear relation similar to the so called Avrami-Erofeev equation[16-18] in this range. Mathematically it can be represented by $\ln [1/(1-\alpha)] = [kt]^m$, where '$\alpha$' is the degree of crystallinity at crystallization time 't', and 'm' & 'k' are Avrami-Erofeev parameters. The data in Fig.2.2 were fitted to the Avrami-Erofeev equation and the results are presented in the Fig.2.3. Excellent linearity of these plots suggests that the crystallization of zeolite beta follows the first order kinetics in accordance with the Avrami-Erofeev equation. It

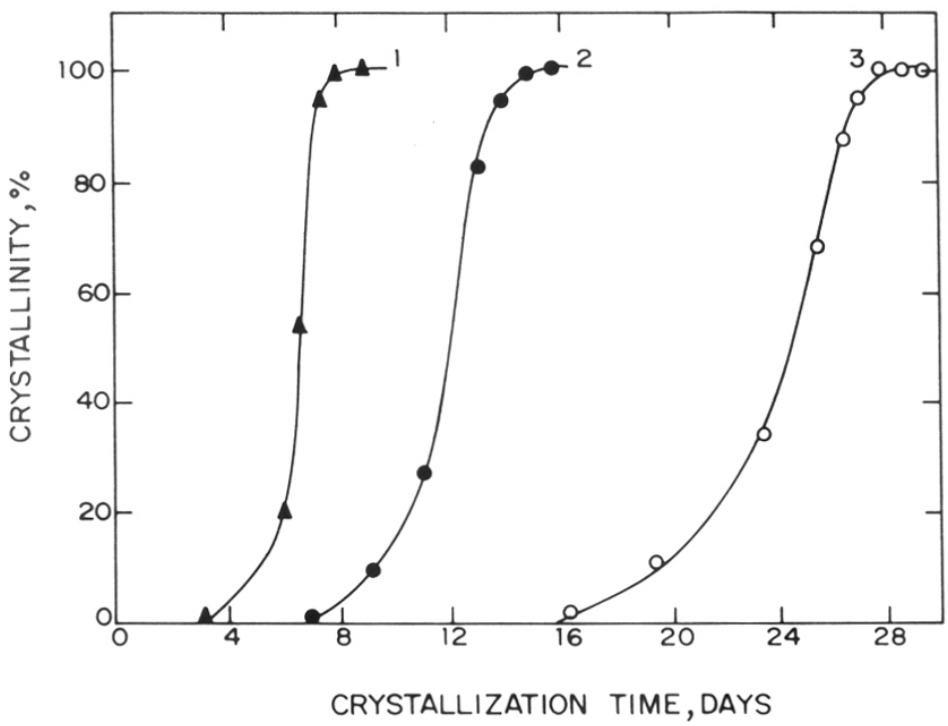

Fig.2.2: Crystallization kinetics of zeolite beta at 1) 413 K, 2) 393 K, and 3) 373 K.

has already been shown in the literature that the crystallization kinetics of many other zeolites[17,18] has been successfully described by similar kinetic equations. The Avrami-Erofeev parameters *i.e.* 'm' and 'k' are evaluated from the slope and intercept from these linear plots (shown in Fig.2.3) are tabulated in Table 2.1. The constant 'k' increases with the increase in temperature and thus indicates the increase in the rate of nucleation on increasing the synthesis temperature. The decrease in the value 'm' with the increase in temperature suggests shorter crystallization periods at higher temperatures.

Table 2.1: Avrami-Erofeev parameters for zeolite beta

Synthesis Temp. (K)	K	m
373	1.18×10^{-24}	8.63
393	2.60×10^{-21}	8.42
413	4.70×10^{-19}	8.00

Apparent activation energy for nucleation (E_n) and crystal growth (E_c)

Since the hydrothermal crystallization of zeolites, is energetically activated process; the apparent activation energy for the process of nucleation (E_n) and for the crystal growth (E_c) are evaluated[16-19] by applying Arrhenius equation. The values of E_n and E_c obtained from the slopes of the linear plots in Fig.2.4 are listed in Table 2.2 and are compared with the reported data[19]. The value of E_n (54.25 KJ/mole) is almost the twice of that reported (29.30 KJ/mole) by Li-jen Leu *et.al*[19]. This may be because they have used TEA-OH as a template whereas in the present study we have used TEA-Br as a template. Since the hydrothermal crystallization of zeolite beta follows a liquid phase transformation mechanism[2,3], the process of nucleation may be easier from the gel containing TEA-OH than that with TEA-Br medium, because of the higher solubility of silicate species in hydroxide than in the bromide salt. In contrast to the trend in E_n values, the E_c value (45.54 KJ/mole) in the present study is lower than that (63.64 KJ/mole) reported[19]. Once the crystallization is set, it is, probably, faster in the gel containing TEA-Br than that with TEA-OH.

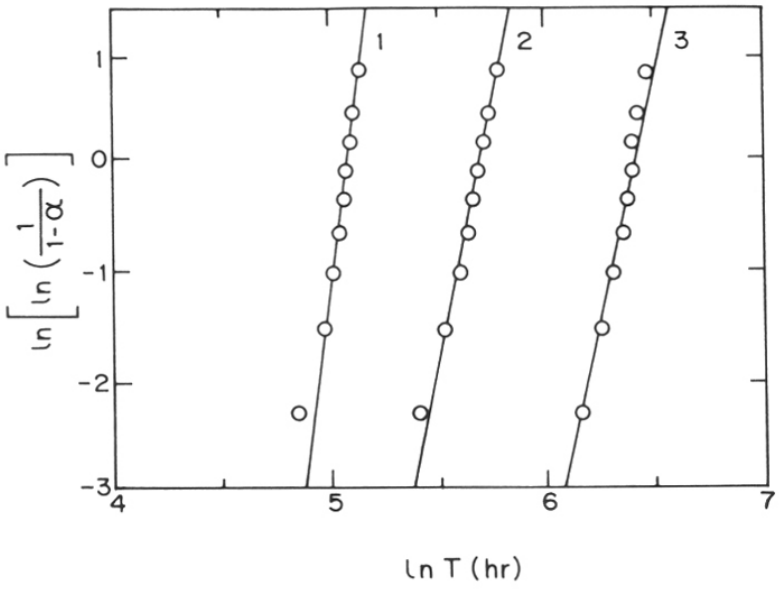

Fig.2.3: Fit of experimental data to the Avrami-Erofeev equation at 1) 413 K, 2) 393 K, and 3) 373 K.

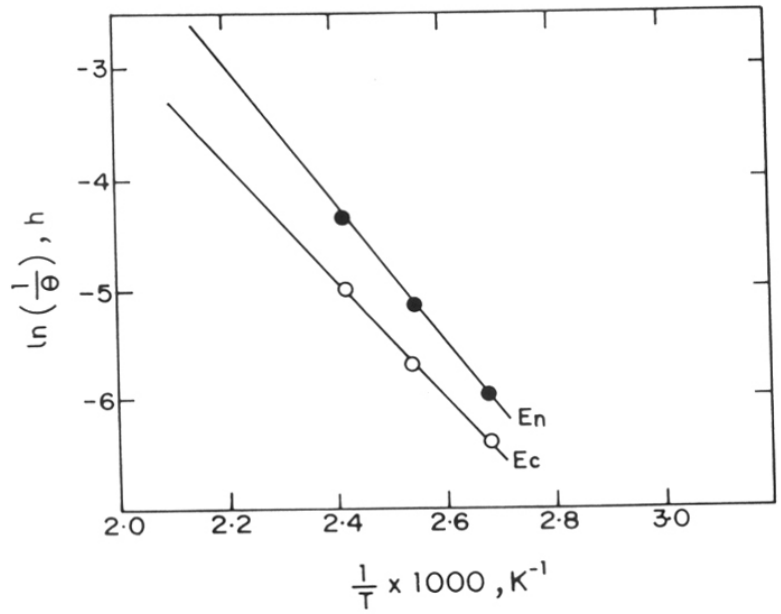

Fig.2.4: Arhenius plots for Crystallization (E_c) and Nucleation (E_n).

Table 2.2: **Activation energies for the synthesis of zeolite beta**

Template	E_n (KJ/mole)	E_c (KJ/mole)
TEA-OH[a]	29.30	63.64
TEA-Br	54.25	45.54

[a]data taken from ref. 28.

ii. Influence of template concentration

The influence of template concentration on the crystallization time is shown in Fig.2.5. At the higher concentration of TEA-Br, the rates of nucleation and crystallization are enhanced. Both the synthesis temperature and the TEA-Br concentration influence the phase purity of zeolite beta. The results are summarized in Table 2.3. At higher concentration of template ($TEA\text{-}Br/SiO_2 = 0.25 - 0.40$), pure zeolite beta with 100 % crystallinity was obtained at 413 K. At 443 K, the concentration of beta in the product decreased to 50 %, the balance being ZSM-12. Below a certain concentration of TEA-Br ($TEA\text{-}Br/SiO_2 < 0.167$), fully crystalline zeolite was not obtained at 413 K. At the lower concentrations of TEA-Br ($TEA\text{-}Br/SiO_2 = 0.1$), the product contained only traces of beta with 30% ZSM-5 and 70 % of ZSM-12. This clearly suggests that the ratio of $TEA\text{-}Br/SiO_2 = 0.25$ is probably the lowest limit for the crystallization of pure zeolite beta.

iii. The effect of gel alkalinity (pH)

The pH was varied by changing the concentration of ammonium hydroxide in the gel. The effect of the alkalinity in the synthesis of zeolite beta is shown in Fig.2.6. At the lower $OH^-/SiO_2 = 0.6$ (curve 3), the rate of crystallization is very low because the hydroxyl ion concentration is not enough to solubilize silicate and aluminate species. At $OH^-/SiO_2 = 1.0$ (curve 2), the induction period was shortened and zeolite beta with 100 % crystallinity was obtained. However, as the alkalinity is increased further to $OH^-/SiO_2 = 1.5$ (curve 1), the rate of crystallization decreases. The excess OH^- ions probably dissolve the nuclei already formed and thereby retard the crystallization rate. This clearly shows that the existance of OH^- ion concentration at

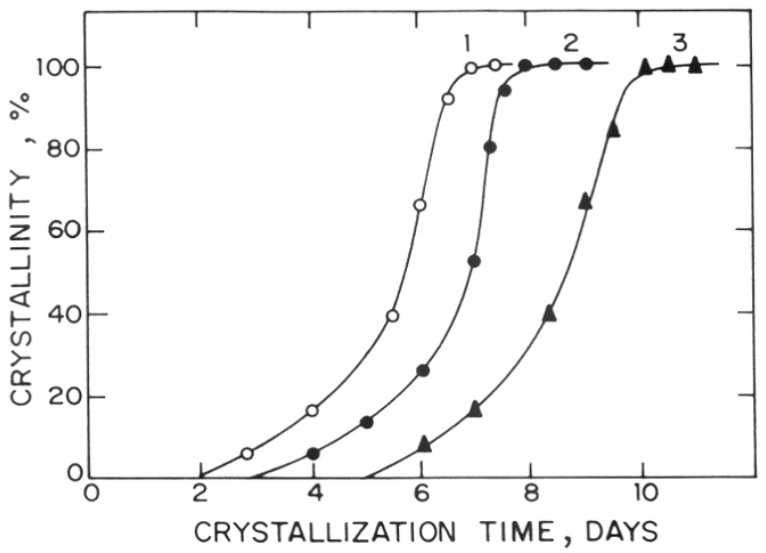

Fig.2.5: The influence of TEA-Br/SiO_2 ratio on the crystallization kinetics of zeolite beta: 1) 0.50, 2) 0.30, and 3) 0.25. SiO_2/Al_2O_3 = 35, OH^-/SiO_2 = 1.0 and H_2O/SiO_2 = 19.

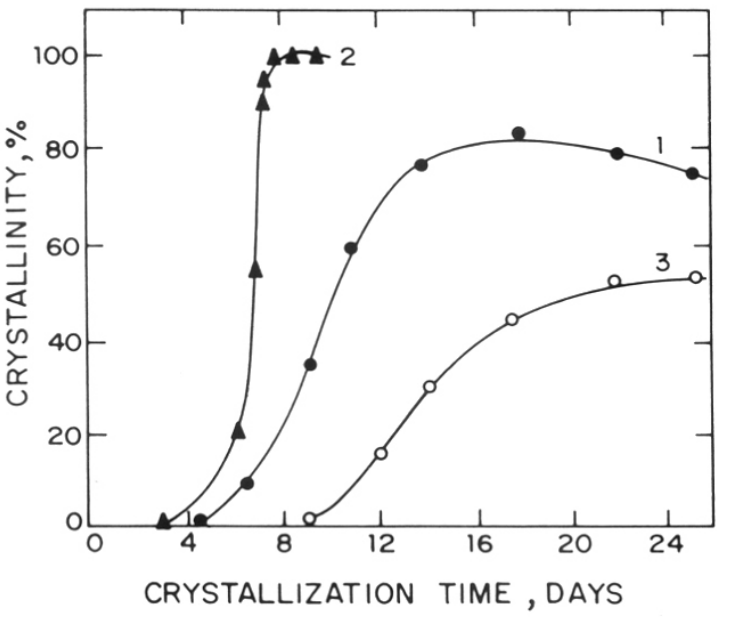

Fig.2.6: The influence of OH^-/SiO_2 ratio on the crystallization kinetics of zeolite beta: 1) 1.5, 2) 1.0, and 3) 0.6. SiO_2/Al_2O_3 = 35, TEA-Br/SiO_2 = 0.30 and H_2O/SiO_2 = 19.

the optimum levels is needed, which is sufficient to depolymerize the source of silica and to initiate the nucleation process but not enough to dissolve the zeolite nuclei and retard the crystallization.

Table 2.3: **Effect of template concentration on the nature of crystalline phases obtained in 8 days from the oxide mole composition**: 3.1 Na_2O: 15$(NH_4)_2O$: x TEA-Br: 35 SiO_2: Al_2O_3: 656 H_2O.

TEA-Br/SiO_2	Crystalline phases obtained at temperature	
	413 K	433 K
0.50	100 % beta	75 % beta + 25 % ZSM-12
0.40	100 % beta	70 % beta + 30 % ZSM-12
0.30	100 % beta	60 % beta + 40 % ZSM-12
0.25	95 % beta + 5 % ZSM-12	50 % beta + 50 % ZSM-12
0.17	95 % beta + 5 % ZSM-12	10 % beta + 90 % ZSM-12
0.10	partly crystalline beta	30 % ZSM-5 + 70 % ZSM-12

iv. The effect of Na+ ion concentration

For the formation of zeolite beta, alkali metal ions are found to be essential[2,3,8]. Attempts made to synthesize the zeolite beta in the absence of alkali metal (Na^+) ion, were not successful. Both the alkali and the TEA^+ ions are found to be required for the crystallization of zeolite beta. In order to optimize the balance between the Na^+ and SiO_2 needed to crystalize zeolite beta, experiments were carried out by adding calculated amount of NaCl to the gel system while keeping the OH^-/SiO_2 ratio constant. The results obtained are shown in Fig.2.7. At higher concentration of Na_2O (Na_2O/SiO_2 = 0.12, curve 2), the induction period was prolonged. The rate of crystallization, however was not affected. Gels having the Na^+ concentration higher than Na_2O/SiO_2 = 0.12, yielded zeolite beta within 13 days of crystallization. It then got transformed to ZSM-5 and mordenite as the crystallization time was increased further. Na_2O/SiO_2 ratio at 0.08 (curve 1) yielded pure zeolite beta within 8 days at 413 K.

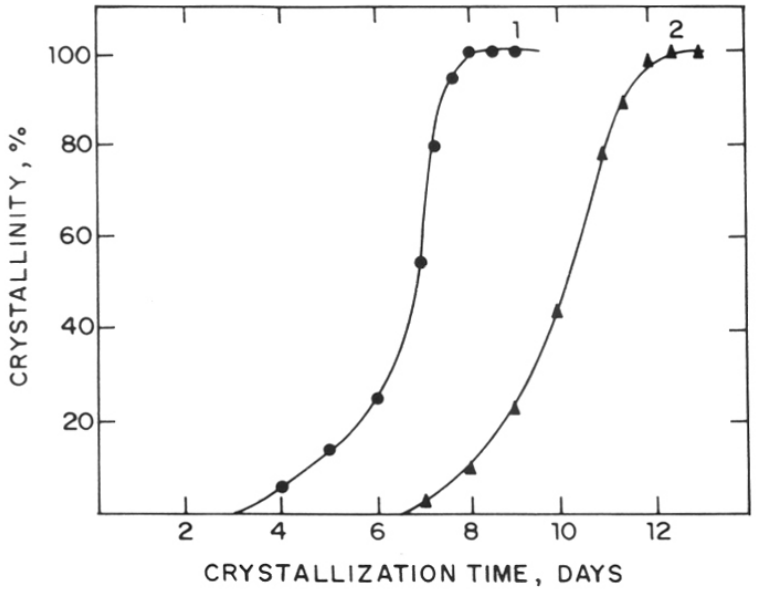

Fig.2.7: The effect of Na_2O/SiO_2 ratio on the crystallization of zeolite beta: 1) 0.08, and 2) 0.12. $SiO_2/Al_2O_3 = 35$, TEA-Br/SiO_2 = 0.30, OH^-/SiO_2 = 1.0 and H_2O/SiO_2 = 19.

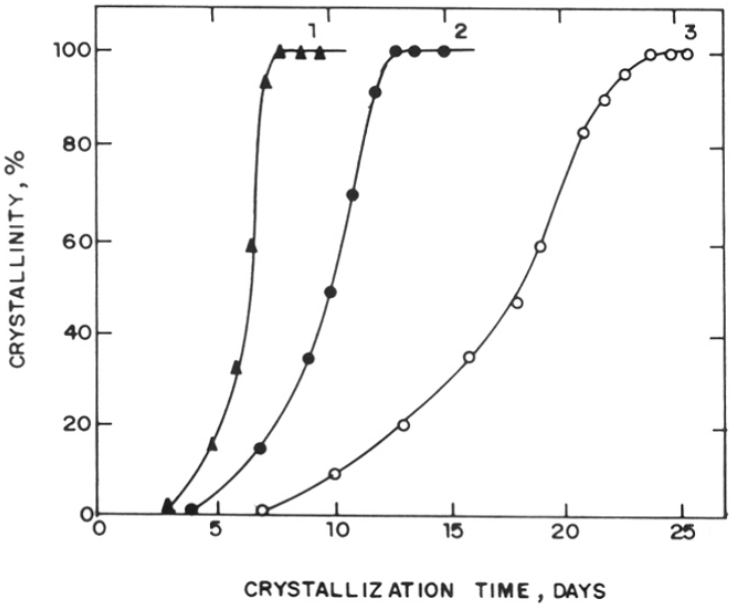

Fig.2.8: The influence of H_2O/SiO_2 ratio on the crystallization kinetics of zeolite beta: 1) 19, 2) 35, and 3) 55. $SiO_2/Al_2O_3 = 35$, OH^-/SiO_2 = 1.0 and TEA-Br^+/SiO_2 = 0.30.

v. The effect of gel dilution (H_2O/SiO_2 ratio)

The influence of water concentration in the gel is shown in Fig.2.8. The gel dilution affects the rate of nucleation only marginally but affects the rate of crystallization appreciably. The crystallization rate was found to be enhanced in the more concentrated systems (curve 1). When H_2O/SiO_2 ratio was increased from 19 to 35 (curve 2), the nucleation and crystallization periods were enhanced from 3 to 4 days and from 8 to 13 days, respectively. On further increasing H_2O/SiO_2 ratio upto 55 (curve 3), the nucleation period was 7 days. It took almost 24 days to get fully crystalline zeolite beta. For H_2O/SiO_2 ratio lower than 19, the water content was found to be too low to get homogeneous gel and hence no crystallization was tried. The faster rates of crystallization in concentrated systems and the larger crystal sizes obtained from dilute solution are common in zeolite synthesis[20]. Scanning electron micrographs of zeolite beta crystals synthesized at different dilution levels are shown in Fig.2.9. Crystals obtained from dilute systems (H_2O/SiO_2 = 55); were some what larger (0.5-0.7 μm) than those obtained from the concentrated systems (H_2O/SiO_2 = 19; 0.3 - 0.5 μm). However, there is no change in the cuboid crystal shape, at different dilution levels.

vi. The effect of gel SiO_2/Al_2O_3 ratio

Fig.2.10 illustrates the influence of SiO_2/Al_2O_3 ratio on the crystallization kinetics of zeolite beta. As the concentration of Al_2O_3 was increased in the gel, the nucleation and crystallization time was marginally increased. It may be noted that, as the aluminium concentration in the gel increases, the incorporation of the silicon into the zeolite framework is more efficient, resulting in a higher yield of solid zeolite beta[3]. Ghamami and Sand[21] also observed the higher crystallization period for lower SiO_2/Al_2O_3 ratios in the ZSM-5 system. These results have been explained by the observation that a higher concentration of aluminate species in the gel **blocks** a larger amount of silica monomers which are needed for nucleation.

Table 2.4 shows some of the solid phases obtained during the synthesis of zeolite beta upon changing the SiO_2/Al_2O_3 ratio and the synthesis temperature. It indicates that pure zeolite beta is obtained between SiO_2/Al_2O_3 = 15-55 at 413 K. On raising the crystallization temperatures above 433 K, zeolites like ZSM-12 and/or ZSM-5 were obtained as an impurity. When the

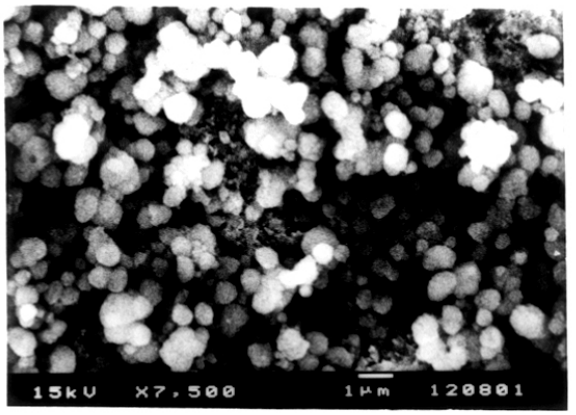

A

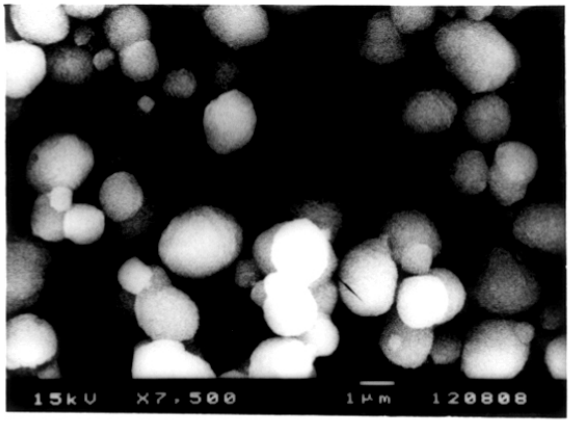

B

Fig.2.9: SEM photographs of zeolite beta: SiO_2/Al_2O_3 = 35, OH^-/SiO_2 = 1.0, TEA-Br/SiO_2 = 0.30 and H_2O/SiO_2 ratio of A) 19, and B) 55.

SiO_2/Al_2O_3 ratio was decreased below 15, increasing concentration of analcime phase was obtained along with the formation of zeolite beta. The gel SiO_2/Al_2O_3 ratio in the range of 15-55 always yielded pure zeolite beta at 413 K. On increasing SiO_2/Al_2O_3 (>100) at 413 K the phase obtained was pure zeolite ZSM-12 instead of beta. When temperature was raised to 433 K with gel SiO_2/Al_2O_3 = 60, zeolite ZSM-12 with impurity of beta and ZSM-5 was obtained.

Table 2.4: Nature of the crytalline phases formed with various SiO_2/Al_2O_3 ratios and temperatures within 8 d.

SiO_2/Al_2O_3	Solid phase	Temp. (K)
6	95 % Analcime + 5 % beta	413
10	30 % Analcime + 70 % beta	413
20	100 % beta	413
35	100 % beta	413
55	100 % beta	413
60	95 % beta + 5 % ZSM-12	413
	50 % beta + 50 % ZSM-12	443
>100	100 % ZSM-12	413

vii. The influence of the nature of the aluminium source

In the present studies sodium aluminate, aluminium sulphate.16 H_2O and aluminium isopropoxide were used as sources of aluminium in the synthesis of zeolite beta. Sodium aluminate proved to be the most reactive aluminium source for the synthesis of zeolite beta with 99 % synthesis yield. It is probable that the basic nature of sodium aluminate may favour the crystallization with the increase in the synthesis yield, compared to other sources of aluminium.

viii. The effect of the nature of organic template

In the kinetics and crystallization of zeolite beta the nature of the organic template also plays an important role. The effect of the template is shown in Fig.2.11. The nucleation was found to be faster with tetraethylammonium hydroxide compared to that with tetraethylammonium bromide; however there is hardly any change in the rate of crystallization. The optimized ratio of OH^-/TEA-Br = 3-6; could be achieved by the addition of either NaOH or NH_4OH. When

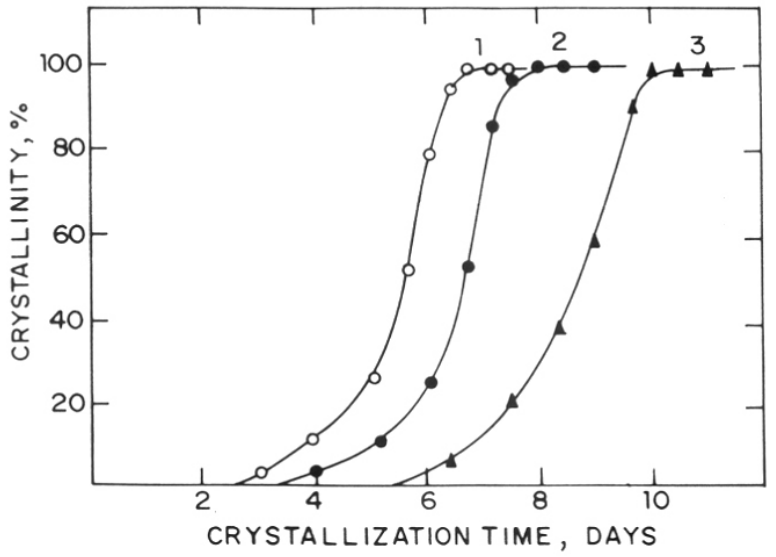

Fig.2.10: The effect of SiO_2/Al_2O_3 ratio on the crystallization kinectics of zeolite beta: 1) 58, 2) 35, and 3) 20. TEA-Br/SiO_2 = 0.30, OH^-/SiO_2 = 1.0 and H_2O/SiO_2 = 19.

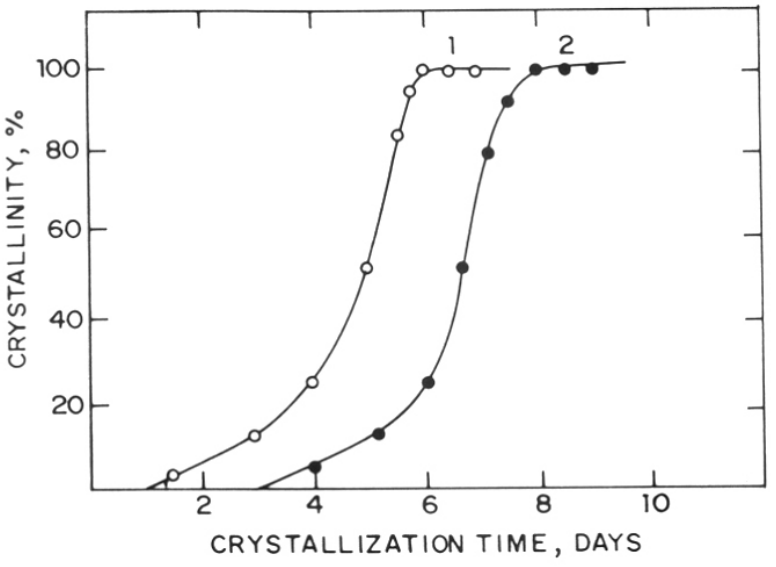

Fig.2.11: Influence of nature of template on the crystallization kinetics of zeolite beta: 1) TEA-OH, and 2) TEA-Br. SiO_2/Al_2O_3 = 35, TEA^+/SiO_2 = 0.30, OH^-/SiO_2 = 1.0 and H_2O/SiO_2 = 19.

NaOH is used to maintain the OH^- ion concentration in the gel, the level of Na^+ ion in the gel increases beyond the optimized concentration of Na^+ ions; and it inhibits the formation of zeolite beta. Therefore, the addition of ammonium hydroxide was essential in order to maintain the OH^- ion as well as Na^+ ion concentrations in the gel.

ix. Reactivity of the source of silica

The reactivity of the source of silica plays a vital role in the synthesis of the zeolites since the dissolution of the silica is the first step. Since the hydrothermal crystallization of zeolite beta follows liquid phase transformation[3], this step seems to be rate controlling. Among the silica sources (TEOS, silica gel and silica sol) used in the present study, silica sol gave a maximum synthesis yield showing its most reactive nature in the formation of zeolite beta.

B. Characterization

i. X-ray Diffraction

X-ray powder diffraction (XRD) patterns for different crystallinity of the samples of zeolite beta are presented in Fig.2.12. Curve 1 in Fig.2.12 corresponds to the XRD pattern of the product at zero time of crystallization and it shows the amorphous nature. As the period of crystallization increases, there is a progress in crystallinity with the appearance of peaks at $2\theta = 7.68°$ and 22.40° (curve 2) which are usually highly intense in the fully crystalline sample. With further increase in the crystallization period there is an advancement in the crystallinity with the increase in the peak intensity and appearance of further peaks (curve 4) especially, a characteristic shoulder peak at $2\theta = 21.42°$. Curve 6 shows the fully crystalline nature of zeolite beta with all the characteristic peaks.

ii. Framework IR

The progress in crystallization was also determined by framework i.r. spectroscopy. The results are summarized in Fig.2.13. Curve 1 in Fig.2.13 shows i.r. spectrum of the amorphous sample at zero crystallization time. It shows a weak shoulder band at 1230 cm^{-1}, a broad band at 1090 cm^{-1} and a medium weak band around 800 cm^{-1} and very weak bands at 560, 534 and 460 cm^{-1}. Similar i.r. spectrum has also been reported by Jacobs and co-workers[2]. As the

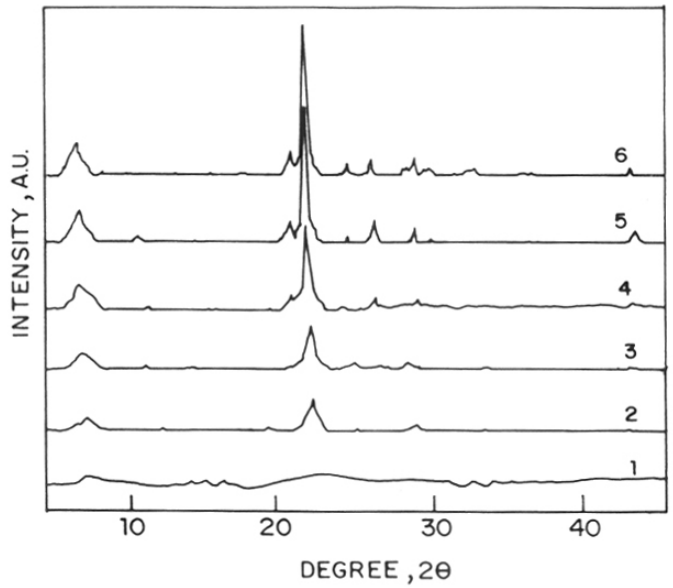

Fig.2.12: XRD patterns of beta zeolite, synthesis time in days: 1) 0, 2) 3, 3) 5, 4) 6, 5) 7, and 6) 8.

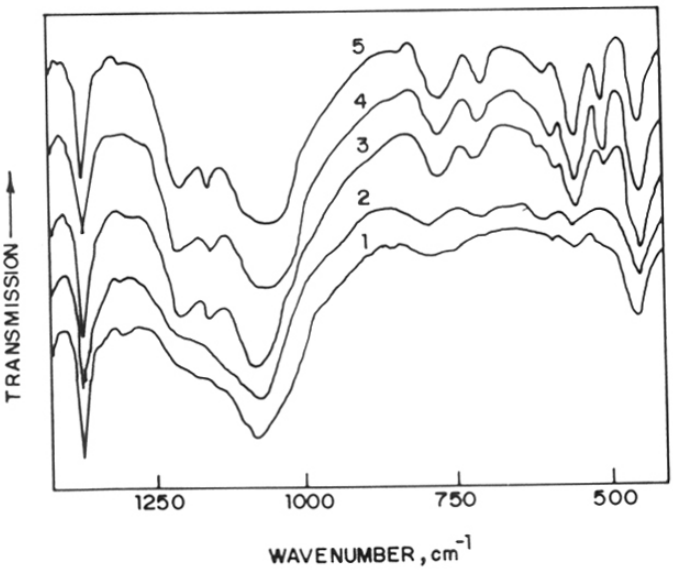

Fig.2.13: Framework i.r. spectra of beta zeolite, synthesis time in days: 1) 0, 2) 3, 3) 5, 4) 7, and 5) 8.

crystallization progresses, the weak shoulder around 1230 cm^{-1} develops into a medium strong band with lowering of its frequency to 1214 cm^{-1}. Similarly a broad structure sensitive band due to external tetrahedral (Si-, Al-) linkages, is shifted to a lower wave number from 1088 to 1066 cm^{-1}. A salient feature of Fig.2.13 is the emergence of a small but sharp band at 1171 cm^{-1} with an increase in the crystallinity of zeolite beta. Also, the weak band around 800 cm^{-1} developes into a small, sharp band at 780 cm^{-1}. The framework i.r. spectrum of 100 % crystalline beta sample (curve 5) is in close agreement with that reported by Jacobs and co-workers[2].

The peak at 590 cm^{-1} exhibits a direct correlation with XRD crystallinity (Fig.2.14). In this figure, the % i.r. crystallinity is calculated from the ratio of the area of the peak at 590 cm^{-1} in the sample to that in the most crystalline sample in this study. The lower value of crystallinity obtained by XRD compared to the relative crystallinity obtained by i.r. is attributed to its inability to "see" the crystallites smaller than about 8 nm[12]. Further, the linear correlation between the crystallinities is also in accordance with the above statement. In a recent study, Jacobs *et.al*[12] showed that although the XRD pattern of the sample was characteristic of an amorphous material, the i.r. spectra show the material to be a ZSM-5 zeolite with crystallite size less than 8 nm.

iii. Thermal analysis (DTA/TG)

The weight and energy loss during the thermal decomposition of the as-synthesized fully crystalline sample is shown in Fig.2.15. An endothermic zone of weight loss at 373 K and three distinct zones of exothermic weight losses are seen in the d.t.a/t.g curves with the peak maxima at 623, 713 and 883 K respectively. Perez-Pariente *et.al*[2] reported three exothermic weight losses at 493-623, 623-773 and 773-973 K, respectively, during the decomposition of TEA-beta zeolites. The endothermic peak at 373 K is due to the physically sorbed water. The exothermic weight loss at 623 K was due to the decomposition of physically occluded TEA-Br. Other two exothermic weight losses at 713 and 883 K were ascribed by them to pyrolysis/oxidative decomposition of occluded TEA-Br and charge balancing TEA^+ cations respectively.

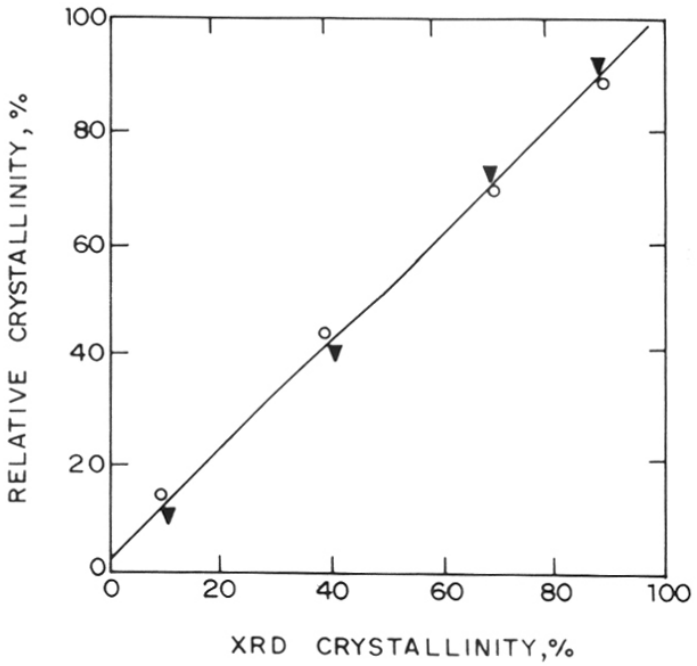

Fig.2.14: Correlation between XRD crystallinity and relative crystallinity estimated from i.r. spectroscopy ( ) and adsorption of *n*-hexane (o).

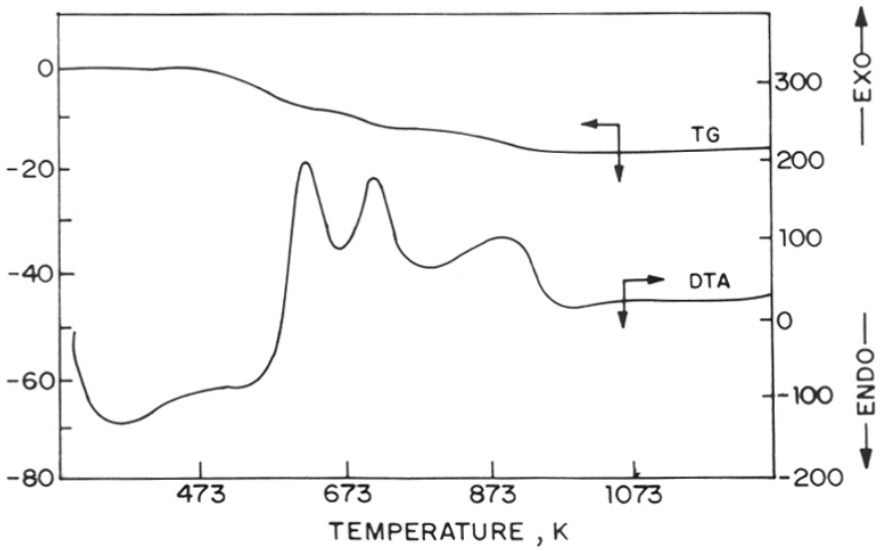

Fig.2.15: Thermo-analytical curves (DTA & TG) of 100 % crystalline zeolite beta.

iv. Adsorption measurements

The crystallization kinetics was also monitored by the adsorption of different probe molecules in the sodium form (calcined at 753 K) of the samples with varying degrees of crystallinity and the results are summarized in Table 2.5. It is seen from Table 2.5 that there is a concurrence between the %crystallinity and the equilibrium sorption. A direct correlation between the XRD crystallinity and the relative crystallinity determined from the amount of n-hexane adsorbed is also shown in Fig.2.14. In this figure, the amount of n-hexane adsorbed by the reference sample was assigned the value of 100 % crystallinity. The average pore volumes (assuming liquid density) for the adsorbates of 100 % crystalline sample matched well with those reported in the literature[1,3]. The results in Table 2.5 confirm the large pore nature (12 MR opening) of zeolite beta.

Table 2.5: Adsorption in beta zeolites[a]

Adsorbate	XRD crystallinity of sample (%)				
	19	41	58	82	100
n-hexane	6.8	8.2	11.2	14.8	16.1
water	9.2	12.9	13.8	16.2	19.2
benzene	5.2	8.3	14.8	17.1	18.9
cyclohexane	6.5	7.9	10.8	15.1	16.4

[a]Temp. = 298 K; $P/P_o = 0.5$

v. Scanning electron microscopy

The scanning electron micrograph of zeolite beta samples showed in Fig.2.9, indicates the absence of any amorphous material and also other crystalline phase impurities. The crystals of 0.5 - 0.7 μm had a uniform crystal size of cuboid shape. The crystal size varies slightly with varying crystallization temperature and also the gel/product SiO_2/Al_2O_3 ratio. The crystalline habit of nearly spherical crystallites however, does not seem to be much affected by the change in these parameters.

2.2. PART-II: MODIFICATION OF ZEOLITE BETA

2.2.1. INTRODUCTION

One of the emerging trends in the area of zeolite catalysis is the isomorphous substitution of Al^{3+} or Si^{4+} by different bivalent (Be), trivalent (B, Ga, Fe and Cr) and pentavalent (P) elements in the framework position and their application in various catalytic reactions[21]. Since the latter ions possess values of charge/radius ratios different from those of Al^{3+}, the intrinsic acidic strength of their associated protons and hence, their catalytic activity/selectivity may vary on such isomorphous substitution[22,23].

Isomorphous substitution of B for Al in pentasil zeolite framework has already been reported[24]. A detailed synthesis of borosilicate analog of NU-1 also has been reported recently[25]. The isomorphous substitution of Ga in to NU-1[25], ZSM-5[26] and faujasite[27] is also reported in the literature. The isomorphous substitution of Fe[28] and Ti[29] into the framework of zeolite beta has been achieved.

The adsorption and catalytic properties of zeolites are modified to a considerable extent by the replacement of Na^+ ions with multivalent cations[30]. The Y type zeolites exchanged with rare earth cations and further modified by the introduction of ammonium or calcium ions are widely used as catalysts in many reactions of industrial importance[31]. The surface acidity of rare earth zeolites is different from that of the parent zeolite[32].

The unique properties of zeolites, high ion exchange capability and a crystalline structure with uniform pore diameters, allow preparation of highly dispersed metals with narrow particle size distributions[33]. Since the pioneering work by Rabo *et al.*[34], noble metals on zeolites have been established as important industrial catalysts and considerable research was focussed on these systems[35]. The objective of combining the catalytic properties of transition metals with the steric constraints imposed by zeolite geometries provides strong incentive for research on active and highly selective zeolite-supported transition metal catalysts[36].

The main aim of this part is to modify the zeolite beta using various post synthesis methods viz.,

1. Isomorphous substitution
2. Cation exchange
3. Impregnation with noble metals

2.2.2. PREPARATION OF MODIFIED BETA ZEOLITES

A. Isomorphous substitution

i). Boron beta (B-beta)

Hydrothermal synthesis of a borosilicate analog of beta was carried out using silica sol (Sycol Bombay, India 28.9 % SiO_2), tetraethylammonium hydroxide (TEA-OH, Aldrich 40 %), orthoboric acid (H_3BO_3 Loba Chemie, 99.5 %) and sodium hydroxide (NaOH, AR pellets). In a typical preparation, 32 g of TEA-OH was added to 40.02 g of silica sol under vigorous stirring. To this solution a 0.92 g of H_3BO_3 in 12 g of water was slowly added. The gel was stirred about 1 h. 0.8 g of Sodium hydroxide was then dissolved in 8 g of distilled water and then added to the above gel. Stirring was continued for 1 more h. The gel was then transferred into a stainless steel autoclave and kept in an oven at 413 K for 11 days. The autoclave was then removed from the oven and quenched in the cold water. The resultant white material was filtered, washed and dried at 393 K in air for 8 h.

ii) Gallium beta (Ga-beta)

Ga-beta was synthesized hydrothermally using tetraethylorthosilicate (TEOS, 98 % Aldrich), tetraethylammonium hydroxide, 40 % Aldrich), gallium nitrate (99.9 %, Aldrich) and sodium hydroxide (AR grade). In a typical preparation 40.2 g of TEOS was added slowly under stirring to 32.2 g of TEA-OH in order to partially hydrolyse the TEOS. To the resultant clear solution, was added a solution of 3.2 g gallium nitrate in 15 g of distilled water under vigorous stirring. To the above mixture, a solution of 0.92 g of NaOH in 10 g of water was added. In order to remove the ethanol formed during the hydrolysis of TEOS, the final clear liquid reaction mixture was then stirred at 353 K for 1 h in an open vessel. It was then transferred to the stainless

steel autoclave. The crystallization was done under static conditions at 413 K for 9 days. After the crystallization was completed, the white solid material was recovered by centrifugation, washed thoroughly with deionised water and dried at 393 K in air for 8 h.

B. Cation exchange

The as-synthesized Al-beta zeolite was calcined at 733 K for 18 h in a flow of air to remove the organics and to obtain the Na-form of the zeolite. The sodium occupancy as a framework charge balancing cation was only 30 % of the total aluminium in the sample. These sodium cations were almost totally exchanged by NH_4^+, Mg^{2+}, Ca^{2+}, Sr^{2+} and La^{3+} ions by contacting the zeolite powder with 15 wt. % aqueous solutions (15 ml/g zeolite) of the nitrate salts of the respective cationic species for 4 h at 368 K. Cation exchange treatments were repeated till the residual sodium in the sample was below 200 ppm.

The B-beta and Ga-beta samples were also calcined at 733 K for 18 h in flow of dry air to remove the organics from the zeolite pores. These organic-free form of the B-beta and Ga-beta zeolite were then ion exchanged with a 15 wt.% solution of ammonium nitrate to get NH_4-B-beta and NH_4-Ga-beta zeolites. The catalytically active form of the zeolites were obtained by calcining the NH_4- form of the zeolites at 733 K for 10 h in a flow of dry air.

C. Impregnation with noble metals.

The NH_4-forms of zeolite beta was used to impregnate the noble metals. The catalysts, Pt/H-beta, containing 0.05-1.0 wt.% platinum were prepared by impregnating the ammonium-beta zeolites with a calculated amount of aqueous $Pt(NH_3)_4Cl_2$ solution. The impregnated catalysts were then dried and calcined in air at 673 K for 3 h. The catalysts, Pt/H-mordenite and Pt/H-ZSM-12, containing 0.3 wt.% platinum were also prepared for the comparison of catalytic activities. Mordenite[37] and ZSM-12[38] were prepared according to the procedures described in the literature.

2.3. CONCLUSIONS

The synthesis of zeolite beta using silica sol and tetraethylammonium bromide has been clearly described. The influence of various synthesis parameters such as nature of silica source, the nature of the organic template, crystallization temperature and time, SiO_2/Al_2O_3, gel alkalinity, gel dilution and alkali metal has been discussed. Zeolite beta could be crystallized at a temperature range from 373-433 K within 6-13 days using TEA-Br and NH_4OH as a template with SiO_2/Al_2O_3 = 15-55, H_2O/SiO_2 = 19 and TEA-Br/SiO_2 = 0.25-0.50. The crystallization process followed the first order kinetic equation. The apparent activation energy for nucleation and crystallization were estimated to be 54.25 and 45.54 KJ, mol^{-1}, respectively.

An increase in crystallization temperature and gel SiO_2/Al_2O_3 ratio favours the formation of zeolite ZSM-12 instead of zeolite beta. Sodium ion concentrations higher than the optimum leads to the formation of zeolite ZSM-5. Gel dilution was found to retard both the rate of nucleation and crystallization. The synthesis efficiency of zeolite beta was found to be almost 100 % when silica sol and sodium aluminate were used as the sources of silica and alumina, respectively.

The synthesis of boron beta (B-beta) and gallium beta (Ga-beta) have been carried out using Al-free source of silicon and, hydroboric acid as a source of boron and gallium nitrate as a source of gallium, respectively.

2.4. REFERENCES

1. Wadlinger, R.L., Kerr, G.T. and Rosinski, E.J., US Pat. 3 308 069 (1967).
2. Perez-Pariente, J., Martens, J.A. and Jacobs, P.A., *Appl. Catal.*,**31**, 35 (1987).
3. Perez-Pariente, J., Martens, J.A. and Jacobs, P.A., *Zeolites*, **8**, 46 (1988).
4. Treacy, M.M.J. and Newsam, J.M., *Nature*, **332**, 249 (1988).
5. Newsam, J.M., Treacy, M.M.J., Koetsier, W.T. and de Gruyter, C.B., *Proc. Royal Soc. Lond. A.*, **420**, 375 (1988).
6. Higgins, J.B., La Pierre, R.B., Schlenker, J.L., Rohrman, A.C., Wood, J.D., Kerr, G.T. and Rohrbaugh, W.J., *Zeolites*, **8**, 446 (1988).
7. Tomlinson, S.M., Jackson, R.A. and Catlow, R.A., *J. Chem. Soc. Chem. Com.*, 813 (1990).
8. Cambloor, M.A. and Perez-Periente, J., *Zeolites*, **11** 202 (1991).
9. Whittam, T.V., Eur. Pat. 55,046 (1981).
10. Wadlinger, R.L., Kerr, G.T. and Rosinski, E.J., US Pat. 3,308,064 (1975).
11. Bhat, R.N. and Kumar, R., *J. Chem. Tech. Biotechnol.*, **48**, 453 (1990).
12. Jacobs, P.A., Derouane, E.G. and Weitkamp, J., *J. Chem. Soc. Chm. Com.*, 591 (1981).
13. Tsitsishvilli, G.V., Krupenikov, A.Yu., Mamulashvili, M.V. and Urushadze, M.V., *Russ. J. Phys. Chem.*, **53**, 975 (1979).
14. Domine, D. and Quobex, J., *Molecular Sieves, Society of Chemical Industry,* London, p.78 (1968).
15. Chao, K.J., Tsai, T.C., Chen, M.S. and Wang, I., *J. Chem. Soc., Faraday Trans.I*, **77**, 547 (1981).
16. a) Avrami, M., *J. Chem. Phys.*, **9**, 177 (1941).
    b) Erofeev, B.V., *C. R. Acad. Sci., USSR*, **52**, 511 (1946).
17. Shiralkar, V.P. and Clearfield, A., *Zeolites*, **9**, 363 (1989).
18. Joshi, P.N., Kotasthane, A.N. and Shiralkar, V.P., *Zeolites*, **10**, 598 (1990).
19. Leu, L.J., Hou, L.Y., Kang, B.C., Li, C., Wu, S.T. and Wu, J.C., *Appl. Catal.*, **69**, 49 (1991).
20. Ernst. S., Jacobs, P.A., Martens, J.A. and Weitkamp, J., *Zeolites*, 7, 46 (1987).
21. Barrer, R.M., *Hydrothermal Chemistry of Zeolites*, Academic Press, London, p.251 (1982).
22. Borade, R.B., *Zeolites*, **7**, 398 (1987).

23. Ball, W.J., Dwyer, J., Garforth, A.A. and Smith, W.J., in "Proceedings of the 7th International Conference, Tokyo, 1986", *Stud. Surf. Sci. Catal.* **26**, 137 (1986).

24. Taramasso, M., Perego, G. and Notari, B. in *"Proceeding of the 5th International Zeolite Conference,"* Napels,, Hayden, London, vol.10. p.642 (1980).

25. Bellussi, G., Millini, R., Carati, A., Maddinelli, G. and Gervasini, A., *Zeolites*, **10**, 642 (1990).

26. Argauer. R.J. and Landolt, G.R., US Pat. 3,702,886 (1972).

27. Kuhl, G.H., *J. Ing. Nucl. Chem.*, **33**, 3261 (1971).

28. Kumar, R., Thangaraj, A., Bhat, R.N. and Ratnasamy, P., *Zeolites*, **10**, 85 (1990).

29. Camblor, M.A., Corma, A., Martinez, A. and Perez-Pariente, J., *J. Chem. Soc. Chem. Com.*, 589 (1992).

30. Tsitsishvilli, G.V. and Andronikashvili, T.G., *"Molecular Sieve Zeolites-II"*, Adv. Chem. Ser., Amer. Chem. Soc., Washington D.C., **102**, 217 (1971).

31. Venuto, P.B. and Landis, P.S., *Advan. Catal.*, **18**, 259 (1968).

32. Naccache, C., Primet, M. and Mathieu, M.V., *"Molecular Sieves-II"*, Adv. Chem. Ser., Amer. Chem. Soc., Washington D.C., **121**, 266 (1973).

33. Breck, D.W., *"Zeolite Molecular Sieves"*, Wiley, New York, 1974.

34. Rabo, J.A., Pickert, P.E. and Mays, R.L., *Ind. Eng. Chem.*, **53**, 733 (1961).

35. Minachev, K.M. and Isako, Y.I., in *"Zeolite Chemistry Catalysis"* (Rabo, J.A. Ed.,). Amer. Chem. Soc., Washington D.C., p.533 (1976).

36. Chow, M., Park. S.H. and Sachtler, W.M.H., *Appl. Catal.*, **19**, 349 (1985).

37. Bajpai, P.K., *Zeolites*, **6**, 2 (1986).

38. Rosinski, E.J. and Rubin, M.K., US Pat. 3,832,449 (1979).

CHAPTER 3

PHYSICO-CHEMICAL CHARACTERIZATION OF BETA ZEOLITES

3.1. INTRODUCTION

The modification of molecular sieves by isomorphous substitution and various secondary synthesis methods is a subject of great interest. In recent years many investigations have been devoted to the modification of the Brönsted acid sites, especially in the case of ZSM-5[1-3]. The incorporation of tetravalent elements like Ge^{4+} and Ti^{4+} does not create any net charge in the framework and no Brönsted acidity can be generated; when Si^{4+} is replaced by other trivalent elements like Al^{3+}, Ga^{3+}, B^{3+} and Fe^{3+}, there is a negative charge associated with each trivalent metal atom and it is balanced by a positive ion, mostly alkali metals, e.g., Na^+, K^+ and H^+, to give electrical neutrality. The strength of Brönsted acid sites thus created varies with different trivalent metal substitution[4]. Because these charge balancing cations are not locked into the framework, they are relatively mobile and can in many cases be easily exchanged for other cations. However, such modifications can alter not only the physico-chemical properties but also their catalytic behaviour.

The adsorption and catalytic properties of zeolites are modified to a considerable extent by replacement of Na^+ ion with hydrogen or multivalent ions[5]. The sorption of nitrogen, not only gives a measure of the surface accessible to molecules comparable in size with nitrogen, but also the surface area of the sample[6]. From the sorption capacities for water, n-hexane, benzene and cyclohexane, the modifications in the pore structure, void volume and hydrophobicity of the zeolites have been determined. The modifications in the crystal structure are studied by X-ray diffraction[7], and infrared spectroscopy[8]. The thermal stability of the zeolite structure can be determined from the thermo-analytical curves. The high temperature exotherm is often used to determine the thermal stability of the zeolites.

The acidity of zeolites has been extensively evaluated by i.r. spectra of chemisorbed bases such as pyridine, piperidine and n-butylamine[9-11]. From the chemisorption of ammonia on zeolites, the number of acid centres are calculated[12,13] and the temperature needed to desorb ammonia completely, is taken as a measure of the acid strength of the site. Isosteric heats of adsorption of ammonia[14] also serves as a measure of zeolite acidity. Takahashi and co-workers[15-18] have reported detailed studies on acidity determination with n-butylamine and differential heats of ammonia sorption in various oxide catalysts and Y type zeolites exchanged with La^{3+}, Ca^{2+} and H^+.

3.2. EXPERIMENTAL

3.2.1. CHEMICAL ANALYSIS

A known quantity of the zeolite sample was heated at high temperature (1073 K) in a platinum crucible for 5 h to constant weight. The sample was then cooled in a desiccator and weighed. The difference in weights gave the loss on ignition. The anhydrous weight of the samples was noted. The anhydrous solid powder was treated with hydrofluoric acid (HF, 40 wt%) and evaporated on a hot plate to remove silicon in the form SiF_4. The HF treatment was repeated three times. From the loss in weight, silica was estimated. The residue was fused in potassium pyrosulfate and dissolved in hot water. This solution was then analyzed by inductively coupled plasma emission (Jobin Yvon JY-38 VHR) and atomic absorption spectroscopy (Hitachi, Z-8000). X-ray flourescence spectrometer (Rigaku 3700) was also used to obtain Si/Al ratios.

3.2.2. X-RAY DIFFRACTION

The X-ray powder diffraction (XRD) patterns of the samples were recorded to ascertain the phase purity and also to detect the change in crystallinity during the framework modification treatments viz., ion exchange and impregnation. The X-ray powder diffraction patterns were recorded on Rigaku (model, D/MAX - VC, Japan) X-ray diffractometer, Ni filtered CuKα -radiation (λ = 1.5404 Å) was used for the analysis of the samples.

3.2.3. INFRARED SPECTROSCOPY

The infrared spectra of the all modified beta zeolite samples were recorded with a PYE UNICAM SP 300 spectrometer in the frequency range of 400-1400 cm^{-1} using nujol mull technique.

3.2.4. THERMAL ANALYSIS

Simultaneous TG-DTA-DTG analysis of all the modified beta zeolites were performed on an automatic derivatograph (SETARAM TG-DTA 92). The thermograms of the samples were recorded under the following conditions.

Weight of the sample	= 40 mg
Heating rate	= 10 K., min^{-1}
Pressure	= Flowing air at atmospheric pressure

Finely powdered α - alumina was used as a reference material.

3.2.5. SOLID STATE MASNMR SPECTROSCOPY

The high resolution MASNMR spectra for ^{29}Si, ^{27}Al, ^{11}B and ^{71}Ga were recorded at room temperature (298 K) on a BRUKER MSL-300 spectrometer, operating in the fourier transform mode. The rotors (sample holders) were spun at 4 KHz. While acquiring ^{29}Si spectra, 2 μs pulse, Larmor frequency 59.595 MHz, a recycle time of 4 seconds was found to be sufficient and the chemical shift was measured with respect to tetramethylsilane (TMS) as an external reference.

The other experimental conditions were, for ^{27}Al: 0.25 seconds recycle time, Larmor frequency 78.172 MHz, 3 μs pulse, spectra collected over 600 scans with $Al(H_2O)_6^{3+}$ as an external reference; for ^{11}B: 2.0 seconds recycle time, Larmor frequency 96.279 MHz, 4.5 μs pulse, spectra collected over 1000 scans with $(CH_3)_2.O.BF_3$ as an external reference; for ^{71}Ga: 0.3 second recycle time, Larmor frequency 91.485 MHz, 3.0 μs pulse, spectra collected over 25,000 scans with $Ga(H_2O)_6^{3+}$ as an external reference.

3.2.6. SCANNING ELECTRON MICROSCOPY

The morphology of zeolite beta samples were investigated using scanning electron microscopy (JEOL, JSM - 5200). The samples were mounted on a carrier made from alumina and were coated with a film of gold to prevent surface charging and to protect the zeolite material from thermal damage by the electron beam. In all the samples, a uniform film thickness of about 0.1 mm was maintained.

3.2.7. ION EXCHANGE CAPACITIES

The calcined samples were treated with 1 N NaCl solution (1 g/50 ml) for 4 h at 403 K to get Na-form of the zeolites. The Na-form was then exchanged with 1 N KCl solution for 4 h at 363 K. The solid was filtered, washed thoroughly with deionized water and dried at 373 K for 5 h. The resultant materials (Na-form & K-form) were analyzed for Na, K and M (M=Al, B and Ga).

3.2.8. SURFACE AREA MEASUREMENTS

A Omnisorb 100 CX (supplied by COULTER corporation, USA) analyser was used for the measurement of low pressure (P/P_o=0.001) nitrogen adsorption to determine the surface area. The samples were activated at 673 K for 2 hours in a high vacuum. After the treatment,

the anhydrous weight of the samples was taken at room temperature. The samples were then cooled to 78 K using liquid nitrogen. After this, the samples were allowed to adsorb nitrogen gas. Finally, the BET surface area was calculated.

3.2.9. ADSORPTION MEASUREMENTS

The sorption measurements for water, cyclohexane, n-hexane and benzene were carried out gravimetrically in a recording electromicrobalance (Model, Cahn-2000 G) (shown in Fig.3.1). The zeolite sample of about 50 mg was pressed into a pellet and was weighed in an aluminium bucket. Then the system was connected to high vacuum and the sample was activated in vacuum (10^{-6} Torr) at 753 K for 4 hours. The sample was then cooled to the desired temperature under high vacuum. Prior to the adsorption, the sorbate vapours were admitted into the sample at a constant pressure and temperature, and the weight gained was recorded continuously as a function of time. After the completion of the experiment, the sample was evacuated and heated to 753 K at 10^{-6} Torr and used for the next measurement.

3.1.10. AMMONIA ADSORPTION

A conventional all glass BET unit (shown in Fig.3.2) was used for the measurement of ammonia adsorption. It consists of three burettes B_1, B_2 and B_3 (B_3 is not shown in Fig.3.2); a manometer M and a sample bulb S. High vacuum systems consisting of a two stage rotary pump, silicon oil diffusion pump, a Mcleod gauge, and a series of liquid nitrogen cold traps, were used for degassing the sample.

The volumes of the burette bulbs were precalibrated with mercury before joining them to the adsorption system. The burettes B_1 and B_2 were immersed in water jackets provided with a thermowell for temperature measurements. The dead space volume in the system was determined by using spectrally pure helium supplied by British Oxygen Co., (U.K.). About 0.25 to 0.30 g of hydrated sample was taken in the sample bulb. The sample bulb was dipped in the thermostatic bath upto a reference mark. The sorption measurements were carried out in the temperature range of 30°C to 180°C. Liquid paraffin was used as a thermostatic medium for controlling the required temperature.

The zeolite sample was degassed at 480°C. The temperature was raised to 480°C with heating rate of 2°C/min. and simultaneous evacuation. The sample was activated at 480°C by evacuating in vacuum (10^{-6}) torr for 8 hours. The sample was cooled and the dead-space volume

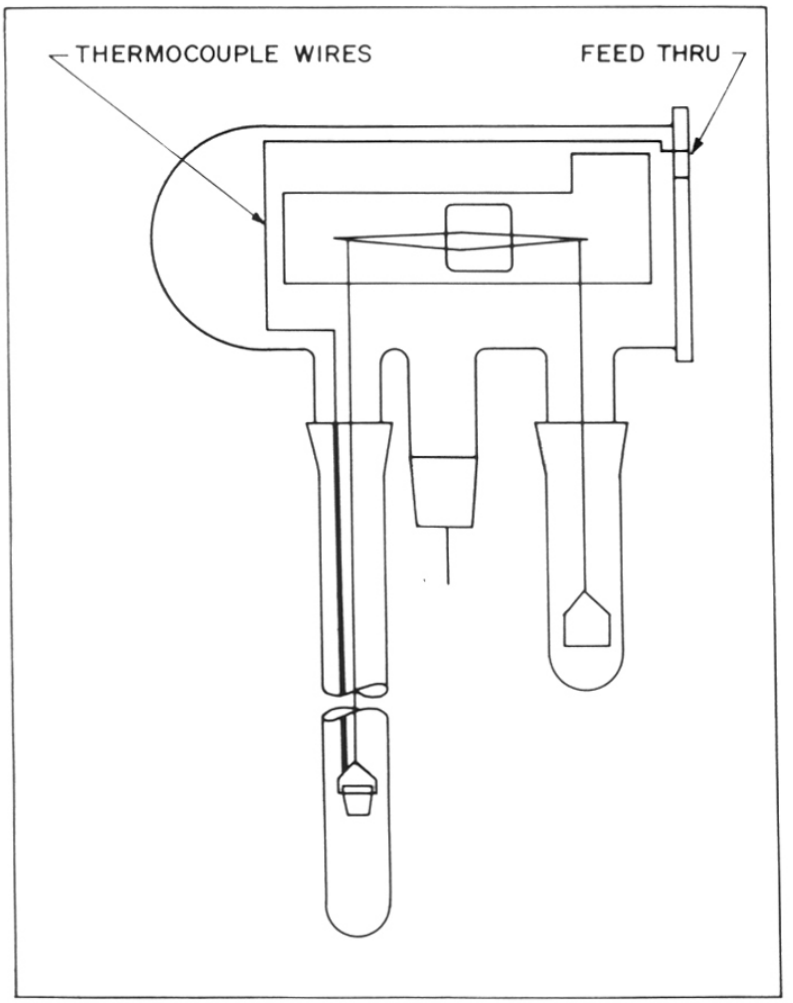

Fig.3.1: Cahn electro micro-balance used for adsorption.

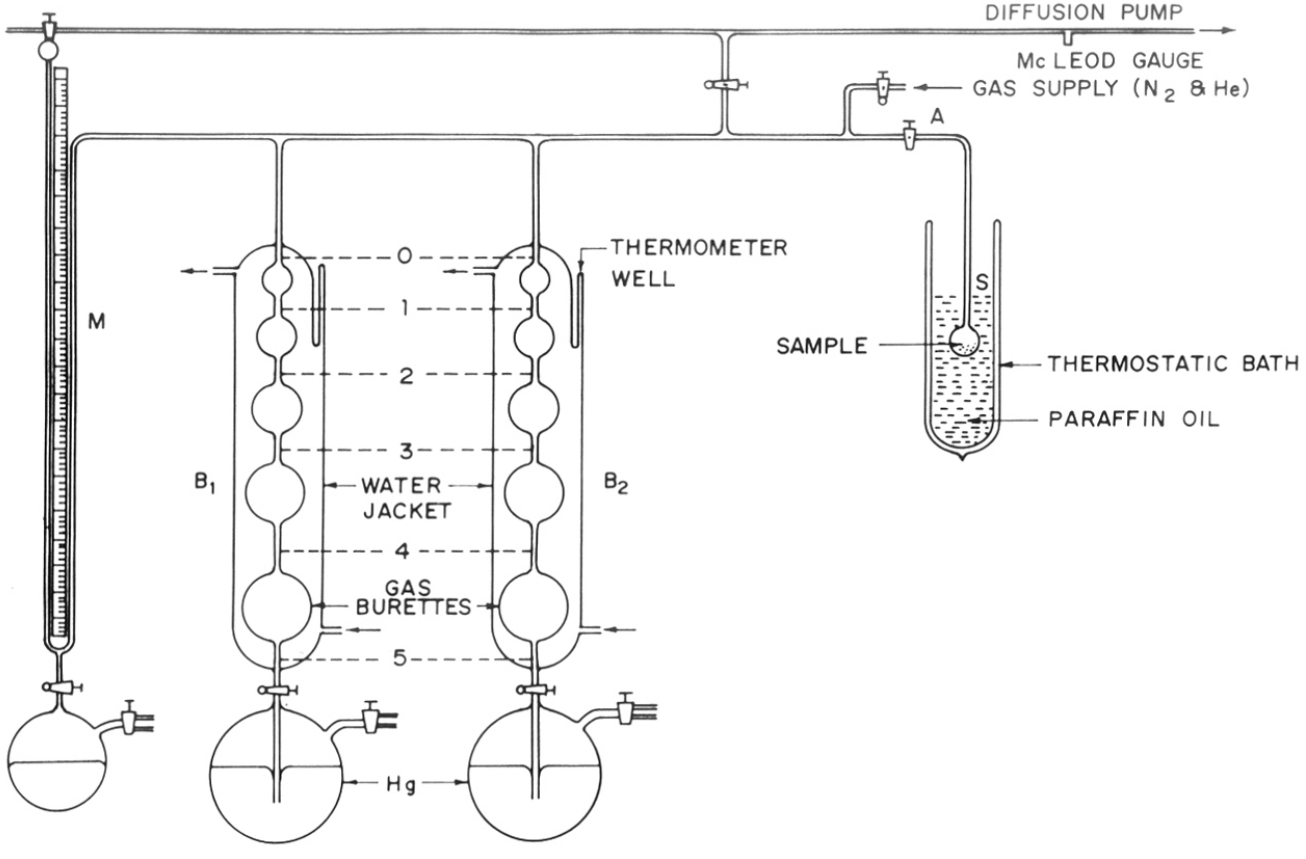

Fig.3.2: Adsorption unit for the measurements of NH_3 sorption.

was determined by using helium at the desired temperature. After pumping out the helium gas, the zeolite sample was evacuated at 480°C by evacuating in vacuum (10^{-6} torr) for 8 hours. Prior to the adsorption isotherms, the sample bulb was cooled and dipped upto the reference mark in the thermostat at the desired temperature for 2 hours before the commencement of the measurements. After this, a known amount of ammonia was admitted. The sample was exposed to ammonia gas at different pressures. The sorption isotherms were measured over a pressure range of 5-500 Torr. The sorption equilibrium was attained within 25-30 minutes. The adsorption measurements were continued by admitting consequent calibrated ammonia doses, until a sufficient number of points were obtained. The sorption isotherm was first measured at 180°C and then at the next lower temperature. The reversibility of the sorption was checked during the desorption measurements.

The volume of gas adsorbed at STP was estimated as follows:

$$V_{ads} = V_1 - V_2 - V_3$$

where V_1, V_2 and V_3 are the volumes of gas taken, remaining in the system, and in the bulb, respectively.

3.3. RESULTS AND DISCUSSION

3.3.1. CHEMICAL ANALYSIS

The unit cell compositions of Al-beta and all modified beta zeolites, obtained from chemical analysis, are given in Table 3.1. On account of the highly pure source of silica (silica sol and tetraethylorthosilicate) used, the concentration of aluminium in B-beta and Ga-beta zeolites was negligible ($SiO_2/Al_2O_3 > 2000$).

Table 3.1: Unit Cell (U.C.) composition (anhydrous basis) of modified beta zeolites.

Zeolite	Unit cell composition	no. of U.C./g. X 10^{-20}
B-beta	$H_{3.99}\ Na_{0.02}\ [(BO_2)_{4.02}\ (SiO_2)_{59.98}]$	1.5989
Al-beta	$H_{4.78}\ Na_{0.02}\ [(AlO_2)_{4.80}\ (SiO_2)_{59.20}$	1.6090
Ga-beta	$H_{4.57}\ Na_{0.01}\ [(GaO_2)_{4.58}\ (SiO_2)_{59.42}]$	1.5112
Na-H-beta	$H_{3.19}\ Na_{1.36}\ [(AlO_2)_{4.55}\ (SiO_2)_{59.45}]$	1.5548
Mg-H-beta	$H_{2.50}\ Na_{0.02}\ Mg_{1.02}\ [(AlO_2)_{4.56}\ (SiO_2)_{59.44}]$	1.5576
Ca-H-beta	$H_{1.07}\ Na_{0.02}\ Ca_{1.59}\ [(AlO_2)_{4.27}\ (SiO_2)_{59.73}]$	1.5410
Sr-H-beta	$H_{1.66}\ Na_{0.02}\ Sr_{1.43}\ [(AlO_2)_{4.54}\ (SiO_2)_{59.46}]$	1.5185
La-H-beta	$H_{1.34}\ Na_{0.02}\ La_{0.94}\ [(AlO_2)_{4.18}\ (SiO_2)_{59.82}$	1.5164

3.3.2. X-RAY DIFFRACTION

The X-ray diffraction pattern of the as-synthesized B-beta, Al-beta and Ga-beta zeolites are given in Fig. 3.3. The corresponding 2 θ and 'd' spacings are given in Table 3.2. The isomorphous substitution of B and Ga for Al, resulted in a change in 'd' spacings, indicating the lattice contraction due to smaller B atoms and expansion due to the larger Ga atoms in the framework positions of beta zeolite. A similar contraction and expansion were also observed for B and Ga substitution in the framework of NU-1 zeolite[19]. There was no significant loss of crystallinity during the process of the ion exchange and impregnation.

3.3.3. INFRARED SPECTROSCOPY

Fig. 3.4 illustrates the framework infrared spectra of as-synthesized samples of B-beta, Al-beta and Ga-beta. The values of some major absorption bands are listed in Table 3.3. In accordance with expectations, most of the lattice vibration bands are shifted to higher frequencies in B-beta and to lower frequencies in Ga-beta compared to Al-beta. For example, the bands at 1175 and 1075 cm^{-1}, due to asymmetric stretching vibration of Si-O-T (T=Al) are shifted to 1180 and 1081 cm^{-1} on isomorphous substitution of Al by smaller B atoms and to 1164 and 1058 cm^{-1} on substitution of Al by the larger Ga atoms in the framework of zeolite beta.

3.3.4. THERMAL ANALYSIS

Fig. 3.5 compares the DTA and TG profiles for B-beta, Al-beta and Ga-beta zeolites. In this we find four distinct steps of weight loss in DTA profiles. The first step is slightly endo-thermic and results from the dehydration of the occluded water and the other three steps are

Table 3.2: 2θ and "d" values of B-, Al- and Ga-beta zeolites.

B-beta		Al-beta		Ga-beta	
2 θ	d (Å)	2 θ	d (Å)	2 θ	d (Å)
7.706	11.463	7.568	11.672	7.556	11.691
11.756	7.522	11.749	7.528	11.742	7.531
16.454	5.383	16.526	5.360	16.388	5.405
21.418	4.132	21.410	4.154	21.392	4.150
22.430	3.961	22.406	3.965	22.376	3.970
25.346	3.511	25.310	3.516	25.208	3.530
26.840	3.319	26.834	3.321	26.827	3.324
29.520	3.022	29.516	3.025	29.480	3.028
33.452	2.676	33.356	2.684	33.332	2.686
43.748	2.068	43.628	2.073	43.580	2.075

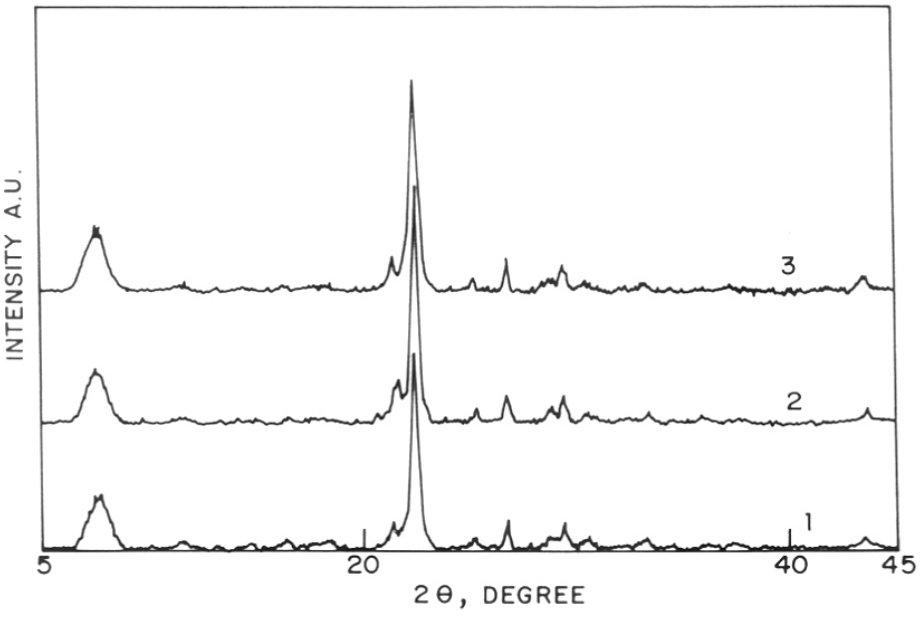

Fig.3.3: XRD patterns of B-, Al-, and Ga-beta zeolites (1, 2, and 3, respectively).

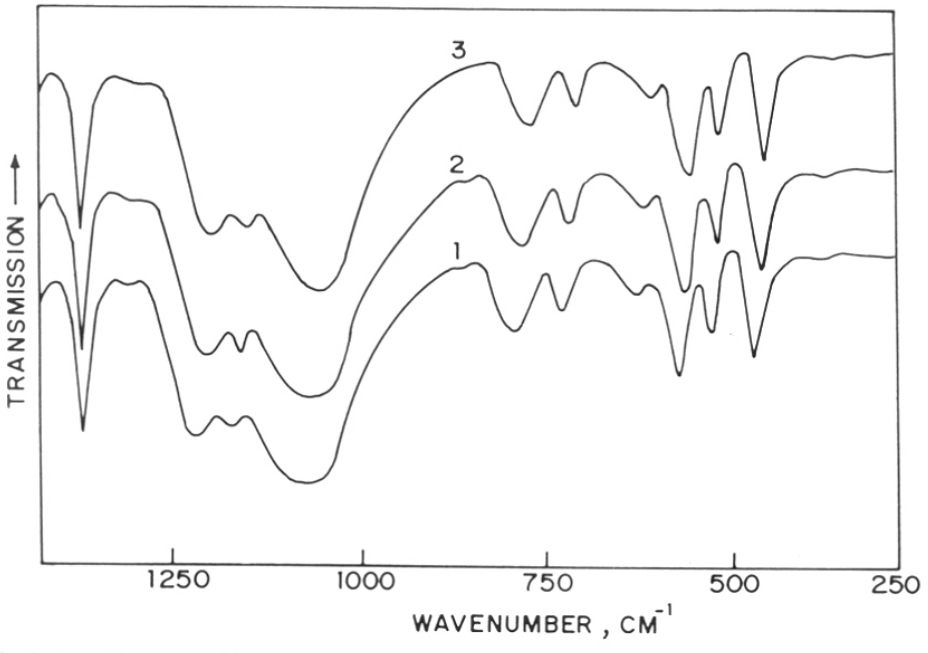

Fig.3.4: Framework i.r. spectra of B-, Al, and Ga-beta zeolites (1, 2, and 3, respectively).

Table 3.3: Framework i.r. vibrations (cm^{-1}) for different isomorphs of zeolite beta.

B-beta	Al-beta	Ga-beta
1180 (w)	1175 (w)	1164 (w)
1225 (w)	1215 (w)	1207 (w)
1081 (w)	1075 (s)	1064 (s)
798 (s)	790 (s)	782 (s)
746 (w)	740 (w)	736 (w)
621 (w)	613 (w)	608 (w)
583 (s)	578 (s)	573 (s)
526 (m)	521 (m)	518 (m)
456 (s)	450 (s)	445 (s)

w = weak, s = strong and m = medium.

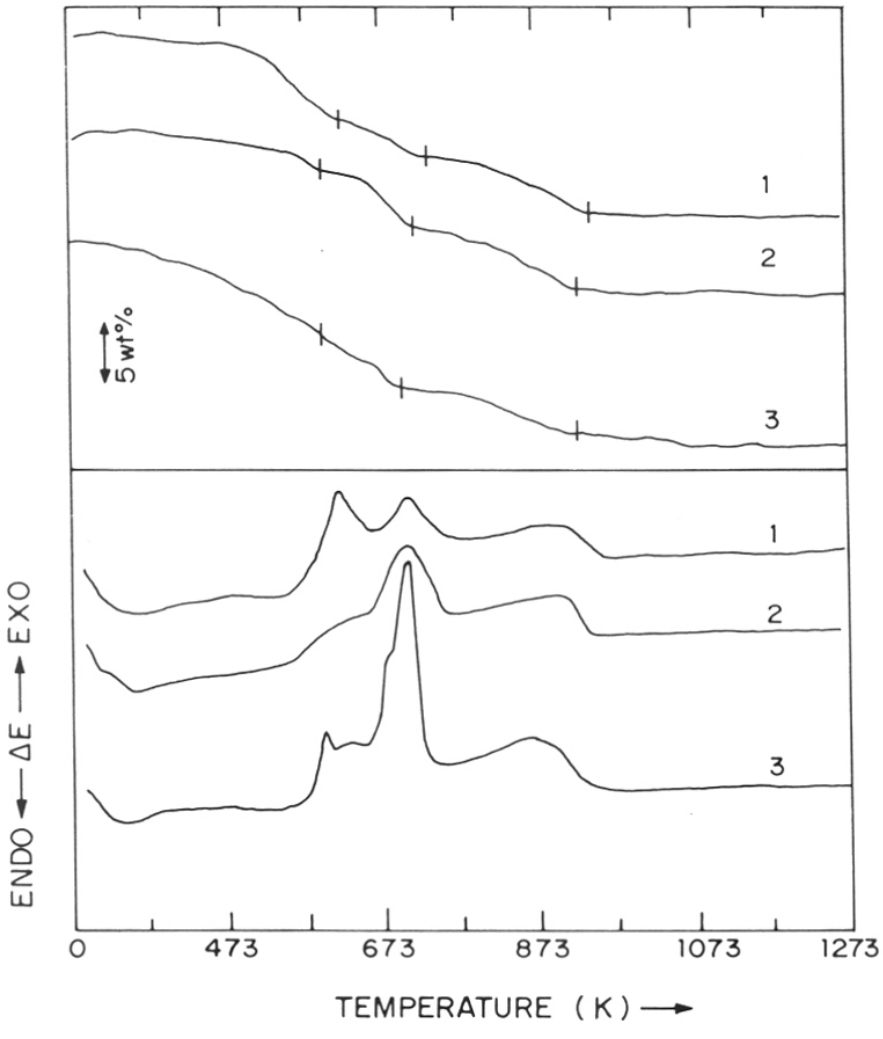

Fig.3.5: DTA (bottom) and TG (top) curves for Al-, Ga-, and B-beta zeolites (1, 2, and 3, respectively).

exothermic and are related to the oxidation of organic material. Perez-Pariente *et al.*[20] also observed similar results in beta zeolites synthesized using tetraethylammonium hydroxide (TEA-OH) as an organic template. The minimum of the endothermic peak shifts from 370 K in Al-beta and Ga-beta to 354 K in B-beta. Corresponding to this endothermic effect the weight loss in TG profiles is only upto 2 wt%.

In the exothermic weight losses, the maxima of the first exotherm shifts to lower temperature from 627 K in Al-beta to 621 K in Ga-beta and to 603 K in B-beta. This exothermic effect is due to the decomposition of physically occluded templating species. The temperature of the maxima of second exothermic peak, due to the oxidative decomposition of TEA^+ cations occluded in the channels, also decreases from 719 K in Al-beta to 712 K in Ga-beta and to 697 K in B-beta. However, the exothermic peak is very sharp in B-beta with a shoulder at 680 K. The loss in weight indicated by TG curves corresponding to the exothermic effect is rather low (3 wt%) in Al-beta correspond to 5 wt% in the other two isomorphic forms.

The temperature of the maxima of the third exothermic peak, due the oxidative decomposition of the TEA^+ cations associated with the framework AlO_4^- tetrahedra also decreases in the sequence Al-beta (918 K) > Ga-beta (913 K) > B-beta (873 K). The decomposition of a part of the template in zeolite beta at temperature as high as 913 K indicates much stronger bonding between some of the template molecules possessing typical framework environment. There is as high as 5 wt% loss corresponding to this exothermic peak.

3.3.5. SOLID STATE MASNMR SPECTROSCOPY

The ^{29}Si and ^{27}Al MASNMR spectra of Al-beta, B-beta and Ga-beta are shown in Fig. 3.6, A, B and C, respectively. The ^{27}Al MASNMR spectra of B-beta and Ga-beta shows the absence of aluminium in the sample. The ^{29}Si MASNMR spectra of as-synthesized B-beta and Ga-beta shows two types of Si environments. A chemical shift of about δ = -102 ppm in Ga-beta, corresponds to Si(1 Ga), indicating Si atoms in the second co-ordination sphere[21].

The ^{11}B MASNMR spectrum of B-beta is shown in Fig. 3.7. The chemical shift at δ = -3.03 ppm [with respect to $(CH_3)_2O.BF_3$] shows the presence of B in tetrahedral co-ordination[19]. The ^{71}Ga MASNMR spectrum of Ga-beta is also shown in Fig. 3.8. The chemical shift at δ = 158 ppm with respect to $Ga(H_2O)_6^{3+}$ is evidence for the tetrahedral Ga^{3+} ions in the framework of zeolite beta[19].

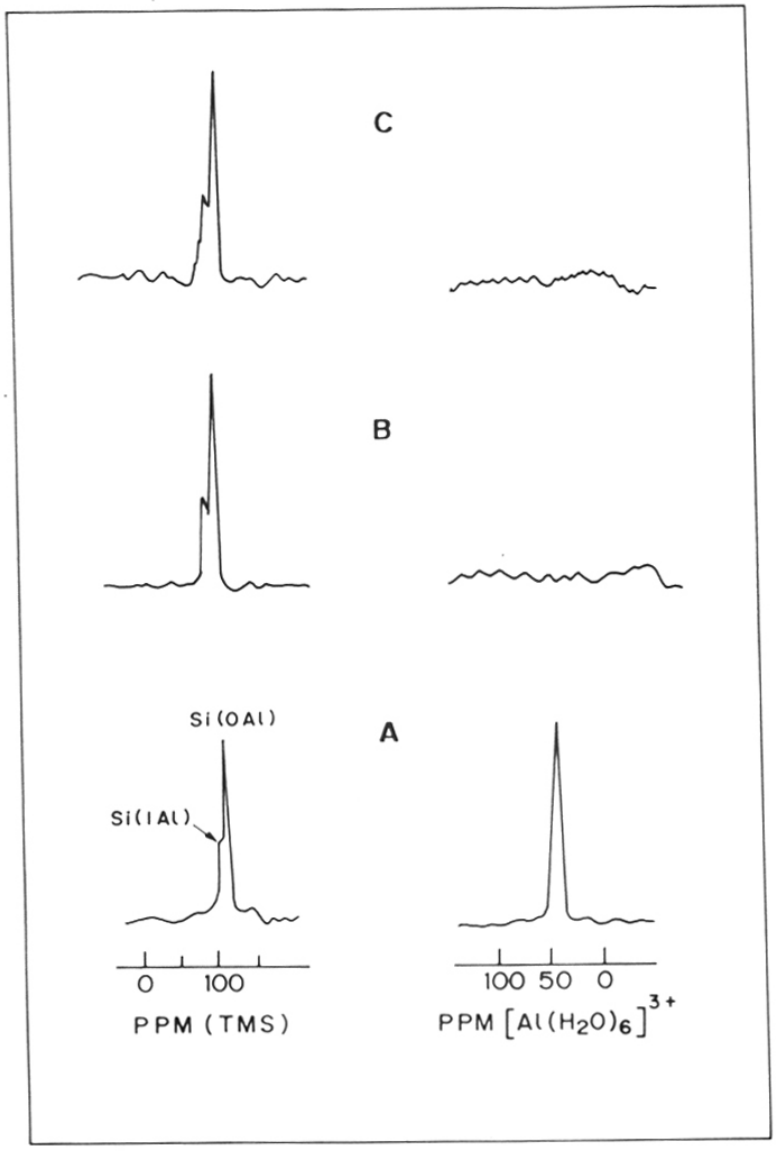

Fig.3.6: MAS NMR spectra of Al-, Ga-, and B-beta zeolites (A, B, and C, respectively).

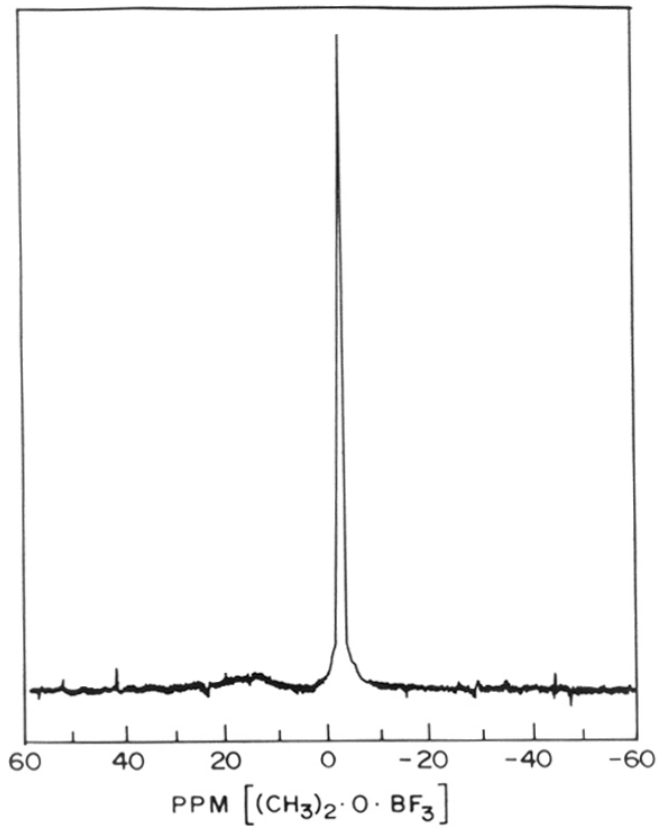

Fig.3.7: ^{11}B MAS NMR spectra of B-beta zeolite.

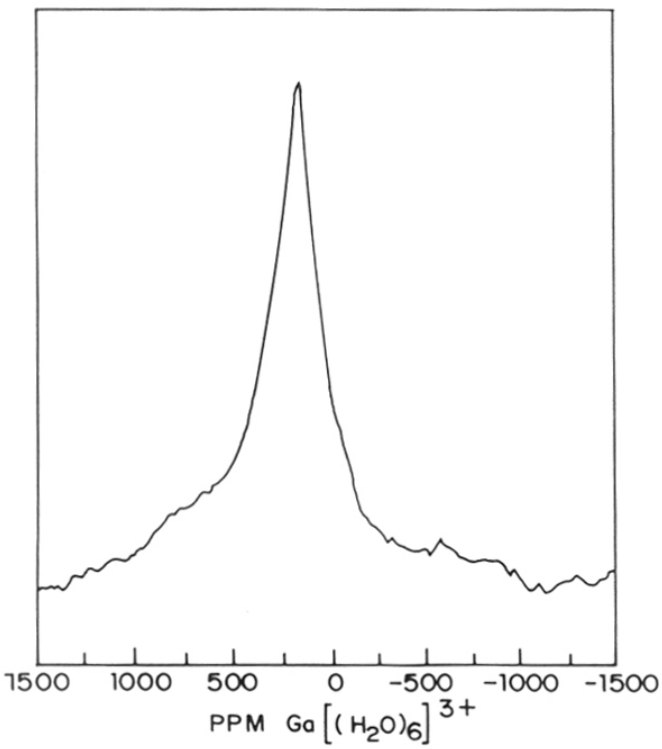

Fig.3.8: ^{71}Ga MAS NMR spectra of Ga-beta zeolite.

3.3.6. SCANNING ELECTRON MICROSCOPY

The scanning electron micrographs (SEM) of as-synthesized Al-beta, B-beta and Ga-beta are shown in Fig. 3.9-A, -B and -C, respectively. The crystallite size of all the zeolites are 0.3 - 0.4 μm. They are nearly spherical in shape. The SEM also confirms the absence of any amorphous material outside the crystals.

3.3.7. ION EXCHANGE CAPACITIES

After saturating the calcined Al-beta, B-beta and Ga-beta zeolite samples with Na^+ ions, the molar ratios of Na/Al, Na/B and Na/Ga in the solid were found to be 0.96, 0.88 and 0.90, respectively. On ion exchange of all the Na-forms of the samples with K^+ ions to get the K-form, the molar ratios K/Al, K/B and K/Ga were 0.91, 0.82 and 0.86, respectively. The ion exchange properties of zeolites are due to the tetrahedral MO_4^- groups (M=Al, B, Ga, Fe etc.,) in the framework position. Recently, Szostak and Thomas[22,23] have demonstrated that the ion exchange capacities of zeolites can be taken as convincing evidence for the presence of M^{3+} ions in the framework positions in the zeolite lattice. Hence, the substantial ion exchange capacities of the calcined B-beta and Ga-beta zeolites is a strong evidence for the presence of the B^{3+} or Ga^{3+} ions in zeolite beta framework.

3.3.8. SURFACE AREA MEASUREMENTS

The low pressure nitrogen adsorption isotherms at liquid nitrogen temperature (78 K) were typically of Langmuir types upto 620 Torr. The BET surface of Al-beta, B-beta and Ga-beta is 690.3, 685.2 and 674.9 m^2/g, respectively. The t-area of the samples was found to be negligible.

3.3.9. ADSORPTION MEASUREMENTS

The adsorption of water, n-hexane, cyclohexane and benzene in the sodium forms of Al-beta, B-beta and Ga-beta samples are given in Table 3.4. It is seen from the Table 3.4 that the equilibrium uptakes for the sorption of all the four sorbate molecules in Al-beta, B-beta and Ga-beta are almost close to each other and these sorption capacities are in agreement with those reported by Wadlinger *et al.*[24]. The salient features of Table 3.4 include almost constant adsorption capacities for n-hexane and cyclohexane giving its pore volume 0.23 ml/g. These adsorption results clearly demonstrate the absence of a significant quantity of any amorphous material occluded inside pores of the zeolite crystals.

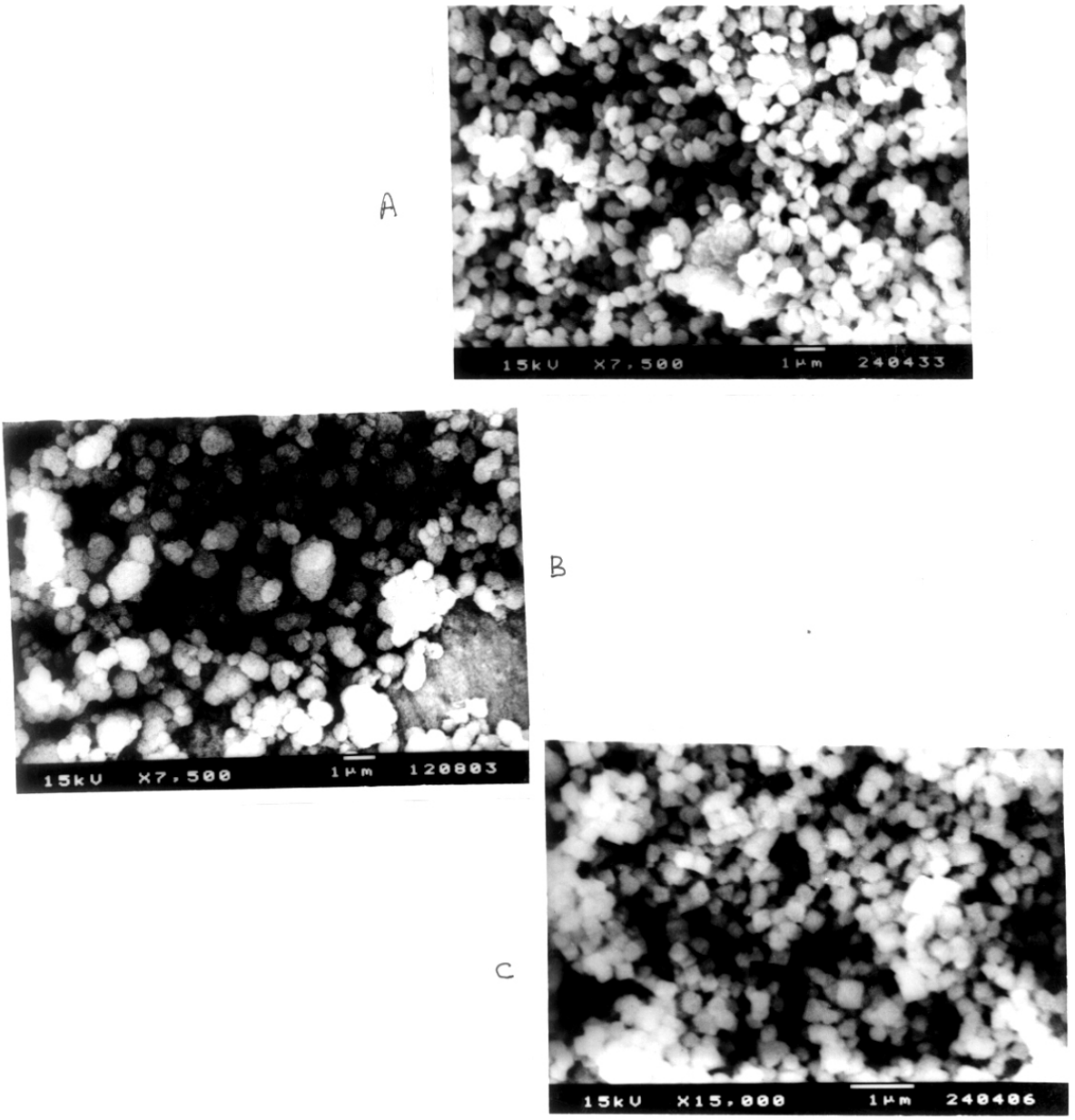

Fig.3.9: Scanning electron micrographs of B-, Al-, and Ga-beta zeolites (A, B, and C, respectively).

Table 3.4: Sorption capacities for modified beta zeolites (P/P_o = 0.5 and Temp.= 298 K).

zeolite	amount sorbed (wt.%)				S.A.,	V.V.,
	H_2O	n-C_6H_{12}	C_6H_{12}	C_6H_6	$m^2/g.$	ml/g.
B-beta	21.09	16.79	20.54	22.52	687	0.279
Al-beta	22.81	19.91	21.67	23.45	708	0.283
Ga-beta	20.87	18.73	19.89	22.71	691	0.291
Na-H-beta	16.87	16.43	18.61	22.42	759	0.311
Mg-H-beta	19.30	19.71	20.02	23.57	684	0.277
Ca-H-beta	16.11	17.42	17.78	22.43	690	0.277
Sr-H-beta	21.62	18.43	21.32	23.91	713	0.290
La-H-beta	19.11	18.25	19.39	22.98	23.91	0.283

S.A = Surface Area, and V.V = Void Volume calculated from Dubinin plots.

3.3.10. AMMONIA ADSORPTION

A. Isotherms of ammonia

Families of isotherms of ammonia sorption in typical cation exchanged beta zeolites are depicted in Fig.3.10. The shape of the isotherms approximates to the type I (langmuir type) according to Kiselev's classification[25]. Almost 75% of the total sorption takes place over a very narrow range of relative pressure. The equilibrium sorption uptake at 400 Torr and especially at lower temperature, follows in the sequence of H-beta > La-H-beta > Mg-H-beta > Na-H-beta > Ca-H-beta > Sr-H-beta. The observed sequence for ammonia sorption capacity is then in accordance with the combined effect of Sanderson's electronegativities and polarizabilities of the cation. At lower pressures (100 Torr) and at higher temperatures the sequence in ammonia sorption capacities becomes rather complicated on account of varying contribution of sorption irreversibiliity which is discussed later.

Cation density in zeolites usually decreases with increase in cationic charge. If these extra-framework cations and protons, produced upon dissociation of water molecules associated with them, act as sorption centres, then the equilibrium amount sorbed of polar molecule like ammonia is expected to decrease with the decrease in cation density in the zeolite framework. Accordingly, Fig 3.10 confirms this general expectation at higher pressure (400 Torr), however, at lower pressure (100 Torr) the amount sorbed in zeolites with decreasing cation density, follows the sequence Na-H-beta < Mg-H-beta < La-H-beta. This shows that at lower pressure (lower

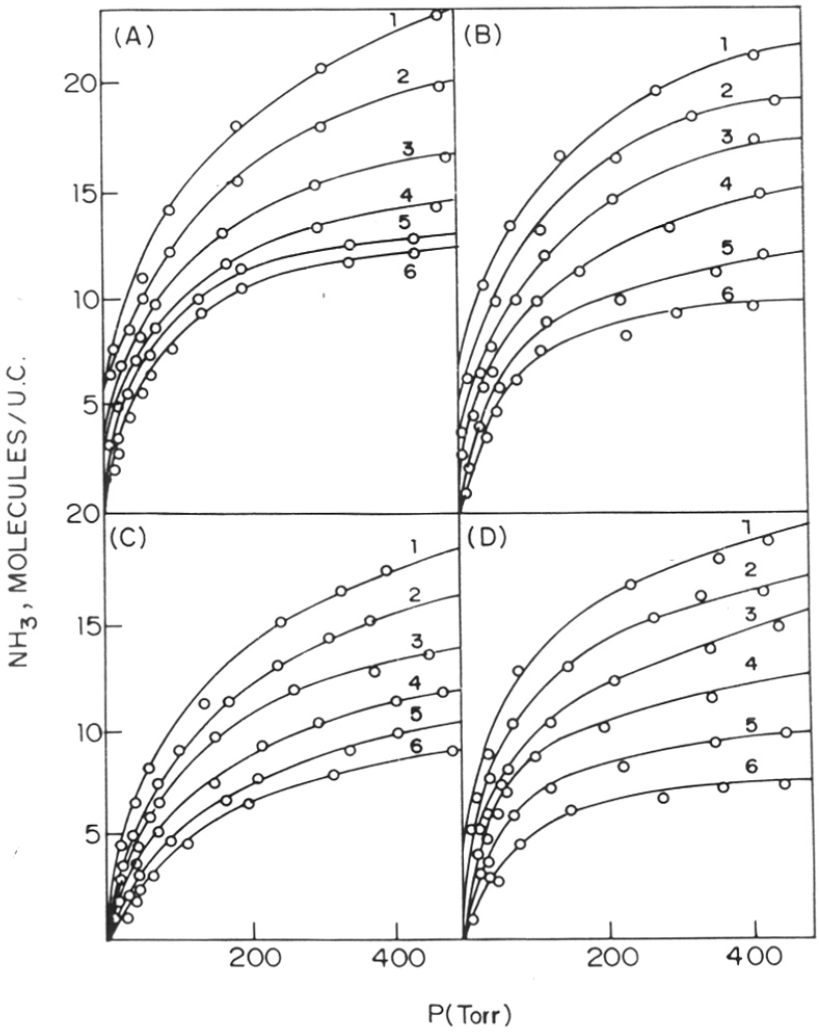

Fig.3.10: Isotherms for ammonia sorption in (A) Hbeta, (B) LaHbeta, (C) NaHbeta, and (D) MgHbeta at 1) 303 K, 2) 333 K, 3) 363 K, 4) 393 K, 5) 423 K, and 6) 453 K.

coverage) sorption capacity seems to be dependent on the cationic charge rather than on the cation density. Similar observation was reported[26] earlier for the carbon dioxide sorption in cation exchanged Y zeolites. In case of cationic species with the same charge (Mg^{2+}, Ca^{2+} and Sr^{2+}), the sorption uptake seems to increase with the decrease in ionic radius. Eventhough only 30% sodium occupancy is there in the parent zeolite Na-H-beta, upon replacement of those sodium cations by protons (via deammoniation of ammonium form) there is at least as much as one and half times increase in the uptake of ammonia molecules. This clearly shows that protons act as stronger sorption centres than other cationic species such as Na^{+}, Mg^{2+}, Ca^{2+}, Sr^{2+} and La^{3+}.

B. Irreversibility of ammonia sorption and acidity

During the desorption experiments under vacuum it was found that all the cation exchanged zeolite beta samples retained certain amount of ammonia irreversibly. Irreversibility in ammonia sorption has also been reported earlier in MnY[27], RuM, CrM and FeM[28,29] zeolites at 303 K. The reversibility of ammonia in zeolites is attributed[27] to (a) formation of ammonia complexes with intrazeolitic cations and to (b) chemisorption. In case of the complex formation[27,28], colour changes were indicated during outgassing and sorption of ammonia in transition metal zeolites. In the present studies irreversibly sorbed ammonia was found to be completely removed on heating the zeolite at 733 K. As the temperature of the desorption was increased, the number of ammonia molecules per cation decreased from 1.5 to nearly 1.0 in the temperature range of 453 to 623 K.

Fig. 3.11 shows the variation in the chemisorbed ammonia with temperature in different cation exchanged beta zeolites. The number of ammonia molecules held on account of chemisorption especially at higher temperatures (> 453K) may be taken as a measure of acidity. At temperature lower than 453 K some ammonia molecules (not necessarily physically sorbed) are held, those are sorbed less strongly on extra-framework cations other than protons and on surface silanol groups and they approximately correspond to α and β peaks on ammonia temperature programmed desorption (TPD)[30]. As the desorption temperature increases NH_4^{+}/H^{+} ratio approaches unity corresponding to γ peak on ammonia TPD. At 733 K all the ammonia molecules were found to be desorbed. The amount of chemisorbed ammonia is highest for H-beta followed by La-H-beta, Mg-H-beta, Ca-H-beta, Sr-H-beta and Na-H-beta; and this clearly is regarded as the sequence of total acidity in the zeolites. It is seen from Fig. 3.11 that

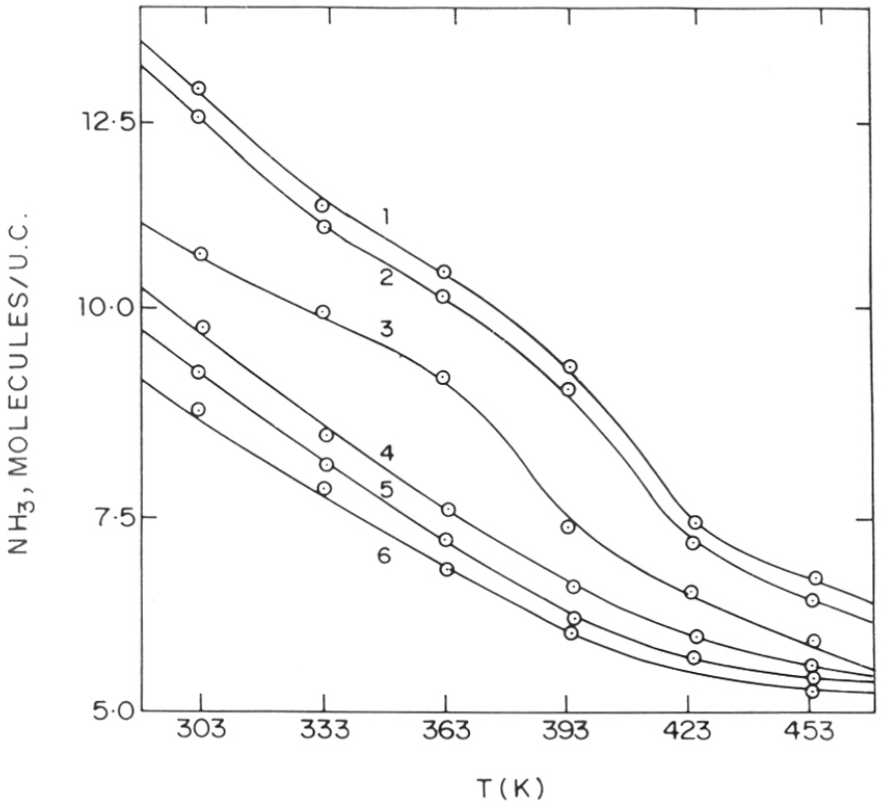

Fig.3.11: Amount of ammonia retained irreversably as a function of temperature in 1) Hbeta, 2) LaHbeta, 3) MgHbeta, 4) CaHbeta, 5) SrHbeta, and 6) NaHbeta.

the decrease in the amount of chemisorbed ammonia with the increase in the sorption temperature is more sharp in the sample retaining more ammonia. The total acidity of the exchanged zeolites, with the exception of Mg-H-beta, follows the sequence of e/r ratio and Sanderson's electro-negativity of the cation.

C. Application of Isotherm Equation

i. Dubinin equation

Polanyi potential theory when modified by Dubinin and Radushkevich[31] takes the form

$$\log(W) = \log(W_o) - B/2.303\ \beta^2\ [T.\ \log\ (P_o/P)]^2$$

where W is the amount sorbed at equilibrium pressure P,

W_o is the total sorption capacity,

B is a constant independent of temperature and is characteristic of the sorbent pore structure and

β is the affinity coefficient.

Dubinin plots were constructed by plotting $(\log P_o/P)^2$ against log W for all the cation exchanged zeolites in the temperature range 303-453 K. In all the samples excellent linear plots were obtained and typical Dubinin plots are shown in Fig. 3.12. The saturation capacities obtained from the intercept of their linear plots were slightly higher than those recorded at 400 Torr experimentally. This seems to be reasonable because the values obtained from the Dubinin plots are extrapolated over higher pressures.

The magnitude of the affinity co-efficient β is inversely proportional to the square root of the factor B/β^2 obtained from the slope. An increase or a decrease in β is usually looked upon as an increase or a decrease in sorption affinity of sorbate molecules towards the sorbent surface. From the linear plots in Fig. 3.12, it is seen that the affinity co-efficient β decreases with the increase in temperature for all the zeolites except for Mg-H-beta and H-beta. Although there does not seem to have any specific trend in the value of β with cationic charge or with polarizability of the extra-framework cationic species; the affinity co-efficient for Na-H-beta is lower than that for other cation exchanged zeolites. In general, the excellent linearity of these plots suggests that the ammonia sorption in cation exchanged beta zeolites could be represented

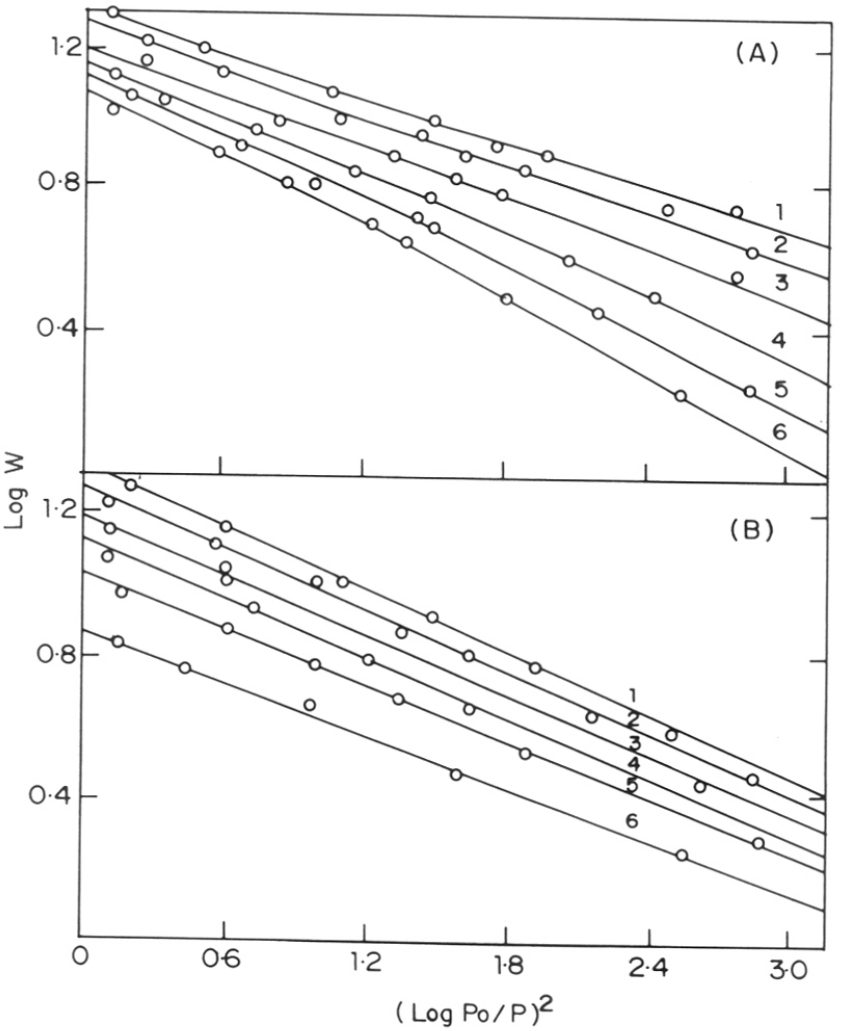

Fig.3.12: Dubinin plots for ammonia sorption in (A) LaHbeta, and (B) MgHbeta at 1) 303 K, 2) 333 K, 3) 363 K, 4) 393 K, 5) 423 K, and 6) 453 K. W is the amount of sorbed molecules/u.c.

satisfactorily by the Polanyi's potential theory of volume filling modified by Dubinin and Radushkevich. Earlier CO_2[26] and NH_3[32] sorption data in cation exchanged Y zeolites were also satisfactorily represented by Dubinin equation.

ii. Langmuir equation

Langmuir sorption isotherm equation has been derived on the assumption of localized monolayer sorption on the sorption centres of equal energy and 1:1 correspondence between the sorption centres and sorbate molecules. Ammonia sorption data in cation exchanged beta zeolites and excellent linear plots (typical of which are shown in Fig. 3.13) were obtained for all the cation exchanged zeolites over entire temperature range of 303-453 K. The excellent linearity of these plots from Fig. 3.13, undoubtedly, indicates the validity of Langmuir equation to describe ammonia sorption in cation exchanged beta zeolites. It seems, therefore, that ammonia sorption in these zeolites is localized with an element of chemisorption indicated by irreversibly retained ammonia discussed earlier. Monolayer capacity (V_m) obtained from the reciprocal of the slope of these linear plots, were rather higher than those recorded experimentally at 400 Torr. It seems to be reasonable that the monolayer capacity (V_m) may not necessarily match the sorption capacity at 400 Torr.

iii. BET equation

The analysis of the ammonia sorption data in terms of BET equation yielded linear plots (Fig. 3.14). The values of monolayer capacities obtained from the slopes and intercept, with the exception of Na-H-beta and H-beta, deviate considerably from the experimental values. This shows that a BET approach, based on the multilayer formation, has only a limited applicability in the present studies of ammonia sorption in cation exchanged beta zeolites.

iv. Sips Equation

Sips equation[33] is based on the localized sorption with sorbate-sorbate interaction usually takes care of any deviation from the Langmuir approach. If the sorption is assumed to be a chemical reaction between the sorption centres and sorbate molecules; Langmuir equation results with 1:1 correspondence between them and if some tolerance is made for the complicating factors, the Sips equation results. Mathematically Sips equation is expressed as,

$$\log [\theta/(1 - \theta)] = \log A + c. \log P$$

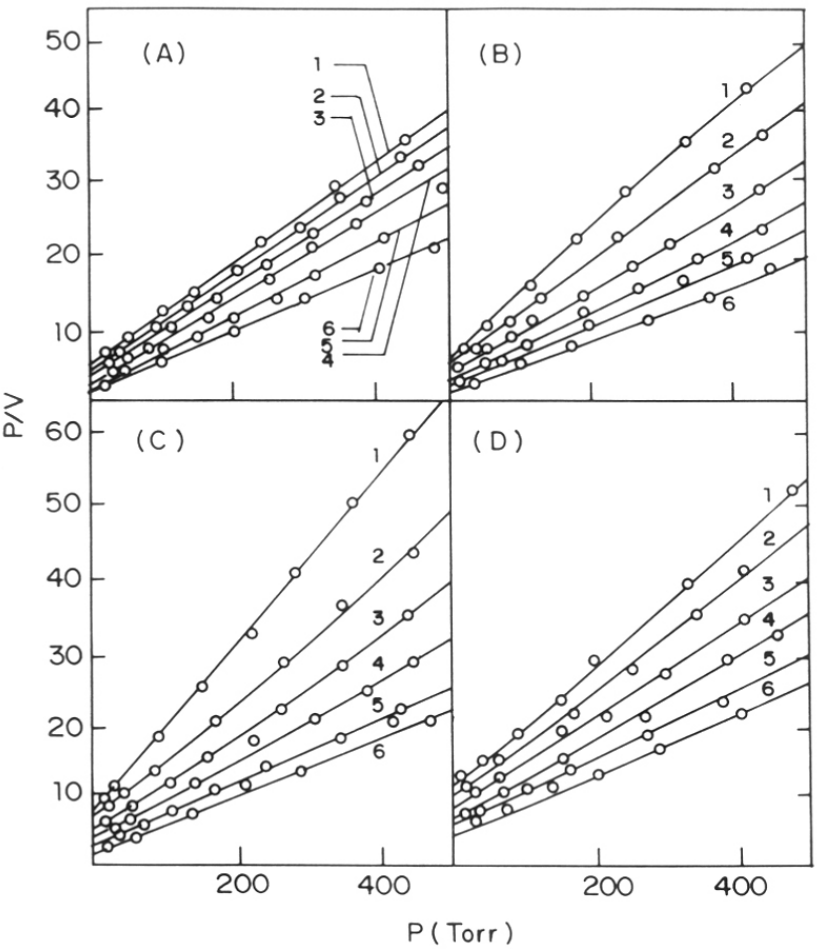

Fig.3.13: Langmuir plots for ammonia sorption in (A) Hbeta, (B) LaHbeta, (C) MgHbeta, and (D) NaHbeta at 1) 453 K, 2) 423 K, 3) 393 K, 4) 363 K, 5) 333 K, and 6) 303 K. V is the amount sorbed molecules/u.c.

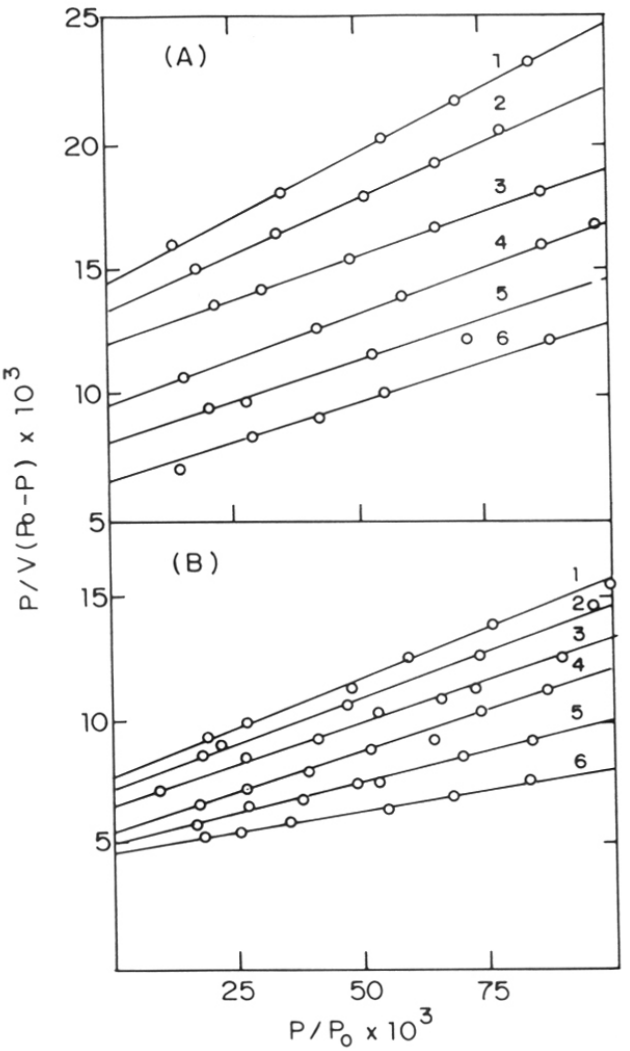

Fig.3.14: BET plots for ammonia sorption in (A) NaHbeta, and (B) Hbeta at 1) 453 K, 2) 423 K, 3) 393 K, 4) 363 K, 5) 333 K, and 6) 303 K. V is the amount sorbed molecules/u.c.

where 'A' and 'c' are constants, 'P' is an equilibrium pressure at coverage θ. 'θ' was calculated by using the monolayer (saturation) capacities obtained by Langmuir equation. In order to check the applicability of Sips equation, the plots of log [θ/1-θ)] against log P for the zeolites were constructed. Fig 3.15 shows the typical Sips plots for ammonia sorption in cation exchanged beta zeolites at 303 K. The linearity of these plots shows the applicability of the Sips equation to the sorption of ammonia in cation exchanged beta zeolites.

As the constant 'c' evaluated from linear plots approaches unity, the Sips equation reduces to Langmuir isotherm and the deviation of 'c' from unity may be taken as a measure of deviation from Langmuir approach. In the present case 'c' always has a value close to unity, irrespective of the nature of the exchanged cation and temperature of the sorption. Therefore, it seems likely that no complicating factors are involved in ammonia sorption to cause deviation from the Langmuir approach. Although the value of 'A' was always lower for the parent zeolite Na-H-beta than that for the cation exchanged forms; it did not show any specific trend with cationic species and with the isotherm temperature.

D. Chemical Affinity and the selectivity of the sorbed phase

When a gas is transferred reversibly and isothermally from the gas phase at a standard pressure P_o into an infinite amount of sorbent-sorbate mixture over which the equilibrium pressure is P, a decrease in chemical potential takes place. Neglecting the non ideality of the sorbate, the chemical affinity may be expressed[32,34]

$$\Delta \mu = RT \ln (P/P_o)$$

the $\Delta \mu$ may be taken as the quantitative measure of the chemical affinity of the sorbate for the sorbent. The plots of $-\Delta \mu$ against the amount sorbed also serve as useful criteria for the comparison of sorption affinities of a probe molecule for various cation exchanged zeolites. The plots of $-\Delta \mu$ against the amount sorbed are shown in Fig. 3.16. In general, it is seen from the Fig. 3.16, that a decrease in chemical potential is comparatively sharper at higher temperature as compared to that at lower temperature.

In the lower coverage region over the entire temperature range Na-H-beta showed lowest chemical potential while both La-H-beta and H-beta showed higher chemical potential over the entire coverage. At the higher coverage the sequence in chemical potential becomes complicated and Na-H-beta shows higher chemical potential than alkaline earth exchanged beta zeolites. In

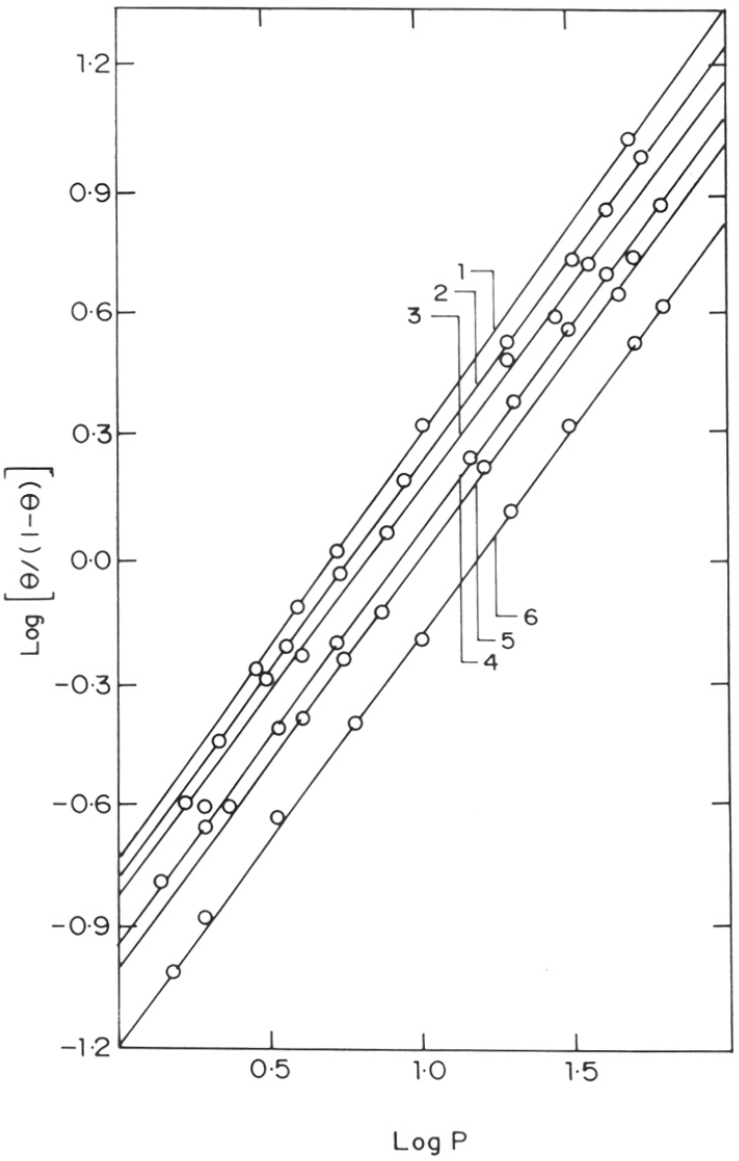

Fig.3.15: Ammonia sorption plots for the Sips equation at 453 K in 1) MgHbeta, 2) SrHbeta, 3) CaHbeta, 4) Hbeta, 5) LaHbeta, and 6) NaHbeta.

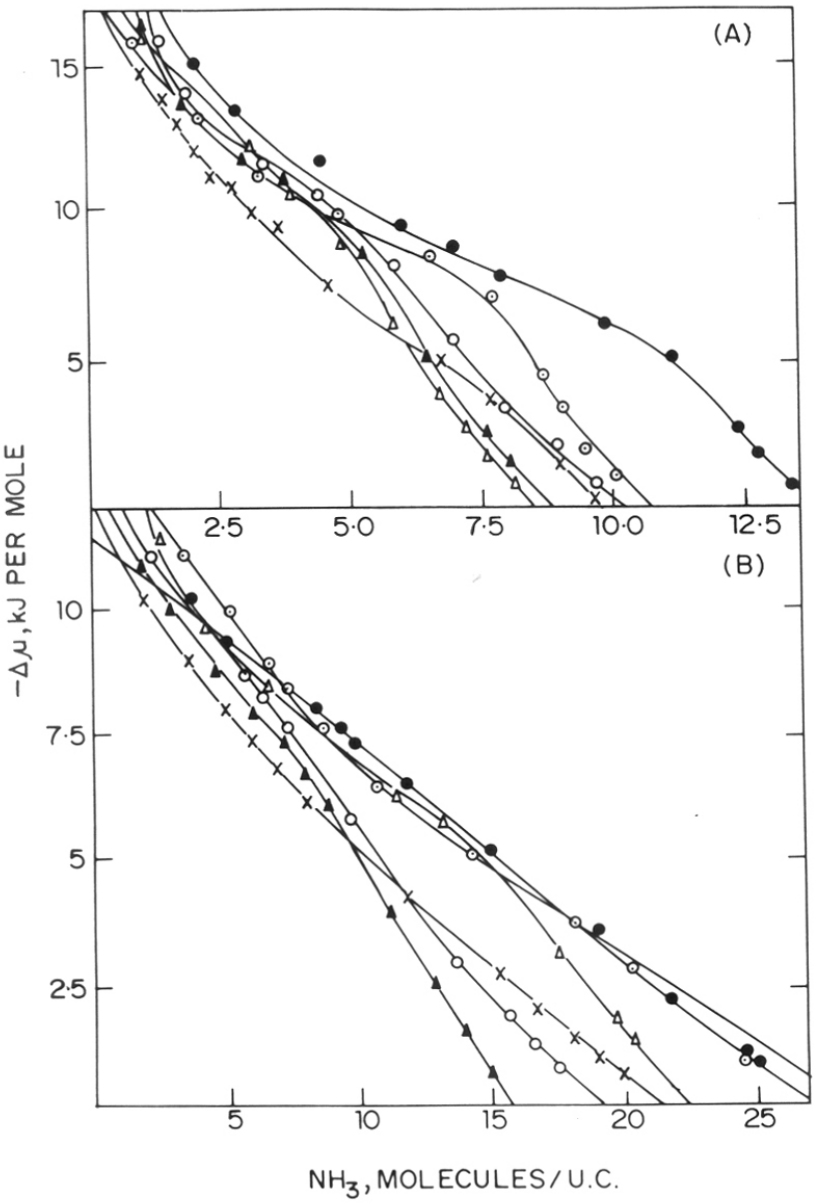

Fig.3.16: Chemical affinity for ammonia sorption at (A) 453 K, and (B) 303 K in (●) Hbeta, (⊖) LaHbeta, (Δ) MgHbeta, (o) CaHbeta, (▲) SrHbeta, and (x) NaHbeta.

the lower coverage region, the ammonia molecule probably interacts with acidic protons, whereas in the higher coverage region it interacts with extra-framework cations. Perhaps in case of Ca-H-beta and Sr-H-beta, Ca^{2+} and Sr^{2+} ions impart more basic character compared to Na^{+} ion to the zeolite lattice. In the higher coverage region the chemical potential for La-H-beta and H-beta are comparable at 303 K. H-beta exhibits a higher chemical potential over the entire coverage at 453 K.

E. Isosteric Heats (Q_{st}) of ammonia sorption

Isosteric heats of ammonia sorption, Q_{st}, are computed from the shift of sorption equilibrium with temperature at constant sorbate loading in accordance with Classius-Clapeyron relationship as follows[35,36].

$$-\Delta H = Q_{st} = R\,[(T_2.T_1)/(T_2-T_1)]\,.\,\ln\,(P_2/P_1)$$

If Q_{st} is assumed to be temperature-independent; the plots of ln P against 1/T were found to be almost linear in the present studies. Fig. 3.17 shows the variation in Q_{st} (obtained from the slope of the linear isosteres) with amount of ammonia sorbed in cation exchanged beta zeolites. The Q_{st} value at a coverage of 0.8 molecule/u.c. follows a sequence Sr-H-beta < Ca-H-beta < Na-H-beta < H-beta < Mg-H-beta < La-H-beta.

All the samples except Na-H-beta, show a wide variation in the Q_{st} value with amount of ammonia sorbed indicating increased surface heterogeneity in cation exchanged beta zeolites as compared to Na-H-beta. Similar surface heterogeneity was also reported[36] by a series of Na^{+}, La^{3+}, Ca^{2+} and H^{+} exchanged Y zeolites. The variation in Q_{st} with the amount sorbed in La-H-beta is from 41 KJ.mole^{-1} at 0.8 molecule/u.c. to 27 KJ.mole^{-1} at 6.5 molecules/u.c. On the contrary, the variation in Q_{st} in Na-H-beta at identical sorption capacity is only 24 to 18 KJ.mole^{-1}.

3.4. CONCLUSIONS

Zeolite beta and its boro- and gallo-silicate analogues have been characterized using different techniques. Evidence for the incorporation of B and Ga into the framework was obtained by XRD, i.r. and MASNMR spectroscopies. All modified beta zeolites exhibited high adsorption capacities indicating the absence of amorphous matter within their pores.

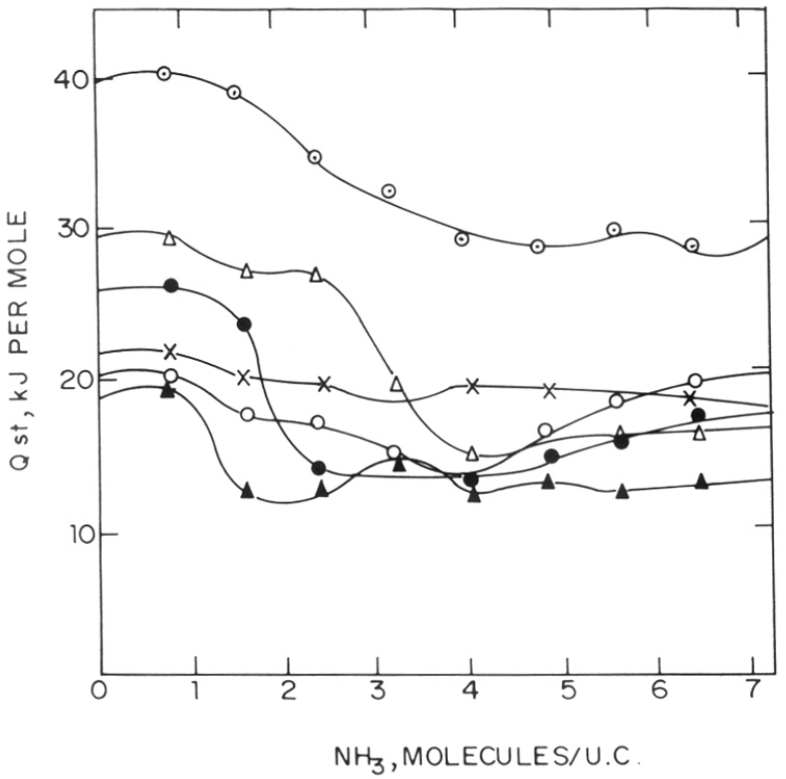

Fig.3.17: Isosteric heats (Q_{st}) for ammonia sorption in (•) Hbeta, (ɵ) LaHbeta, (Δ) MgHbeta, (o) CaHbeta, (▲) SrHbeta, and (x) NaHbeta.

Ammonia sorption isotherms were measured in cation exchanged beta zeolites. Sorption data were analyzed in terms of Dubinin, Langmuir, BET and Sips adsorption isotherm models. H-beta and La-H-beta exhibited higher chemical potential than other cation exchanged zeolites over the entire coverage and temperature range. La-H-beta showed the highest Q_{st} value and Sr-H-beta showed the lowest Q_{st} value over the entire coverage.

3.4. REFERENCES

1. Barrer, R.M., *Hydrothermal Chemistry of Zeolites,* Acadamic press, London p. 251 (1983).
2. Szostak, R., *Molecular sieves, Principles of synthesis and identification*, Van Nostrand Rheinhold, New York, p. 83 (1989).
3. Tielen, M., Geelen, M. and Jacobs, P.A., *Acta Phys. Chem.*, **31**, 1 (1985).
4. Chu, C.T.W. and Chang, C.D., *J. Phys. Chem.*, **89**, 1569 (1985).
5. Tsitsishvilli, G.V. and Andronikashvili, T.G., *Adv. Chem. Ser.*, **102**, 217 (1971).
6. Tsitsishvilli, G.V., *Adv. Chem. Ser.*, **121**, 291 (1973).
7. Smith, J.V., *Adv. Chem. Ser.*, **101**, 171, (1971).
8. Flanigen, E.M., Khatami, H. and Szymanski, H.A., *Adv. Chem. Ser.*, **101**, 201 (1971).
9. Yates, D.J.C., *"Molecular sieves"*, Soc. Chem. Ind. London, p. 334 (1968).
10. Ward, J.W., *Adv. Chem. Ser.*, **101**, 380 (1971).
11. Jacobs, P.A. and Heylen, C.F., *J. Catal.*, **34**, 267 (1974).
12. Mapes, J.E. and Eischens, R.P., *J. Phys. Chem.*, **58**, 1059 (1954).
13. Mamoru, A., *J. Catal.*, **52**, 16 (1978).
14. Vogt, V.F., Wolf, H., Bremer, H., Rubinstein, A.M., Klyachko, A.L., Brueva, J.R. and Mishin, I.V., *Z. Anorg. Alleg. Chem.*, **439**, 153 (1978).
15. Tsutsumi, K., Quikoh, H., Hagiwara, S. and Takahashi, H., *Bull. Chem. Soc. Japan*, **48**, 3756 (1975).
16. Masuda, T., Taniguchi, H., Tsutsumi, K., and Takahashi, H., *Bull. Chem. Soc. Japan*, **51**, 1965, 1970 (1978).
17. Masuda, T., Taniguchi, H., Tsutsumi, K., and Takahashi, H., *Bull. Chem. Soc. Japan*, **52**, 2849 (1979).
18. Masuda, T., Taniguchi, H., Tsutsumi, K., and Takahashi, H., *J. Japan Petro. Inst.*, **22**, 67 (1979).
19. Bellussi, G., Millini, R., Carati, A., Maddinelli, G. and Gervasini, A., *Zeolites*, **10**, 642 (1990).
20. Perez-Pariente, J., Martens, J.A. and Jacobs, P.A., *Appl. Catal.*, **31**, 35 (1987).
21. Khodakov, A.Y., Kustov, L.M., Bondarenko, T.N., Dergachev, A.A., Kazansky, V.B., Minachev, K.M., Borbely, G. and Beyer, H.K., *Zeolites*, **10**, 603 (1990).
22. Szostak, R. and Thomas, T.L., *J. Catal.*, **100**, 555 (1986).
23. Szostak, R. and Thomas, T.L., *J. Chem. Soc. Chem. Com.*, 113 (1986).
24. Wadlinger, R.L., Kerr, G.T. and Rosinski, E.J., US Pat. 3 308 069 (1967).

25. Kiselev, A.V., *Discuss. Faraday Soc.*, **40**, 205 (1965).
26. Shiralkar, V.P. and Kulkarni, S.B., *Zeolites*, **4**, 330 (1984).
27. Coughlan, B. and McEntee, J.J., *Proc. R. Irish Acad. Sect. B*, **76**, 473 (1976).
28. Coughlan, B. and McCann, W.A., *J. Chem. Soc., Faraday Trans. I*, **75**, 1969 (1979).
29. Coughlan, B. and Larkin, P.M., *Chem. Ind.*, 275 (1976).
30. Topsoe, N., Pederson, K. and Derouane, E.G., *J. Catal.*, **70**, 41 (1981).
31. Dubinin, M.M. and Radushkevich, L.V., *Proc. Acad. Sci.* USSR, **55**, 327 (1974).
32. Shiralkar, V.P. and Kulkarni, S.B., *J. Colloid & Interface Sci.*, **108**, 1 (1985).
33. Sips, R.J., *Chem. Phys.*, **16**, 491 (1948).
34. Barrer, R.M. and Coughlan, B., *"Molecular sieves", Soc. Chem. Ind. London*, 141, 231, 241 (1968).
35. Shiralkar, V.P. and Kulkarni, S.B., *Zeolites*, **5**, 37 (1985).
36. Shiralkar, V.P. and Kulkarni, S.B., *J. Colloid & Interface Sci.*, **109**, 115 (1986).

CHAPTER 4

CATALYTIC REACTIONS OVER BETA ZEOLITES

4.1. INTRODUCTION

Zeolite beta has a three dimensional, 12-membered ring pore system made up of two different types of channels with diameters of 7.3 and 5.5 Å[1], respectively (shown in Fig.1.5). On account of its rigid three-dimensional network of large pores with high framework SiO_2/Al_2O_3 ratio it is a potential catalyst in many hydrocarbon conversion processes of industrial importance. In addition, the comparatively smaller dimension of one of the two types of pores (5.5 Å) offers a certain level of shape selectivity similar to that observed in medium pore zeolites.

Zeolite beta is an active catalyst in the alkylation of benzene with dodecene, leading to phenyl decanes[2]. It has also been used in the formation of diphenylmethane from benzene and trioxane[3]. Dealuminated zeolite beta loaded with noble metal behaves as a bifunctional zeolite catalyst which is able to dewax hydrocarbon feedstocks mainly by isomerization of the waxy components[4-6]. It is effective in lowering the pore point of petroleum oil by isomerizing the normal alkanes contained therein to their branched isomers, rather than cracking them to lighter alkanes, as is done by other zeolites such as ZSM-5 or erionite[4,5]. The shape selective catalytic properties of zeolite beta, especially in the cracking of alkanes and in the isomerization of m-xylene have been investigated[7-9]. Zeolite beta is also used in the disproportionation of cumene to produce diisopropylbenzenes[10]. It is also a promising catalyst in the conversion of gas-oil to LPG and gasoline[11], and in the isomerization of n-hexane to dimethylbutanes[12].

Cumene, an important intermediate for the production of phenol and acetone, is obtained by using of solid phosphoric acid (SPA) on silica[13] and Friedel-Craft catalysts, like aluminium chloride[14]. Alkylation of benzene with propylene to produce cumene is a well-known reaction. A vapour-phase process with a phosphoric acid on kieselguhr catalyst and liquid-phase alkylation in the presence of sulfuric acid are used[15]. Zeolites also serve as a catalysts for a variety of alkylation reactions involving formation of ethylbenzene[16,17] and xylenes[18,19]. Zeolites are also used in the isopropylation of benzene to produce cumene[20-24].

Cymenes (isopropyltoluenes and methylcumenes), especially, the m- and p-isomers are important intermediates in the production of cresols and isopropylphenols which are major intermediates for resins[25]. In addition, they are also used as raw materials for plasticizers. p-Cymene is also used as a heat transfer medium and a starting material in many organic syntheses. The other applications of cymenes are in polymers, perfumery, fungicides, pesticides and special solvents. The alkylation of toluene with propylene to produce cymenes over zeolites

has also been done[26]. In addition to avoiding environmental and corrosion problems associated with Fridel-Crafts as well as phosphoric acid catalysts, the use of the zeolite catalysts were found to prolong the useful cycle length of the process.

The main aim of this chapter is to examine the catalytic properties of zeolite beta in the isopropylation of benzene and toluene to cumene and cymenes, respectively.

4.2. EXPERIMENTAL

The catalytic reactions were carried out in a fixed bed, down flow, vertical silica reactor having an inner diameter of 1.5 cm and 30 cm length. It was equipped with a thermocouple in a thermowell for sensing the reaction temperature. The powder form of the zeolites was pressed using hydraulic press into pellets. These pellets were then crushed to 10-20 mesh size and then were used in the catalytic reactions. A 1.0 g (anhydrous basis) of catalyst was loaded in the central zone of the reactor in such a way that the catalyst bed was sandwiched between inert porcelain beads. The reactor was placed in a double-zone furnace (Fig.4.1). The catalyst was activated at 753 K for 8 h in a flow of dry air before use. The catalyst was then flushed with dry nitrogen and cooled to reaction temperature. The liquid reactants were injected using a syringe pump (Sage Instruments, Model 352, USA) at the required rate .

The reaction products were passed through the condenser cooled by chilled water. The condensed liquid products were collected periodically. The products were analysed in a gas chromatograph (Hewlett Packard 5880 A) equipped with a capillary column (50 m X 0.25 mm crosslinked methyl silicone gum). The products were identified by GC-MS (Shimadzu QCMS-QP2000A). Benzene, toluene and isopropanol used were of AnalaR grade.

4.3. RESULTS AND DISCUSSION

4.3.1. ISOPROPYLATION OF BENZENE

The main reaction schemes can be presented as:

benzene	+	isopropanol	--------->	cumene + H_2O
cumene	+	isopropanol	--------->	diisopropylbenzene (DIPB) + H_2O
DIPB	+	benzene	--------->	2 cumene
cumene			--------->	benzene + propylene
cumene			--------->	n-propylbenzene

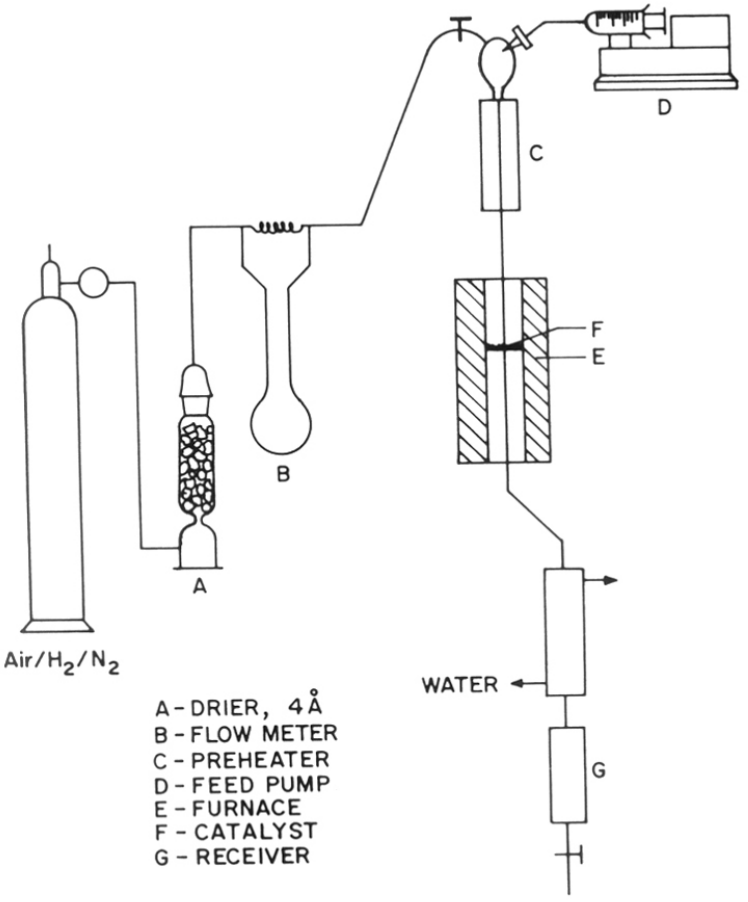

Fig.4.1: **Fixed bed, down flow reactor used for reactions in this study.**

a. Effect of SiO_2/Al_2O_3 ratio

The influence of the SiO_2/Al_2O_3 ratio of H-beta on the product distribution in the alkylation of benzene with isopropanol is shown in Table 4.1. This reaction is known to proceed through the activation of propene formed[27], during the dehydration of alcohol by the catalyst. The activated propene then reacts with benzene and cumene to produce cumene and diisopropyl-benzenes (DIPB), respectively. The conversion of isopropanol in all the cases was more than 99 % and independent of the SiO_2/Al_2O_3 ratios. The higher formation of DIPB over the sample with SiO_2/Al_2O_3 of 58 is expected as: i) the rate of alkylation of cumene is faster than the rate of alkylation of benzene[27] and ii) the transalkylation reaction needs higher acidity[28]. This shows that the secondary reaction such as disproportionation of DIPB is more significant at the lower SiO_2/Al_2O_3 ratios. In this reaction, in addition to the alkylation (which yields isopropyl and diisopropylbenzenes), other undesired reactions such as isomerization, cracking and dispro-portionation of alkyl aromatics also occur. Formation of such products consume reactants (benzene and alcohol) without producing the desired product, and, hence, leads to the lower selectivity to cumene.

It is also observed (Table 4.1) that with the increase in SiO_2/Al_2O_3 ratio from 20 to 58, the concentration of n-propylbenzene decreases. Elimination of the some of the acid sites, wherein the isomerization of cumene occurs, is probably one of the reasons for the lesser concentrations of n-propylbenzene. Hence, the further studies were carried out over SiO_2/Al_2O_3 of 26 with varying reaction parameters such as reaction temperature, weight hourly space velocity (WHSV), reactant mole ratio and the nature of the alkylating agent. In this reaction, all the results were tabulated after 4 h time-on-stream.

b. Effect of temperature

Temperature has shown a marked effect on the product distribution (Table 4.2). Formation of DIPB decreases at high temperatures, due to the transalkylation of DIPB with benzene to cumene. The disproportionation and isomerization of cumene also occurs at temperatures above 210° C. At the higher reaction temperatures, the formation of side products like toluene, ethylbenzene, n-propylbenzene and C_{10} aromatics is also seen. Formation of these products is due to the isomerization and cracking reactions of alkylbenzenes taking place above 210° C.

Table 4.1: Effect of SiO_2/Al_2O_3 ratio over H-beta zeolites in isopropylation of benzene. Temp.=210° C; benzene/isopropanol mole ratio=8 and space velocity=4 h^{-1}.

	SiO_2/Al_2O_3 ratio			
Products (wt.%)	20	26	42	58
C_3 conversion	99.98	99.94	99.90	99.90
Aliphatics	0.16	0.16	0.19	0.23
Benzene	81.56	81.50	81.61	81.69
Toluene + xylenes	0.46	0.43	0.49	0.48
Cumene	16.91	16.84	16.62	16.41
n-propylbenzene	0.09	0.05	0.02	0.01
C_{10} aromatics	0.19	0.26	0.26	0.28
1,3-DIPB[a]	0.42	0.50	0.54	0.61
1,4-DIPB	0.19	0.21	0.25	0.28
Selectivity (%)				
Cumene	93.94	93.55	92.33	91.16
(Cumene + DIPB)	98.95	99.39	98.84	98.51

[a] DIPB = diisopropylbenzene.

Table 4.2: Effect of temperature in isopropylation of benzene over H-beta. SiO_2/Al_2O_3 = 26, Temp.=210° C; benzene/isopropanol mole ratio=8 and space velocity=4 h^{-1}.

Products (wt.%)	Temperature (°C)					
	150	180	210	230	250	270
C_3 conversion	99.80	99.87	99.94	99.93	99.90	99.94
Aliphatics	0.14	0.21	0.16	0.31	0.43	0.48
Benzene	82.79	81.83	81.50	81.82	82.49	82.68
Toluene + xylenes	0.21	0.33	0.43	0.49	0.63	0.81
Cumene	14.21	15.78	16.84	16.51	15.46	14.98
n-propylbenzene	0.01	0.02	0.05	0.06	0.07	0.09
C_{10} aromatics	0.19	0.31	0.26	0.21	0.34	0.42
1,3-DIPB[a]	1.50	0.93	0.50	0.32	0.28	0.25
1,4-DIPB	0.72	0.32	0.21	0.10	0.09	0.08
Selectivity (%)						
Cumene	78.88	87.67	93.55	91.72	85.89	83.22
(Cumene + DIPB)	97.15	98.00	99.39	95.17	88.96	85.95

[a] see foot note in Table 4.1.

c. Effect of space velocity (WHSV)

Fig.4.2 shows that, while the overall selectivity to cumene plus DIPB is almost constant; the selectivity to cumene decreases with increasing space velocity. The reason for the higher selectivity to cumene at higher contact times (lower WHSV), is due to the transalkylation of DIPB with benzene. At higher contact times cumene is also isomerized to n-propylbenzene (shown in Fig.4.2).

d. Effect of benzene/isopropanol mole ratio

Higher benzene-to-isopropanol mole ratios favour the selective formation of cumene (Fig.4.3). At lower mole ratios, the formation of DIPB is observed in higher concentration. A decrease in the selectivity of isopropanol to cumene is observed at lower mole ratios. The higher concentration of isopropanol over the catalyst, leads to higher DIPB. This results in the preferential alkylation of cumene (rather than that of benzene), to form DIPB. Due to the steric hindrance the formation of 1,2-DIPB isomer did not occur.

e. Effect of the alkylating agent

The specific alkylating agent may exert an influence on the selectivity and stability of the catalyst. Hence, to study the effect of an alkylating agent, isopropylation reaction was carried out using propylene and isopropanol (Table 4.3). In both the cases, the selectivity to cumene is almost same with identical product distribution pattern. However, a faster deactivation is observed when propylene is used as an alkylating agent. The stronger adsorption of olefin on the active site may be one of the reasons for the faster deactivation. Also, the alkylation of benzene with n-propanol did not yield more n-propylbenzene. The major product was isopropylbenzene. The propyl cation formed during this reaction, rearranges rapidly to the more stable isopropyl (secondary carbonium ion) cation and reacts with benzene.

f. Effect of time-on-stream

The activity of this catalyst was tested for more than 500 h (Fig.4.4). During this study the selectivity to cumene decreased only marginally, but the overall selectivity to cumene and DIPB remained almost constant. A steady but slow deactivation was noticed with time-on-stream.

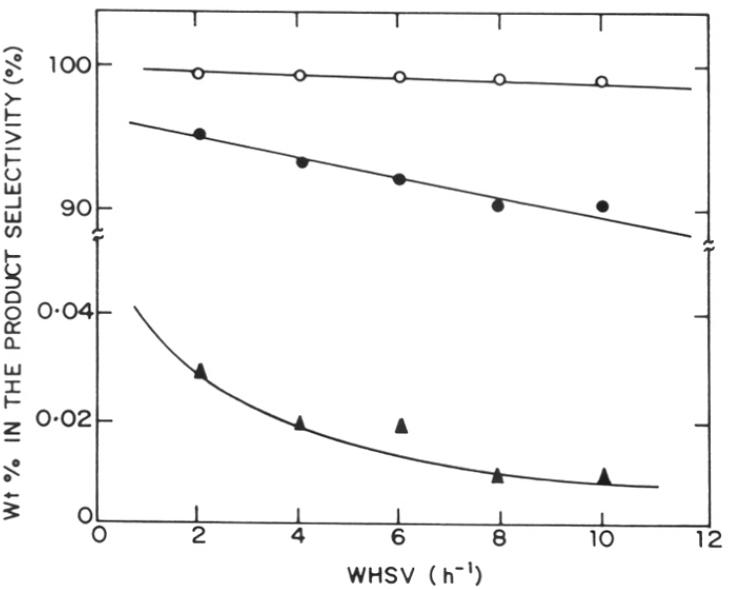

Fig.4.2: **Effect of space velocity on product distribution. Reactants mole ratio = 8, temperature = 210°C; (o) cumene, (o) [cumene + DIPB] and (▲) *n*-propylbenzene.**

Table 4.3: Effect of alkylating agent over H-beta in isopropylation of benzene. SiO_2/Al_2O_3=26, Temp.=210° C; benzene/C_3 mole ratio=8 and space velocity=4 h^{-1}.

Products (wt.%)	alkylating agent	
	Isopropanol	Propylene
C_3 conversion	99.94	99.91
Aliphatics	0.16	0.21
Benzene	81.50	81.43
Toluene + xylenes	0.43	0.69
Cumene	16.84	16.58
n-propylbenzene	0.05	0.08
C_{10} aromatics	0.26	0.29
1,3-DIPB[a]	0.50	0.48
1,4-DIPB	0.21	0.23
Selectivity (%)		
Cumene	93.55	92.11
(Cumene + DIPB)	99.39	97.94

[a] see foot note in Table 4.1.

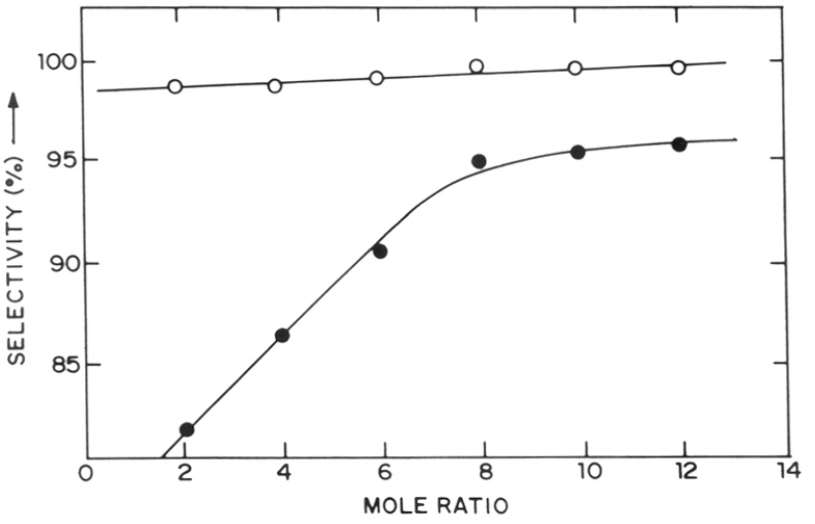

Fig.4.3: Effect of reactants mole ratio on the selectivity of isopropanol. Temperature = 210°C, space velocity = 4 h^{-1}; (●) cumene and (o) [cumene + DIPB].

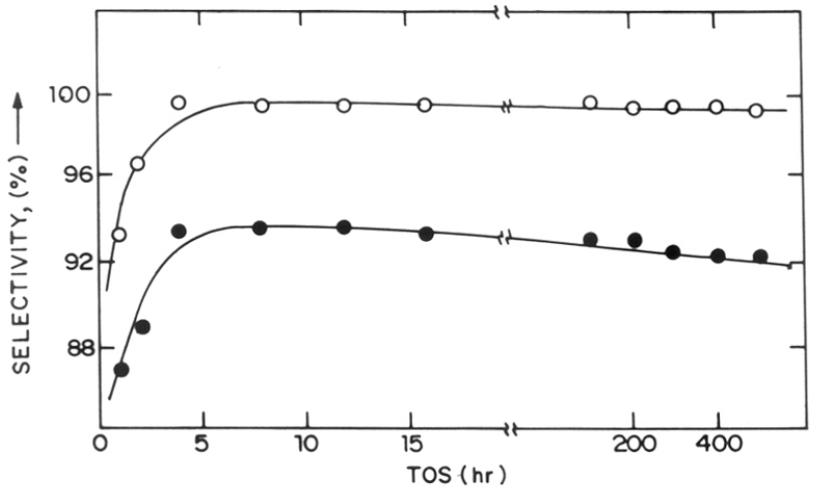

Fig.4.4: Effect of time-on-stream on the selectivity of isopropanol. Temperature = 210°C, space velocity = 4 h^{-1}, reactants mole ratio = 8; (●) cumene and (o) [cumene + DIPB].

g. Effect of isomorphous substitution

Table 4.4 compares the catalytic activity for H-Al-beta, H-Ga-beta and H-B-beta zeolite catalysts. The conversion of isopropanol is >99 % over all three zeolites. The selectivity towards cumene follows the sequence H-Al-beta > H-Ga-beta > H-B-beta and the selectivity towards the DIPB is found to be in the reverse order. The formation of cracked products such as toluene and ethylbenzene is also found to be less in H-Ga-beta and H-B-beta than the H-Al-beta catalyst. This indirectly suggests that the H-Ga-beta and H-B-beta catalysts are less acidic as compared to that of Al analogue[29]. The higher concentration of DIPB over H-Ga-beta and H-B-beta shows that the transalkylation ability of these catalysts is lower than that of H-Al-beta catalyst under the experimental conditions.

h. Effect of the zeolitic structure

The catalytic activity and selectivity in the isopropylation of benzene with isopropanol over H-mordenite, H-ZSM-12 and H-beta is compared in Table 4.5. The physico-chemical properties of these three zeolites are presented in Table 4.6 and structural differences are also shown in Fig.4.5. In all the zeolites, the conversion of isopropanol is more than 99 %. A fast deactivation was noticed within 10 h over H-mordenite; while a steady activity was observed in H-ZSM-12 and H-beta even after 400 h of time-on-stream. The selectivity to cumene is also high in the case of the latter two zeolites. The side products like aliphatics, toluene and C_8 aromatics etc., are higher in H-mordenite, resulting in a decrease in the selectivity to cumene. Among H-ZSM-12 and H-beta zeolites, H-beta showed higher selectivity towards cumene. Among the twelve-membered ring zeolites studied, H-beta was found to be the best catalyst for the isopropylation of benzene followed by H-ZSM-12 and H-mordenite. Eventhough H-ZSM-12 and H-beta zeolites are highly siliceous and more stable in the isopropylation reaction, but the higher selectivity to cumene in H-beta may be attributed to its typical interconnecting channel system with no cavities.

i. Effect of the exchanged cation

The influence of the exchanged cation on Na-H-beta and the product distribution is shown in Table 4.7. Although in H-beta and La-H-beta the conversion of isopropanol is high, with higher selectivity towards cumene, selectivity to DIPB was found to be low. In Na-H-beta, Mg-H-beta and Ca-H-beta the conversion of isopropanol and selectivity to cumene was found to be comparatively low, though the selectivity to DIPB is higher.

Table 4.4: Effect of Isomorphous substitution over H-beta zeolites in isopropylation of benzene. Temp.=210° C; benzene/C_3 mole ratio=8 and space velocity=4 h^{-1}.

Zeolite	B-beta (30)[b]	Al-beta (26)	Ga-beta (24)
Acidity (m.M of NH_3/g.)	0.235	0.286	0.259
Products (wt.%)			
C_3 conversion	99.90	99.94	99.91
Aliphatics	0.10	0.16	0.14
Benzene	82.47	81.50	81.91
Toluene + xylenes	0.17	0.43	0.16
Cumene	15.62	16.84	16.22
n-propylbenzene	0.01	0.05	0.01
C_{10} aromatics	0.18	0.26	0.19
1,3-DIPB[a]	0.91	0.50	0.62
1,4-DIPB	0.51	0.21	0.31
Selectivity (%)			
Cumene	86.78	93.55	90.11
(Cumene + DIPB)	98.41	99.39	98.63

[a] see foot note in Table 4.1..

[b] bracketed figures indicates SiO_2/M_2O_3 ratio, M = B, Al and Ga.

Table 4.5: Isopropylation of benzene in large pore zeolites.
Temp.=210° C; benzene/isopropanol mole ratio=8 and space velocity=4 h^{-1}.

Products (wt.%)	zeolite		
	H-mordenite	H-beta	H-ZSM-12
C_3 conversion	99.91	99.94	99.90
Aliphatics	0.22	0.16	0.18
Benzene	82.58	81.50	81.41
Toluene + xylenes	0.58	0.43	0.31
Cumene	14.91	16.84	16.48
n-propylbenzene	0.32	0.05	0.01
C_{10} aromatics	0.41	0.26	0.25
1,3-DIPB*	0.72	0.50	0.61
1,4-DIPB	0.31	0.21	0.27
Selectivity (%)			
Cumene	82.83	93.55	91.56
(Cumene + DIPB)	91.32	99.39	98.82

* see foot note in Table 4.1.

Table 4.6: Structural and Physico-chemical properties of zeolites.

Zeolite	Beta	Mordenite	ZSM-12
Channel structure	three-dimensional interconnecting channels	Uni-dimensional interconnecting channels	Uni-dimensional non interconnecting channels
Pore opening	12 MR 7.3 X 6.8 Å (straight channel) 5.6 X 6.8 Å (sinusoidal channel)	12 MR 6.5 X 7.0 Å (12 MR) 2.6 X 5.7 Å (8 MR)	12 MR 5.5 X 5.9 Å
Unit cell crystal symmetry	monoclinic and tetragonal	orthorhombic	monoclinic
Si/Al ratio	13	6.8	62
Acidity (m.M of NH_3/g.	0.286	0.534	0.067
sorption capacity (wt.%)[a]			
benzene	21.9	9.8	13.2
n-hexane	19.1	11.9	14.2
cyclohexane	19.4	9.3	10.8

[a] P/P_o = 0.5 and temperature = 298 K.

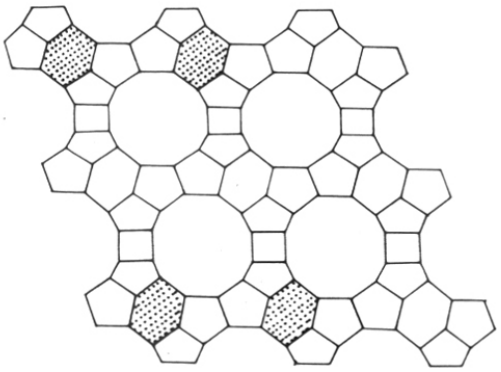

(A)

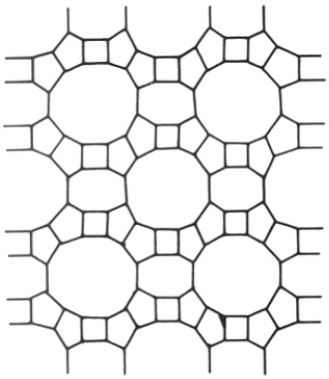

(B)

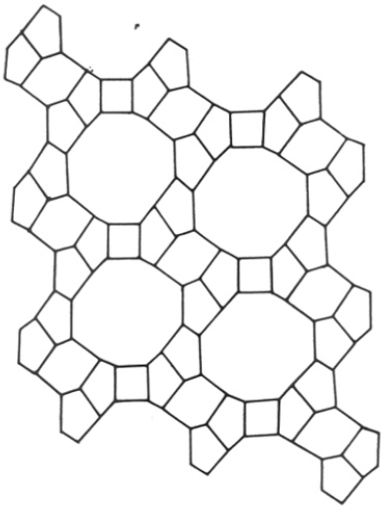

(C)

Fig.4.5: Structure of various large pore zeolites (A) beta (B) mordenite and (C) ZSM-12.

Table 4.7: Effect of cation exchange on beta zeolite in the isopropylation of benzene. SiO_2/Al_2O_3 = 26, Temp.=210° C; benzene/isopropanol mole ratio=8 and space velocity=4 h^{-1}.

Products (wt.%)	Zeolite				
	H-beta	La-H-beta	Na-H-beta	Mg-H-beta	Ca-H-beta
C_3 conversion	99.94	98.73	92.33	95.30	94.14
Aliphatics	0.16	0.14	0.48	0.12	0.14
Benzene	81.50	82.26	83.28	83.91	83.62
Toluene + xylenes	0.43	0.26	0.19	0.17	0.17
Cumene	16.84	16.31	14.72	14.51	13.80
n-propylbenzene	0.05	0.01	0.03	0.02	0.02
C_{10} aromatics	0.26	0.17	0.19	0.15	0.18
1,3-DIPB[a]	0.50	0.51	0.62	1.03	1.33
1,4-DIPB	0.21	0.22	0.28	0.45	061
Selectivity (%)					
Cumene	93.55	90.61	81.77	80.61	76.67
(Cumene + DIPB)	99.39	96.62	89.22	92.83	92.66

[a] see foot note in Table 4.1.

The relative rates of the formation of cumene and DIPB reflect their diffusion-controlled transport in the modified pore system and may, therefore, form the basis of characterizing the pore structure. Among these cation exchanged zeolites La-H-beta is as active as H-beta. The increase in activity of La-H-beta may be attributed to protons produced upon the hydrolysis of the water molecules associated with the rare-earth cation[30].

4.3.2. TRANSALKYLATION OF BENZENE WITH DIPB

The transalkylation of benzene with DIPB to cumene is shown in Table 4.8. The formation of cumene is possible either by transalkylation of DIPB with benzene or dealkylation of DIPB. During the transalkylation reaction, one mole of benzene and DIPB each reacts to form two moles of cumene. During the dealkylation reaction, one mole of DIPB gives one mole of cumene. From the Table 4.8, it is concluded that the transalkylation of DIPB is more favourable than the dealkylation resulting in the higher yield of cumene.

4.3.3. ISOPROPYLATION OF TOLUENE

a. Effect of SiO_2/Al_2O_3 ratio

The influence of the SiO_2/Al_2O_3 on the isopropylation of toluene with isopropanol over H-beta is shown in Table 4.9. The main reactions are:

toluene	+	isopropanol	--------->	cymenes + H_2O
cymene	+	isopropanol	--------->	diisopropyltoluene (DIPT) + H_2O
DIPT	+	toluene	--------->	2 cymenes
cymene			--------->	toluene + propene
2 Toluene			--------->	xylenes + benzene

The conversion of isopropanol is more than 99 % in all the cases. Although the product pattern obtained over all these samples was similar, a small increase in the yield of DIPT is observed over the sample with a SiO_2/Al_2O_3 ratio of 58. This increase may also be attributed to i) the rate of alkylation of cymenes being higher than the rate of alkylation of toluene[27] and ii) the transalkylation reaction requiring higher acidity[28]. The detailed studies on this reaction were carried out over the sample with $SiO_2/Al_2O_2O_3$ = 26, by varying reaction parameters. The results at 2 h time-on-stream are utilised in the discussion below.

Table 4.8: Transalkylation of benzene with DIPB over beta zeolite. SiO_2/Al_2O_3 = 26; benzene/DIPB mole ratio=16 and space velocity=4 h^{-1}.

Products (wt.%)	Temperature (°C)		
	Feed	200	220
DIPB conversion	---	90.28	93.10
Aliphatics	0.08	0.02	0.02
Benzene	88.87	83.74	82.33
Toluene + xylenes	----	0.49	1.10
Cumene	----	14.64	14.87
n-propylbenzene	----	0.02	0.04
C_{10} aromatics	----	0.02	0.15
1,3-DIPB[a]	9.94	0.75	0.56
1,4-DIPB	0.26	0.24	0.15
Selectivity (%)			
Cumene	----	95.57	93.94

[a] see foot note in Table 4.1.

Table 4.9: Effect of SiO_2/Al_2O_3 ratio on isopropylation of toluene over H-beta zeolites. Temp.=180° C; toluene/isopropanol mole ratio=8 and space velocity=4 h^{-1}.

	SiO_2/Al_2O_3 ratio			
Products (wt.%)	20	26	42	58
C_3 conversion	99.92	99.90	99.91	99.89
Aliphatics	0.05	0.04	0.04	0.04
Benzene	0.17	0.16	0.18	0.15
Toluene	81.79	81.87	82.12	82.41
Xylenes	0.41	0.40	0.34	0.30
Cumene	0.39	0.41	0.36	0.31
m-Cymene	10.64	10.61	10.40	10.29
p-Cymene	5.07	5.02	4.78	4.63
o-Cymene	0.83	0.89	0.77	0.69
Σ DIPB[a]	0.09	0.10	0.14	0.16
Σ DIPT[b]	0.47	0.48	0.82	0.99
Selectivity (%)				
Cymenes	96.05	95.93	92.62	90.65
DIPT	3.92	4.01	6.85	8.28

[a] DIPB = diisopropylbenzene

[b] DIPT = diisopropyltoluene

b. Effect of temperature

The influence of temperature on the isopropylation of toluene is shown in Table 4.10. The concentration of DIPT decreased at higher temperatures, due to dealkylation reactions and transalkylation of DIPT with toluene to cymenes. The disproportionation of cymenes also increased with increase in the reaction temperature. At higher reaction temperatures, the formation of the by-products such as benzene, xylenes, cumene and DIPB are enhanced.

c. Effect of space velocity (WHSV)

Lower space velocities are found to be favourable for the selective formation of cymenes (Fig.4.6). Total selectivity to cymenes plus DIPT is similar over the entire range of space velocities. The selectivity to cymenes alone increases at lower space velocities. The reason for the higher selectivity to cymenes at higher contact times (lower WHSV), is the transalkylation of DIPT with toluene to yield cymenes.

d. Effect of the toluene/isopropanol mole ratio

At higher toluene-to-isopropanol mole ratios the selectivity to cymenes is very high (Fig.4.7). At lower mole ratios the formation of DIPT is more. A decrease in the selectivity of isopropanol to cymenes is observed at lower mole ratios. This is probably due to the higher isopropanol concentration over the catalysts, resulting in the preferential alkylation of cymenes (rather than that of toluene) to form DIPT. The direct conversion of isopropanol to aromatic hydrocarbons can also complicate picture.

e. Effect of time-on-stream

The product distribution as a function of time-on-stream (TOS) is shown in Fig.4.8. Although the catalyst is still active at TOS of 200 h, a very slow deactivation is noticed with the duration of run. During this slow deactivation, coke induced para selectivity[31] is observed, resulting in a higher concentration of p-cymene.

f. Effect of zeolitic structure

The catalytic performance of the three large pore zeolites, H-mordenite, H-ZSM-12 and H-beta has been compared in Table 4.11. The conversion of isopropanol is almost complete in all three zeolites. The by-products like xylenes, benzene, toluene and cumene produced through dealkylation reactions are high, and the selectivity to cymenes plus DIPT ise low in

Table 4.10: Effect of temperature on isopropylation of toluene over H-beta SiO_2/Al_2O_3 ratio=26; toluene/isopropanol mole ratio=8 and space velocity=4 h^{-1}.

Products (wt.%)	Temperature (°C)			
	160	180	200	220
C_3 conversion	98.52	99.90	99.89	99.90
Aliphatics	0.05	0.04	0.05	0.05
Benzene	0.10	0.16	0.36	0.59
Toluene	82.70	81.87	81.43	79.63
Xylenes	0.15	0.40	0.47	0.55
Cumene	0.16	0.41	0.42	0.55
m-Cymene	9.05	10.61	10.99	11.34
p-Cymene	5.23	5.02	4.75	4.51
o-Cymene	1.21	0.89	0.80	0.71
Σ DIPB[a]	0.09	0.10	0.11	0.10
Σ DIPT[b]	1.20	0.48	0.43	0.39
Selectivity (%)				
Cymenes	89.95	95.93	96.05	96.16
DIPT	10.03	4.01	3.59	3.26

[a,b] see foot notes in Table 4.9.

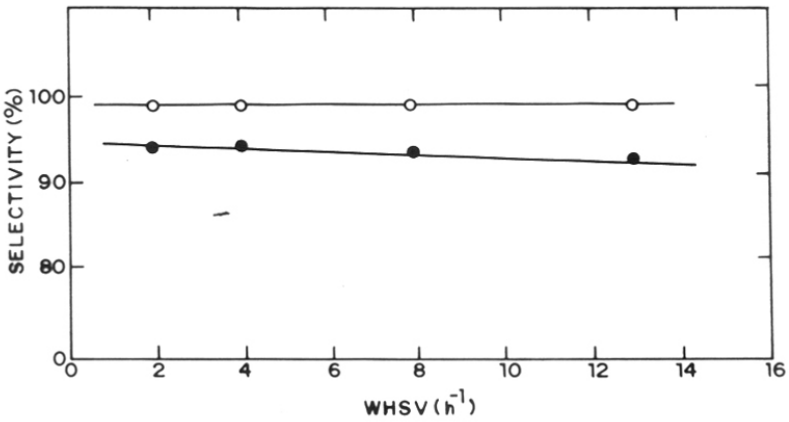

Fig.4.6: Effect of space velocity in the isopropylation of toluene. Reactants mole ratio = 8, temperature = 180°C; (•) cymenes and (o) [cymenes + DIPT].

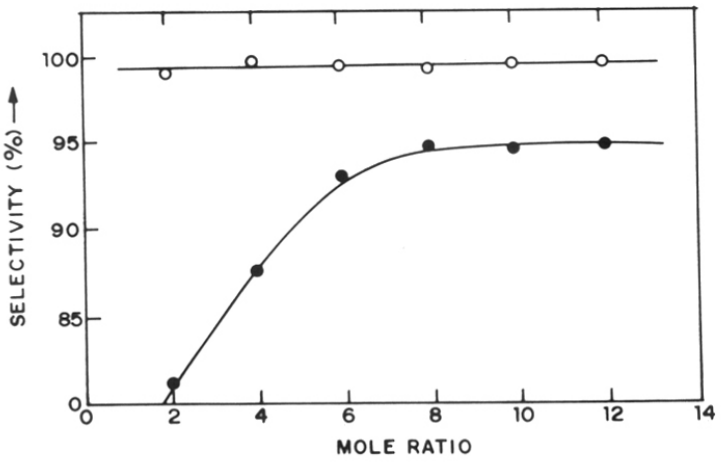

Fig.4.7: Effect of reactants mole ratio on the isopropylation of toluene. Temperature = 180°C, space velocity = 4 h^{-1}; (•) cymenes and (o) [cymenes + DIPT].

Table 4.11: Isopropylation of toluene in large pore zeolites.
Temp.=180° C; toluene/isopropanol mole ratio=8 and space velocity=4 h^{-1}.

Products (wt.%)	Zeolite		
	H-beta	H-mordenite	H-ZSM-12
C_3 conversion	99.90	99.91	99.84
Aliphatics	0.04	0.02	0.02
Benzene	0.16	0.86	0.09
Toluene	81.87	79.32	83.01
Xylenes	0.40	1.78	0.13
Cumene	0.41	0.63	0.13
m-Cymene	10.61	10.56	9.06
p-Cymene	5.02	4.91	5.45
o-Cymene	0.89	0.75	1.33
p/(*o*+*m*) cymenes	0.44	0.43	0.52
Σ DIPB[a]	0.10	0.13	0.09
Σ DIPT[b]	0.48	0.38	0.90
Selectivity (%)			
Cymenes	95.93	94.19	91.98
DIPT	4.01	3.18	7.52

[a,b] see foot notes in Table 4.9.

case of H-mordenite, while beta and ZSM-12 exhibit better selectivity to cymenes and DIPT. Between H-beta and H-ZSM-12, the selectivity to cymenes is more in the case of H-beta zeolite. It is likely that beta with a more open structure, larger pore dimensions and comparatively lower SiO_2/Al_2O_3 ratio (higher acid site density) is able to transalkylate more of the DIPT with toluene to yield cymenes than H-ZSM-12.

A comparison of the activity and stability of these three zeolites is presented in Fig.4.9. All the catalysts showed the same initial conversion; but a faster deactivation is noticed in H-mordenite. However, H-beta and H-ZSM-12 zeolites have a steady and stable activity even after 200 hours on-stream. The phenomenon of deactivation in H-mordenite is probably related to its uni-dimensional pore system and the higher acid site density of the catalyst[32]. A higher acidity results in more pronounced dealkylation as in the case of H-mordenite. The by-products formed during the reaction, in particular the olefins, act as a coke precursors and deactivate the catalysts. Further, the unidirectional pore system of mordenite is also more prone to pore blockage by coke.

The para selectivity among the cymene isomers follows the order H-ZSM-12 > H-beta ≅ H-mordenite. The observed para selectivities can be rationalized on the basis of differences in pore geometry of these zeolites (shown in Fig.4.5). Two parameters i.e., the diameter of the channels and the presence of large cavities exert influence on the p-selectivity among cymenes produced. While zeolite beta has pore intersections, mordenite has side pockets and ZSM-12 has non-interconnecting channels. ZSM-12 with a comparatively smaller pore diameter and with non-interconnecting channels is found to be the most p-selective.

When reaction mechanisms are the same in a particular hydrocarbon conversion reaction over large pore zeolites[33], the zeolite pore structure could influence their stability and product distribution pattern. Among the 12-membered ring zeolites studied, zeolite beta is found to be the best catalyst for the isopropylation of toluene, and exhibited good stability and high selectivity towards cymenes followed by ZSM-12 and mordenite (Table 4.11 and Fig.4.9). Eventhough, ZSM-12 and beta zeolites are highly siliceous and more stable in this reaction, the higher selectivity to cymenes in case of beta can be attributed to its interconnecting pore system.

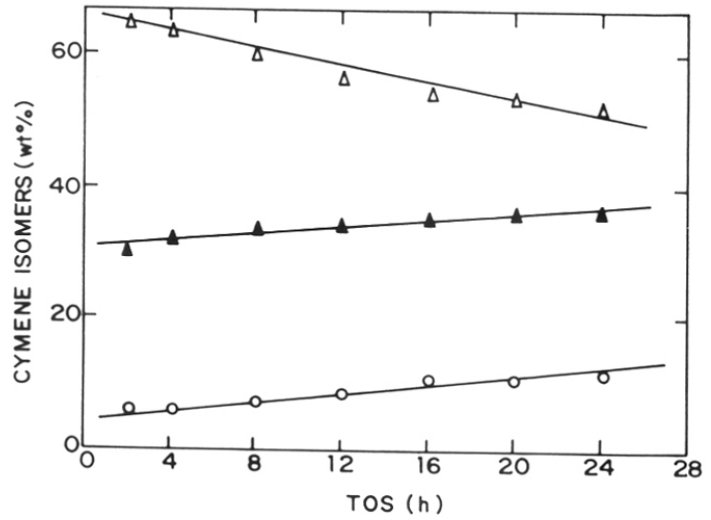

Fig.4.8: Concentration of cymene isomers with time-on-stream (TOS). Temperature = 180°C, reactants mole ratio = 8; (Δ) *m*-cymene, (▲) *p*-cymene and (o) *o*-cymene.

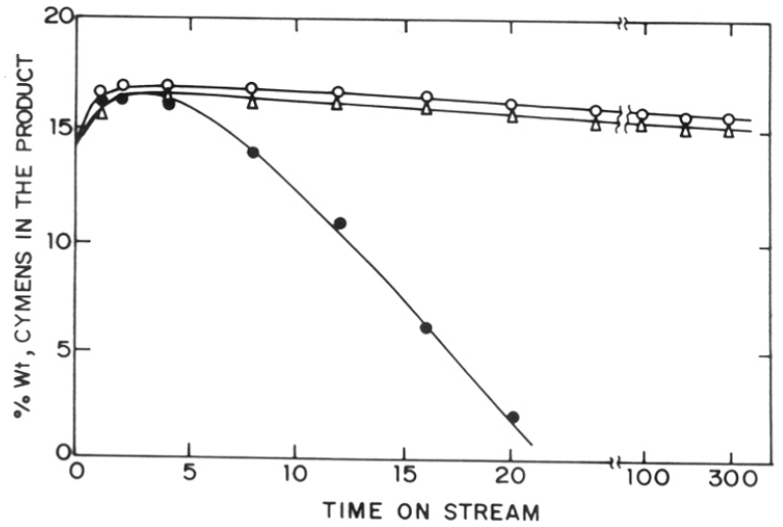

Fig.4.9: Catalytic performance of the large pore zeolites in the isopropylation of toluene with time-on-stream. Temperature = 180°C, space velocity = 4 h^{-1}, reactants mole ratio = 8; (o) beta, (Δ) ZSM-12 and (●) mordenite.

4.3.4. TRANSALKYLATION OF TOLUENE WITH CUMENE

The results of the transalkylation of toluene with cumene at various temperatures and space velocities are presented in Tables 4.12 and 4.13. As expected the conversion of cumene is low at lower reaction temperatures and higher space velocities. Another possible product during this reaction is DIPB, which is formed by the disproportionation of cumene. However, at higher toluene to cumene mole ratios (8 or higher), this reaction is not favoured.

4.3.5. TRANSALKYLATION OF TOLUENE WITH DIPB

A typical product distribution of the transalkylation of DIPB with toluene is presented in Table 4.14. In this reaction, the formation of cumene is possible either by the transalkylation of one mole of DIPB with one mole of toluene or by the dealkylation of DIPB. If two moles of toluene and one mole of DIPB react, two moles of cymenes will be formed. Other reactions such as the disproportionation of DIPB are negligible when toluene is present in excess. The catalyst is very active and selective towards cymenes without any cracked products like propylene, but the conversion of DIPB decreased from 99 to 63 % within 24 h of time-on-stream.

4.4. CONCLUSIONS

The isopropylation of benzene and toluene have been studied over zeolite beta. The activity and selectivity of beta is compared with those of other large pore zeolites mordenite and ZSM-12. The activity and stability are dependent on the acidic and structural properties of zeolites. Zeolite beta exhibited highest activity and selectivity in these reactions.

Table 4.12: Influence of temperature on the transalkylation of toluene with cumene in H-beta. Temp.=180° C; toluene/cumene mole ratio=8 and space velocity=4 h^{-1}.

	temperature (°C)		
Products (wt.%)	200	220	240
cumene conversion	65.25	66.21	71.42
Aliphatics	0.01	0.03	0.03
Benzene	5.23	5.50	6.55
Toluene	78.50	77.79	79.55
Xylenes	0.66	0.90	1.51
Cumene	5.92	5.77	4.87
m-Cymene	5.85	5.95	5.62
p-Cymene	2.67	2.73	0.43
o-Cymene	0.41	0.44	0.19
Σ DIPB[a]	0.34	0.33	0.21
Σ DIPT[b]	0.14	0.16	0.08
Selectivity (%)			
Cymenes	92.26	92.23	79.42
DIPT	1.44	1.65	0.82

[a,b] see foot notes in Table 4.9.

Table 4.13: Influence of space velocity on the transalkylation of toluene with cumene over H-beta. Temp.=180° C; toluene/cumene mole ratio=8 and space velocity=4 h^{-1}.

Products (wt.%)	Space velocity (WHSV)		
	4	8	15
Cumene conversion	66.21	59.62	53.34
Aliphatics	0.03	0.02	0.03
Benzene	5.50	4.71	3.96
Toluene	77.79	79.82	81.29
Xylenes	0.90	0.55	0.25
Cumene	5.77	6.89	8.14
m-Cymene	5.95	4.81	3.69
p-Cymene	2.73	2.19	1.77
o-Cymene	0.44	0.34	0.23
Σ DIPB[a]	0.33	0.36	0.39
Σ DIPT[b]	0.16	0.12	0.08
Selectivity (%)			
Cymenes	92.23	88.75	86.91
DIPT	1.65	1.23	0.82

[a,b] see foot notes in Table 4.9.

Table 4.14: Transalkylation of toluene with DIPB over H-beta zeolite. toluene/DIPB mole ratio=8 and space velocity=4 h^{-1}.

Products (wt.%)	temperature (°C)		
	180	210	230
DIPB conversion	86.10	98.37	99.29
Aliphatics	0.05	0.07	0.06
Benzene	1.97	2.48	2.71
Toluene	83.27	82.20	79.47
Xylenes	0.72	0.94	1.12
Cumene	4.59	3.62	0.62
m-Cymene	5.19	6.26	10.61
p-Cymene	2.11	2.87	4.31
o-Cymene	0.35	0.45	0.92
Σ DIPB[a]	1.38	0.26	0.07
Σ DIPT[b]	0.27	0.15	0.08
Selectivity (%)			
Cymenes	65.26	77.83	96.70
DIPT	3.54	1.48	0.78

[a,b] see foot note in Table 4.9.

4.5. REFERENCES

1. Newsam, J.M., Treacy, M.M.J., Koetsier, W.T. and de Gruyter, C.B., *Proc. Royal Soc. London Ser.* **A 420**, 375 (1988).
2. Young, L.B., Eur. Pat. Appl., 30,084 (1981).
3. Tobias, M.A., US Pat. 3,728,408 (1973).
4. La Pierre, R.B. and Patridge, R.D., Eur. Pat. Appl. 94,827 (1983).
5. La Pierre, R.B., Patridge, R.D., Chen, N.Y. and Wong, S.S., Eur. Pat. Appl. 95,203 (1983).
6. La Pierre, R.B., Patridge, R.D., Chen, N.Y. and Wong, S.S., US Pat. 4,501,926 (1986).
7. Martens, J.A., Perez-Pariente, J. and Jacobs, P.A., *Acta. Phys. Chem.*, **31**, 487 (1985).
8. Martens, J.A., Perez-Pariente, J., Sastre, E., Corma, A. and Jacobs, P.A., *Appl. Catal.* **45**, 85 (1988).
9. Corma, A., Fornes, V., Melo, P. and Perez-Pariente, J., ACS Symp. Preprints, Div., Petroleum Chem., p. 632 (1987).
10. Tsai, T.C. and Ay, C.L. and Wang, I., *Appl. Catal.*, **77**, 199 (1991).
11. Bonetto, L. Camblor, M.A., Corma, A. and Perez-Pariente, J., *Appl. Catal.*, **82**, 37 (1992).
12. Leu, L-J., Hou, L-Y., Kang, B-C., Li, C., Wu, S-T. and Wu, J-C., *Appl. Catal.*, **69**, 49 (1991).
13. Jones, E.K. and Dettner, D.D., US. Pat. 2,860,173 (1958).
14. Miki, H., US Pat. 4,347,393 (1982).
15. McAllister, S.H., Anderson, J. and Bullard, E.F. *Che. Engg. Prog.*, **43**, 189 (1947).
16. Chandavar, K.H., Kulakarni, S.B. and Ratnasamy, P., *Appl. Catal.* **4**, 287 (1982).
17. Becker, K.A., Karge, H.G. and Streubel, W.D., *J. Catal.*, **28**, 403 (1973).
18. Young, L.B., Butter, S.A. and Kaeding, W.W., *J. Catal.*, **76**, 418 (1982).
19. Nunan, J., Cronin, J. and Cunningham, J., *J. Catal.*, **87**, 77 (1984).
20. Kaeding, W.W. and Holland, R.E., *J. Catal.*, **109**, 212 (1988).
21. Chandavar, K.H. Hegde, S.G., Kulkarni, S.B. and Ratnasamy, P., *J. Chem. Technol. & Biotechnol.*, **34A**, 165 (1984).
22. Reddy, K.S.N., Shiralkar, V.P. and Rao, B.S., *Appl. Catal.*, communicated.
23. Pradhan, A.R. and Rao, B.S., *J. Catal.*, **132**, 79 (1991).
24. Pradhan, A.R., Kotasthane, A.N. and Rao, B.S., *Appl. Catal.*, **72**, 311 (1991).
25. Ito, K., *Hydrocarbon Processing*, **52** (8), 89 (1973).
26. Yen, Y.C., *Stanford Res. Inst. Econ. Rep.*, **49** (1969).

27. Harper, E.F., Ko, D.Y., Lese, H.K., Sabourin, E.T. and Williamson, R.C. in Albright, L.F. and Goldsby, A.R. Eds., *Industrial and Laboratory Alkylations*, (ACS Symp. Series No. 55) p.371 (1977).

28. Meshram, N.R., Kulkarni, S.B. and Ratnasamy, P., *J. Chem. Technol. & Biotechnol.*, **34 A**, 119 (1984).

29. Cynthia, T.W.C. and Chang, C.D., *J. Phys. Chem.*, **89**, 1569 (1985).

30. Jacobs, P.A., *Carboniogenic Activity of Zeolites*, Elsevier, Amsterdam p.46 (1977).

31. Bhatia, S., Beltramini, J. and Do, D.D., *Catal. Rev. Sci. & Engg.*, **34** (4), 431 (1989).

32. Karge, H.G. and Boldingh, E.P., *Catalysis Today*, **3**, 53 (1988).

33. Tsai, C.T. and Wang, I., *J. Catal.*, **133**, 136 (1992).

CHAPTER 5

ISOMERIZATION OF *n*-HEXANE OVER ZEOLITE BETA

5.1. INTRODUCTION

Light gasoline of a high octane number can be obtained by isomerization of C_5-C_6 alkanes. The lower is the reaction temperature the greater is the proportion of branched alkanes at thermodynamic equilibrium and hence the greater the octane number[1,2]. Highly chlorinated Pt-alumina catalysts, which can be considered to be superacids, are used at low temperatures (120-180°C). However, these catalysts are very sensitive to the accidental deactivation (by water or aromatics, etc.). That is why certain isomerization processes employ bi-functional zeolite catalysts (such as Pt-mordenite), which are less active and therefore operate at higher temperature (about 250°C).

The activity, the stability and the selectivity of acidic zeolites depend on their framework Si/Al ratio, hence on their acid site density[3-10] and structural features[11,12]. For most of the zeolites a maximum activity was found for the value of the Si/Al ratio above which none of the AlO_4^- (hence none of the acid sites) is in the nearest neighbourhood. Above this value the activity per acid site is constant, the strength of the isolated sites being maximal[3,4].

This chapter describes the hydroisomerization of *n*-hexane over large pore zeolites, beta, mordenite and ZSM-12 loaded with 0.3 wt.% platinum.

5.2. EXPERIMENTAL

The NH_4-forms of zeolites were used to impregnate the platinum. The catalysts, Pt/H-beta, containing 0.05-1.0 wt.% platinum were prepared by impregnating the ammonium-beta zeolites with a calculated amount of aqueous $Pt(NH_3)_4Cl_2$ solution. The impregnated catalysts were then dried and calcined in air at 673 K for 3 h. The catalysts, Pt/H-mordenite and Pt/H-ZSM-12, containing 0.3 wt.% platinum were also prepared in a similar manner. The physico-chemical properties of the zeolites (H-forms of beta, mordenite and ZSM-12) are shown in Table 4.6.

Prior to the experiments, the catalysts were pre-reduced in situ with hydrogen gas at 673 K for 2 h. The catalytic reactions were carried out at atmospheric pressure in the manner described in chapter 4. The products were analyzed with an on-line GC (HP 5890 series II) equipped with a capillary column (50 m X 0.5 mm crosslinked methylsilicone gum).

5.3. RESULTS AND DISCUSSION

The isomerization of *n*-hexane was then studied under the following conditions: temperature 453-553 K; WHSV = 1.0 h^{-1}; H_2/H.C. (molar ratio) = 10; pressure 1 atm. Catalytic activities as a function of reaction temperature are shown in Fig.5.1. At 493 K and 513 K, the conversion of *n*-hexane is maximum and C_6-isomers are the only primary products. The deactivation rate depends on the Si/Al ratio of the catalyst, and hence the lower is the acid site density, the lower is the deactivation (Fig.5.2). The deactivation rate also decreases with time-on-stream. The activity of the catalysts decrease in the order: Pt/H-beta (13) > Pt/H-mordenite (6.8) > Pt/H-ZSM-12 (62). Where the numbers in parenthesis represent the Si/Al ratio of the zeolite. The relatively low activity for Pt/H-ZSM-12 (62) may be due to its low acid site concentration (shown in Table 4.6). Pt/H-beta catalyst showed significant catalytic activity even after 50 h. run.

The Research Octane Number (RON) for the various C_6 isomers are 34.0, 73.4, 74.5, 92.3, and 103.5 for *n*-hexane, 2-methylpentane (2-MP), 3-methylpentane (3-MP), 2,2-dimethylbutane (2,2-DMB) and 2,3-dimethylbutane (2,3,-DMB), respectively. Therefore, high yields of 2,2-DMB and 2,3-DMB are desirable for a good isomerization catalyst. Fig.5.3 shows the product distribution at various temperatures. The isomer distribution depends on the total conversion and also on the nature of the catalyst. Pt/H-beta catalyst with higher catalytic activity also gives higher yields of (2,2-DMB + 2,3-DMB). The yield of DMB increases with temperature. Pt/H-mordenite gave a lower yield of DMB, although it has a higher activity compared to Pt/H-ZSM-12. The amount of DMB increased only slightly with temperature over Pt/H-mordenite.

In order to investigate the appropriate platinum content for *n*-hexane isomerization at 493 K, a series of catalysts were prepared based on zeolite beta loaded with 0, 0.05, 0.1, 0.3, 0.5, 0.7 and 1.0 wt.% of platinum. The catalytic activity and selectivity are shown in Fig.5.4. The activity increases with platinum content up to a maximum at about 0.3 wt.% platinum, then levels off. This behaviour, typical of a bifunctional catalyzed reaction, means that at low platinum content the hydro-dehydrogenation steps are kinetically limiting[13], while for 0.3 wt.% Pt and above isomerization of *n*-hexenes into isohexenes is the limiting step.

Guisnet *et.al*[13] proposed two shemes for the isomerization of *n*-hexane over zeolites.

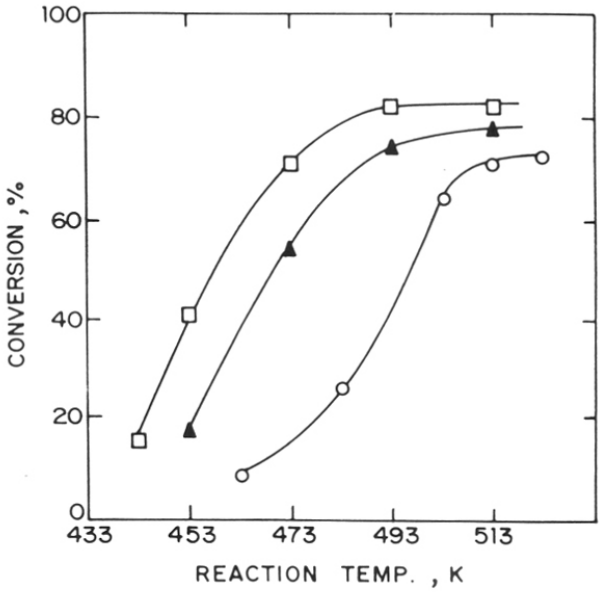

Fig.5.1: Catalytic activities varied with the reaction temperature over zeolites loaded with 0.3 wt.% platinum and WHSV=1 h^{-1}. (□) Pt/H-beta, (▲) Pt/H-mordenite and (o) Pt/H-ZSM-12.

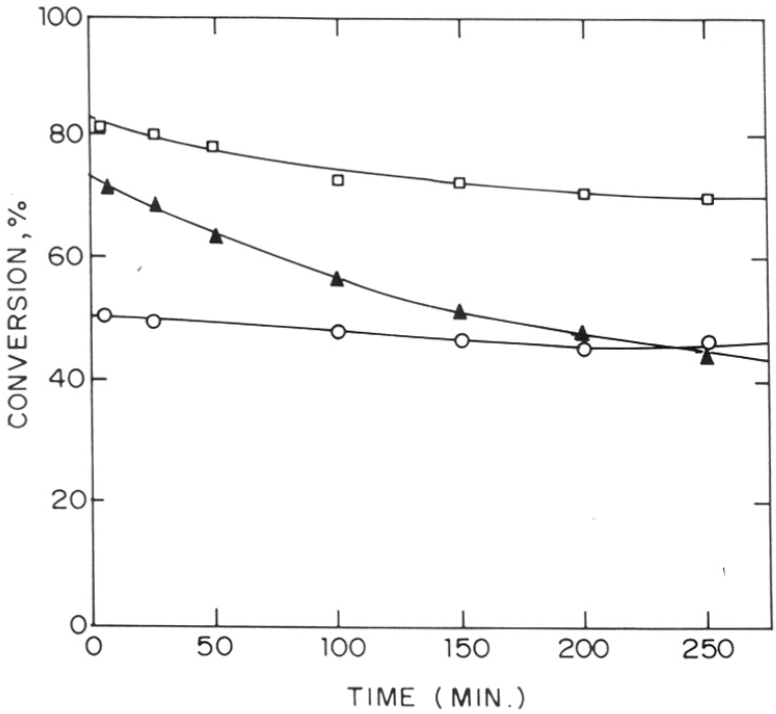

Fig.5.2: Conversion of *n*-hexane at 493 K as a function time-on-stream. WHSV=1 h^{-1}, symbols as in Fig.5.1.

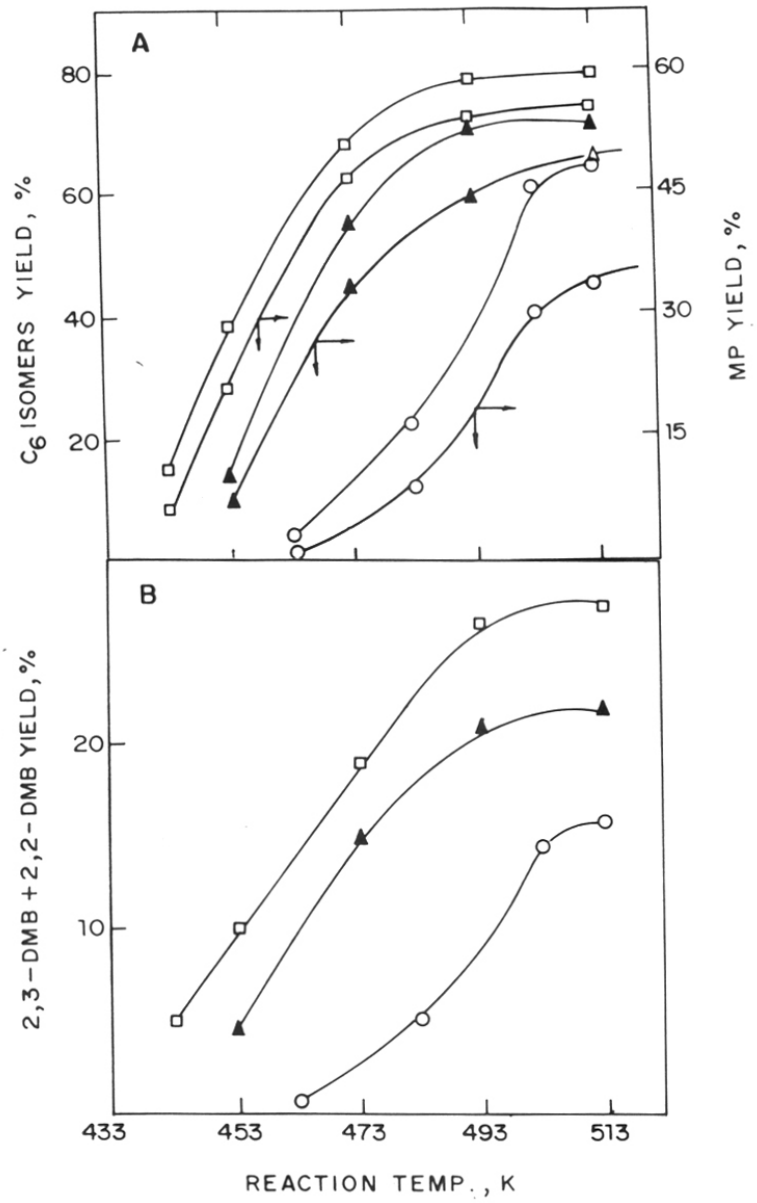

Fig.5.3: Effect of reaction temperature on the yield of C_6-isomers (A) and the yield of 2,2-DMB + 2,3-DMB (B). WHSV=1 h^{-1}, symbols as in Fig.5.1.

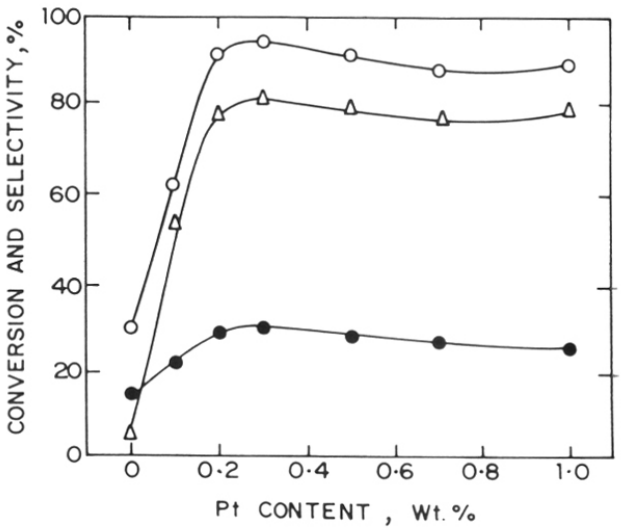

Fig.5.4: Effect of platinum content on the catalytic activity and selectivity of *n*-hexane isomerization over Pt/H-beta. WHSV=1 h^{-1}, Temp.= 493 K. (o) Selectivity of isomerization, (Δ) conversion of *n*-hexane and (•) selectivity of DMB.

For the catalysts with low acid site density the isomerization mechanism follows as in scheme I. For the catalysts with high acid site density the isomerization mechanism follows as shown in scheme II. Methylpentanes (MP) are the only primary products, 2,3-DMB then 2,2-DMB are formed successively. Irrespective of the nature of catalysts, methylpentanes are formed in their equilibrium ratio (2 MP/3 MP = 1.5).

5.4. CONCLUSIONS

Pt/H-beta was found to be more active and selective than Pt/H-mordenite, for the isomerization of *n*-hexane into methylpentanes and dimethylbutanes. Catalysts based on beta were also more stable than those based on mordenite or ZSM-12. The catalytic activities of Pt-loaded zeolite catalysts follow the sequence: Pt/H-beta > Pt/H-mordenite > Pt/H-ZSM-12. The lower yields of 2,2-DMB and 2,3-DMB over Pt/H-ZSM-12 catalyst were attributed to its low acid site density.

5.5. REFERENCES

1. Franck, J.P., *Procedes Chimiques, Techniques de l' ingenieur*, Paris, J5910 (1983).
2. Kouwenhoven, H.W., *'Molecular Sieves'* (Meier, W.M. and Uytterhoeven, J.B., Eds.) Adv. Chem. Ser., Americal Chemical Society, Washington, **121**, 529 (1973).
3. Bolton, A.P., *'Zeolite Chemistry and Catalysis'*, (Rabo, J.A., Eds.) American Chemical Society, Washington, ACS Monograph **171**, 714 (1976).
4. Barthomeuf, D., *Mater. Chem. Phys.*, **17**, 49 (1987).
5. Barthomeuf, D., *Stud. Surf. Sci. and Catal.*, **38**, 17 (1988).
6. Tsutsumi, K. and Takahashi, H., *J. Catal.*, **24**, 1 (1972).
7. Koradia, P.B., Kiovsky, J.R., and Asim, M.V., *J. Catal.*, **66**, 290 (1980).
8. Namba, S., Hosonuma, N. and Yashima, T., *J. Catal.*, **72**, 16 (1981).
9. Fajula, F., Ibarra, R., Figueras, F. and Gueguen, C., *J. Catal.*, **89**, 60 (1984).
10. Corma, A., *Stud. Surf. Sci. and Catal.*, **49 A**, 49 (1989).
11. Pradhan, A.R., Rao, B.S. and Shiralkar, V.P., *Stud. Surf. Sci. and Catal.*, **65**, 347 (1991).
12. Tsai, T.C. and Wang, I., *J. Catal.*, **133**, 136 (1992).
13. Guisnet, M., Fouche, V., Belloum, M., Bournonville, J.P. and Travers, C., *Appl. Catal.*, **71**, 283 (1991).

CHAPTER 6

SUMMARY AND CONCLUSIONS

CONCLUSIONS

Zeolite beta possesses a three-dimensional, 12-membered pore system and belongs to a family of zeolites, the two end members of which have tetragonal (Polymorph A) and monoclinic (Polymorph B) symmetry. In both the crystallographic systems, twelve-membered ring straight channels are present in two crystallographic directions, while the twelve-membered ring channel in the third crystallographic direction is sinusoidal. The main difference between the two polymorphs is in the pore dimensions of the straight channel which is narrower for the tetragonal structure. Moreover, the sinusoidal channels are more tortuous in the tetragonal compared to those in the monoclinic structure. Zeolite beta is the only high silica zeolite to have a fully three dimensional twelve-membered ring pore system. It is also the only large pore zeolite to posses chiral pore intersections. Finally, unlike other zeolites, but similar to mordenite, it is the only zeolite to have a near-random degree of stacking faults and yet maintain full sorption capacity.

This thesis describes the synthesis, characterization and catalytic properties of modified beta zeolites. The major objectives of this work were 1) to synthesize zeolite beta using commercially economic raw materials such as silica sol and tetraethylammonium bromide (TEA-Br) instead of the conventionally used tetraethylorthosilicate (TEOS) and tetraethylammonium hydroxide (TEA-OH), respectively. 2) A study of the physico-chemical and catalytic properties of the beta zeolites modified by a) isomorphous substitution b) cation exchange with di- and tri-valent ions c) loading with noble metals.

Zeolite beta was synthesized using silica sol, tetraethylammonium bromide, sodium aluminate, sodium hydroxide and ammonium hydroxide. Factors influencing the synthesis of zeolite beta, such as the influence of synthesis temperature, template concentration, alkali metal ion concentration, hydroxyl ion concentration and gel dilution were also studied. Zeolite beta could be crystallized in a temperature range from 373-433 K within 6-13 days using TEA-Br and NH_4OH with SiO_2/Al_2O_3 = 15-55, Na_2O/SiO_2 = 0.8, H_2O/SiO_2 = 19 and TEA-Br/SiO_2 = 0.25-0.50. The crystallization process followed the first order kinetic equation. The apparent activation energies for nucleation and crystallization were estimated to be 54.25 and 45.54 KJ mol^{-1}, respectively.

An increase in the crystallization temperature, gel SiO_2/Al_2O_3 ratio and decrease in the TEA-Br concentration leads to the co-crystallization of ZSM-12. Sodium ion concentrations higher than the optimum level lead to the formation of zeolite ZSM-5. Gel dilution was found to retard both the rate of nucleation and crystallization. The yield of zeolite beta was found to be almost 99% when silica sol and sodium aluminate were used as the sources of silica and alumina, respectively.

The synthesis of boron beta (B-beta) and gallium beta (Ga-beta) have been carried out successfully using Al-free source of silicon and hydroboric acid or gallium nitrate, respectively.

The physico-chemical characterization was done by XRD, framework i.r., chemical analysis, MASNMR and adsorption of different probe molecules. XRD showed the presence of a typical zeolite beta phase. XRD data indicate a slight contraction in the B-beta and an expansion in the Ga-beta framework, suggesting the incorporation of B and Ga ions in lattice positions. Lattice vibration frequencies in the i.r region are shifted (relative to those in the Al-beta) to higher wave numbers due to the presence of smaller B ions (B-beta) and lower wave numbers due to the presence of heavier Ga ions (Ga-beta). Scanning electron microscopy showed the absence of any amorphous matter, outside the pores of crystals. Equilibrium sorption capacities of water, cyclohexane, *n*-hexane, benzene and nitrogen showed the absence of significant amount of amorphous material inside the pores of zeolite beta.

^{29}Si MASNMR spectra of B-beta and Ga-beta exhibited a signal around δ = -102 ppm. ^{11}B MASNMR spectra showed the signal at δ = -3.03 ppm (indication of B^{3+} ions in tetrahedral positions). ^{71}Ga MASNMR spectra showed a signal at δ = 159 ppm due Ga^{3+} ions are in the Td symmetry. ^{27}Al MASNMR spectra of B-beta and Ga-beta showed the absence of significant amounts of aluminium. The higher ion-exchange capacities of B-beta and Ga-beta also suggest that trivalent ions are in framework positions.

The strength of acid sites of the cation exchanged beta zeolites was determined by ammonia adsorption isotherms. The amount of ammonia retained irreversibly is in the order of H-beta > La-H-beta > Mg-H-beta > Ca-H-beta > Sr-H-beta > Na-H-beta. The physical state of the sorbed phase was analyzed in terms of various thermodynamic parameters. Adsorbed ammonia on H-beta and La-H-beta exhibited a higher chemical potential than over other cation-exchanged zeolites over

the entire coverage and temperature. The decrease in chemical potential with coverage was, however, sharper in Na-H-beta and Sr-H-beta as compared to that in other zeolites. La-H-beta showed the highest Q_{st} value and Sr-H-beta showed the lowest Q_{st} value over the entire coverage. The initial isosteric heats seems to be influenced by Sanderson's electronegativity and e/r ratio of the exchanged cation.

Zeolite beta is a potential catalyst for the production of cumene from benzene isopropanol. The major by-product is 3-4% diisopropylbenzenes. At higher reaction temperatures *n*-propylbenzene is also produced along with other higher aromatic compounds. The formation of cumene is more at lower SiO_2/Al_2O_3 ratio, lower space velocities and higher benzene/isopropanol mole ratios. The optimum conditions for the selective formation of cumene at atmospheric pressure are: temperature 210°C, space velocity = 4 h^{-1} and benzene to isopropanol mole ratio of 8. H-Al-beta is more selective catalyst for the formation of cumene than the boron and gallium analogs.

Zeolite beta is also an active catalyst in the isopropylation of toluene to cymenes. The activity and selectivity of beta was compared with those of other large pore zeolites such as mordenite and ZSM-12. The selectivity to cymenes is more at lower space velocities and higher reactant mole ratios. Coke induced *para* selectivity was observed with time-on-stream among the cymene isomers. In terms of activity, stability and selectivity, zeolite beta is superior to mordenite and ZSM-12 for the formation of cymenes. The transalkylation of toluene with cumene and di-isopropylbenzene takes place on beta zeolite with good selectivities to cymenes.

The hydro-isomerization of *n*-hexane (to methyl pentanes and dimethyl butanes) was investigated over zeolite beta, mordenite and ZSM-12. The catalytic activities decreased in the order: Pt/H-beta > Pt/H-mordenite > Pt/H-ZSM-12. The lower yields of 2,2-DMB and 2,3-DMB over Pt/H-ZSM-12 (compared to the other two catalysts) were attributed to its low acid site density. 0.3% Pt/H-beta (Si/Al = 13) was found to be a useful catalyst for *n*-hexane isomerization, especially for the higher yields of dimethylbutanes.